UNIVERSITY OF SOUTHAMPTON

Diffusion of Boron and Silicon in Germanium

Suresh Uppal

Doctor of Philosophy

Materials Research Group
School of Engineering Sciences
September 2003

UNIVERSITY OF SOUTHAMPTON

ABSTRACT

FACULTY OF ENGINEERING
ENGINEERING MATERIALS

Doctor of Philosophy

DIFFUSION OF BORON AND SILICON IN GERMANIUM

by Suresh Uppal

This study used, for the first time, a combination of ion implantation and Secondary Ion Mass Spectroscopy (SIMS) to dope and characterise diffusion profiles of B and Si in Ge. By comparison of concentration profiles of B implanted in different orientation in crystalline and pre-amorphised Ge targets, it has been established that the channelling phenomenon plays an important role. For diffusion studies, B was introduced in Ge to different doses and energies. Subsequently the specimens were subjected to various thermal budgets using furnace annealing in the temperature range 800–900 °C, either with a surface protection layer or in evacuated ampoules. Annealed boron profiles showed an immobile concentration peak and a diffusion tail. Diffusion coefficients were derived by computer simulation using concentration profiles of as implanted and annealed samples. The measured diffusivity, around two orders of magnitude lower than reported previously using electrical techniques, was consistent with the variation in implantation dose, annealing ambient and protective layer. Using B doped epitaxial Ge layers grown by Molecular Beam Epitaxy, it was further confirmed that implantation induced defects are not responsible for slow B diffusion. An activation energy of $4.6(\pm 0.3)\,\mathrm{eV}$ and a pre-exponential factor of $1.2\times10^{5}\,\mathrm{cm^2/s}$ can be assigned for B diffusion in Ge in the temperature range studied. The results cast doubt over the prevailing belief of a vacancy diffusion mechanism for B diffusion in Ge. Additionally, the solid solubility of B in Ge at 875 °C has been estimated to be $\sim 2\times10^{18}\,\mathrm{atoms/cm^3}$.

For Si diffusion in Ge, studied in the temperature range 750–875 °C using furnace annealing, an activation energy of $3.2\,(\pm 0.3)\,\mathrm{eV}$ and a pre-exponential factor of $9.7\,\mathrm{cm^2/s}$ is assigned which agrees well with the values from the literature. The anomalous surface peak observed in the annealed profiles is attributed to implantation induced defects. The similarity of the activation energy of Si diffusion in Ge and Ge self-diffusion is suggestive of a similar diffusion mechanism for both the processes.

It is well known that boron shows a diffusion behaviour which is opposite to all other dopants as well as to Ge diffusion in Si-rich Si-Ge alloys. As an implication of the present study to B diffusion in Si-Ge alloys, it seems highly unlikely that a changeover of diffusion mechanism occurs as a function of Ge content in the alloy spectrum.

Contents

List of Figures

List of Tables

Acknowledgements

I would like to express my sincere gratitude to my supervisor, Arthur Willoughby, for his exceptional guidance and advice throughout this project. His optimism and continuous encouragement provided me constant inspiration to overcome the challenges. I am thankful to my advisor, Janet Bonar, for her helpful assistance, constructive criticism and invaluable suggestions.

I wish to thank members of Advanced SIMS Project group, University of Warwick, particularly Mark Dowsett for his helpful advice on interpreting and understanding the SIMS profiles. I am grateful to Richard Morris and Graham Cooke for performing SIMS measurements on difficult samples. My thanks are extended to Evan Parker and Tim Grasby, also at the University of Warwick, for growing boron doped epitaxial germanium layer. Alain Claverie of CNRS/CEMES (France) is thanked for arranging the Transmission Electron Microscopy analysis of epitaxial germanium. I am further grateful to Nick Cowern at the University of Surrey for his helpful suggestions and discussions at various stages of the project.

A special thank is reserved for Andreas Strohm (University of Stuttgart) and Harmut Bracht (now at Universität Münster) for their valuable suggestions and help in the design of the experimental setup for ampoule making.

To all the staff of the clean room at Southampton University Microelectronics Center and at Engineering Materials Laboratory, I express my sincere thanks for helping me learn various skills. A thanks is due to Clive Goddman, Chemistry Department, University of Southampton for making the ampoules and training me the skill of making good ampoules.

I am indebted to my parents and family for their support, love and affection. A special gratitude is owed to all my friends near and far for being there whenever required.

Chapter 1

Introduction

1.1 History

In 1947, the first junction transistor was built on germanium. Subsequent research concentrated mainly on achieving higher levels of material purity and improving device performance. By early 1950's germanium technology had advanced to produce rectifiers and transistors on an industrial scale. Diffusion, being an important process in junction formation, was studied for various dopants using p-n junction and radiotracer methods available at the time. Silicon was also researched as an alternative material which then was relatively difficult to purify because of its higher melting point and vulnerability to oxidation. Soon it was realised that native oxide of silicon could be utilised as a masking layer for impurity doping and also as a useful shield against contamination. On the other hand, germanium oxide was soluble in water and decomposes at higher temperature. The higher bandgap of silicon provided further advantages of higher operating temperatures and lower junction leakage currents. These advantages, coupled with industrial demands, shifted the research interest towards silicon based devices. Meanwhile, usage of germanium was confined to detectors, power transistors and substrates for III-V solar cells.

Recently, germanium has made a comeback! During last ten years the interest of research community has switched towards a new material silicon-germanium (Si-Ge). Silicon and germanium are miscible over the entire alloy composition range. The two materials possess very similar lattice constants but differ in other important properties such as electron & hole mobility and band gap [1]. Thus by adding a suitable amount of one into the other, such properties can be tailored. The major advantage of Si-Ge is its compatibility with the existing silicon technology. Today, a variety of applications for Si-Ge material with up to 70% germanium can be found. Quite recently, a germanium channel based MOSFET (Metal-Oxide-Semiconductor Field Effect Transistor) has been proposed and fabricated with some success [2].

1.2 Motivation for this work

Realisation of the potential of Si-Ge as a better alternative for a variety of devices has led to an intensification of research into the material. Diffusion processes which influence electrical behaviour of semiconductors form an integral part of the device technology. Quantification of dopant diffusion and understanding the responsible diffusion mechanisms is very important for optimisation and development of new Si-Ge based devices. Thus self- and dopant diffusion in Si-Ge alloys is currently being researched extensively.

Boron is an important p-type dopant in both silicon and Si-Ge alloys. Its diffusion behaviour in silicon has been investigated immensely in the past and in Si-Ge alloys (up to ~25% germanium) more recently. It is interesting to note that with addition of germanium the diffusivity of boron in Si-Ge alloys has exhibited a reduction (for at least up to 50% germanium). In pure germanium, however, the reported values were several orders of magnitude higher than in pure silicon. Whether this reduction is a long range strain, composition or mixed effect of both, is still debated although many experiments have been carried out aiming to resolve this issue (see Chap. 3). Understanding boron diffusion in Si-Ge as a function of germanium concentration requires a sound knowledge of its diffusion behaviour in pure germanium [3], especially given that another important dopant, antimony, does not behave similarly to boron in Si-Ge alloys. Thus a comprehensive study of boron diffusion in germanium was deemed important.

A review of literature shows that boron diffusion in germanium has not been investigated sufficiently. In fact, the main studies were conducted about three decades ago when diffusion was commonly quantified using electrically active impurity concentrations only. Incremental resistance and pn-junction profiling, which are somewhat crude by today's standards, were the techniques used at that time. Today, with advances in technology, characterisation techniques such as Secondary Ion Mass Spectroscopy (SIMS) are available which can measure the true elemental concentration of impurities directly. Furthermore we are able to exploit ion implantation as a way of introducing controlled amounts of impurities into the substrate in place of rudimentary techniques used in previous studies.

During device formation Si-Ge alloys are exposed to high temperatures. Thus an understanding of self-diffusion in these alloys also becomes relevant. Although germanium diffusion in silicon and Si-Ge alloys has been studied in the past and also quite recently (see Sec. 3.2.1), silicon diffusion in Si-Ge and pure germanium has not been explored well enough. Thus combining the advanced techniques of ion implantation and high resolution SIMS, efforts have also been undertaken to examine silicon diffusion in germanium. Due to the very similar nature of silicon and germanium this study may help to shed some light on self-diffusion processes in Si-Ge alloys.

1.3 Organisation of work

This dissertation has been organised as follows:

Chapter 2 is a general introduction to the subject of diffusion. Here an attempt is made to describe various kinds of defects found in semiconductors which are thought to be responsible for diffusion. The chapter outlines basic diffusion theory, relevant concepts and related mathematics. Possible mechanisms for dopant and self-diffusion in semiconductors are also discussed briefly.

Chapter 3 is devoted to a review of literature. Starting with a review of self- and impurity diffusion in silicon, it develops with a discussion on dopant and self-diffusion in germanium. A discussion on self- and impurity diffusion in Si-Ge alloys is also included. Studies involving boron implantation into germanium will also be examined.

Chapter 4 is an appraisal of the experimental techniques. Since ion implantation is the method used to introduce boron and silicon in germanium wafers in this study, this chapter deals with the basics of implantation and also a brief mathematical formulation used to express impurity profile after implantation. Discussion of the principle technique used for analysis, i.e. SIMS, forms second part of this chapter. It also outlines the method of obtaining concentration profiles from the raw SIMS data. The complications faced in annealing germanium and the measures taken to overcome the difficulties are also detailed.

The experimental program for implantation in germanium is described in chapter 5. The results of boron and silicon implantation in germanium are presented and discussed.

Chapter 6 outlines the experimental program for the diffusion study. The obtained diffusion results for boron as well as silicon are then analysed and discussed in detail. The implications of this study on boron diffusion in Si-Ge alloys is discussed and a consistent picture in the light of our measurement is attempted.

Finally chapter 7 forms the conclusions and suggests possible directions for future work in this area.

Chapter 2

Diffusion: theory, mechanisms and concepts

Atomic diffusion is a phenomenon by which atoms move in the lattice. Usually, the movement of atoms is due to a concentration gradient. Atoms move from high concentration to low concentration regions until a chemical equilibrium is reached. Self-diffusion, however, occurs even in the absence of a concentration gradient. Thus, practically speaking, if one isotope of an element is migrating in the matrix of another isotope of the same element, the process would be described as *self-diffusion* e.g. diffusion of ^{71}Ge in ^{72}Ge. If atoms of one element diffuse in the matrix of another element it is known as *impurity diffusion* e.g. diffusion of boron in germanium or silicon. The measurement of diffusion is possible only if there is a detectable difference between the host and the diffusing atoms.

2.1 Defects in semiconductors

All real crystals are imperfect due to the presence of defects. Defects fall into point, line or planar categories. Depending on the abundance of these defects, they may strongly affect the diffusion process. Point defects are further classified broadly into (a) intrinsic defects which are native to the crystal e.g. vacancies and interstitials, and (b) extrinsic defects, induced by impurities e.g. doping or by non-equilibrium processes like ion-implantation. A point defect can be *isolated* or *associated* with an impurity/host atom.

2.1.1 Intrinsic point defects

At finite temperatures, lattice atoms undergo continuous vibrations around their equilibrium lattice positions. In the process some atoms may acquire enough energy to detach themselves from a regular lattice site to form intrinsic defects. An absence of an atom from a regular lattice site is called a vacancy and is denoted by V (also known as a *Schottky defect*). The presence of a self atom out of a regular lattice site is called a self-interstitial and is denoted

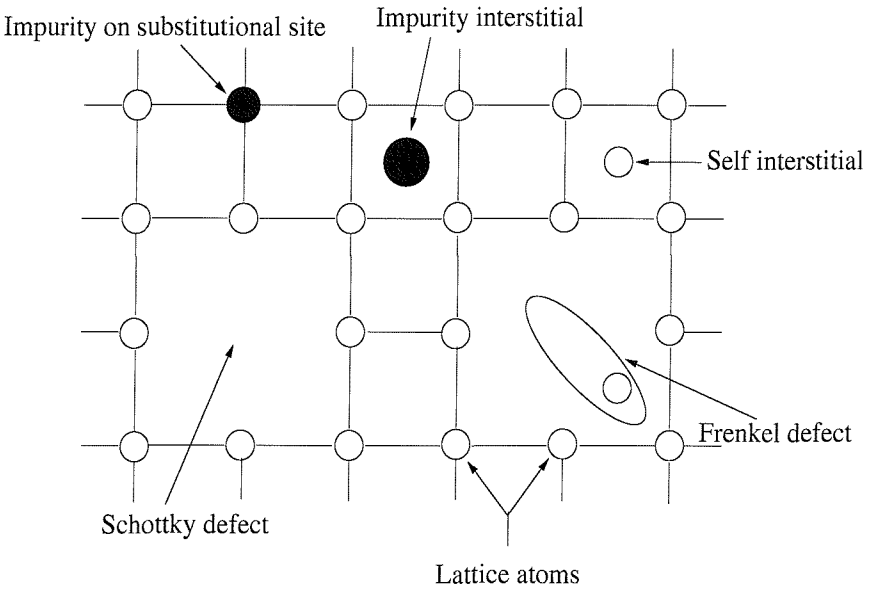

Figure 2.1: Two dimensional representation of various point defects present in semiconductors. These defects are present in all real crystals and their concentration may influence the diffusion process significantly.

by I (see Fig. 2.1). A *Frenkel defect* is said to be formed when a host atom occupies an interstitial position adjacent to a vacancy. Frenkel defects are generally very unstable. Unless the generated vacancy and the interstitial are separated immediately, they annihilate each other due to thermally activated movement. The vacancies and self-interstitials may exist in various charge states. For example, a vacancy can act as an acceptor by acquiring an electron as

$$V + e \rightleftharpoons V^{-}.$$

More than doubly charged states are, however, thermodynamically unstable in silicon and germanium [4].

A concept of *extended point defects* (V, I) has also been introduced by Seeger *et al.* [4] to explain some experimental observations of diffusion in silicon and germanium. In this configuration, the distortion introduced by a point defect is distributed over many lattice sites.

2.1.2 Extrinsic point defects

Impurity atoms, added intentionally or even unintentionally to a semiconductor, form extrinsic point defects. They can occupy either regular lattice sites (substitutional) or interstitial sites. We denote a dopant atom at a substitutional site by A and one at an interstitial site as A_i. A simplified configuration of impurity atoms at substitutional and interstitial sites is depicted in Fig. 2.1. Impurity atoms are easily ionised when they are in a different matrix to

their own and can interact with native defects already present in the crystal. Even a small fraction of such defects can affect the electrical properties of semiconductors significantly.

Another configuration of the interstitial defect has been suggested and is named *interstitialcy*[1] [6]. In this configuration, two non-substitutional atoms are located about a regular lattice site. Practically, it is difficult to differentiate between an interstitial and interstitialcy configuration.

If the intrinsic defect concentration and/or impurity doping is too high, defect-impurity pairs or larger complexes may form. These complexes can also affect the self- or impurity diffusion. The diffusion phenomenon occurring via such pairs is known as *pair-diffusion* [6].

A dopant in a lattice may occupy a substitutional site next to a vacancy and form a *dopant-vacancy* pair which is designated here by AV. In the interstitialcy defect configuration, if one of the atoms is a dopant atom, the defect is known as a *dopant-interstitialcy* pair which is symbolised by AI.

2.1.3 Thermodynamics of point defects

2.1.3.1 Equilibrium concentration

At any temperature, a finite concentration of native point defects (vacancies and interstitials) exists in thermal equilibrium with the lattice. Such dynamic equilibrium displays the fact that these defects minimise the free energy of the crystal. The equilibrium concentration of a defect species X, C_X^* ($X = V$ or I), can be written as [7]

$$C_X^* = C_L \theta_X \exp\left[\frac{G_X^f}{kT}\right] = C_L \theta_X \exp\left[\frac{S_X^f}{k}\right] \exp\left[\frac{-H_X^f}{kT}\right], \tag{2.1}$$

where C_L is number of available lattice sites in the crystal, θ_X is the number of degrees of freedom of the defect on a lattice site, G_X^f, S_X^f and H_X^f are the Gibb's free energy, entropy and enthalpy of formation of the defect X, respectively. The variables k and T are Boltzmann's constant and absolute temperature, respectively. Equilibrium defect concentrations in elemental semiconductors are smaller than that in pure metals [4]. Various direct experiments have been performed to measure defect concentrations in semiconductors [7]. Information on point defect properties of semiconductors can also be obtained from metal (such as Au, Cu) or dopant diffusion experiments rather indirectly [8].

If the defect exist as an impurity-point defect pair ($AX, X = V$ or I, A), then the thermal equilibrium concentration of such pairs is given by [6]

$$C_{AX}^* = \frac{C_A C_X}{C_L} \theta_{AX} \exp\left[\frac{E_{AX}^b}{kT}\right], \tag{2.2}$$

where E_{AX}^b is the binding energy of the AX defect, C_X the concentration of point defect which are not associated with dopants, θ_{AX} the number of equivalent ways for AX defect

[1] Strictly speaking, the term interstitialcy was first used by Seitz [5] to explain a diffusion mechanism.

formation at a particular site and C_A the concentration of impurity atoms. A positive binding energy reflects that the formation energy of a point defect is lowered in the proximity of dopant atoms. Thus the formation energy of the native point defects is affected by the presence of impurity atoms.

2.1.3.2 Charged defect concentrations

As stated earlier, point defects may also exist in a number of charged states. Due to acceptor or donor nature of dopants, a Coulombic interaction between charged defects and ionised dopants may become significant and affect diffusion. The formation energy of a charged defect depends on the energy level of the particular defect in the band gap, denoted in the following by E_X, relative to the Fermi level. The concentration of a charged defect which is not associated with dopant atoms can be written as [6]

$$\frac{C_{X^-}}{C_{X^0}} = \frac{\theta_{X^-}}{\theta_{X^0}} \exp\left[-\frac{E_{X^-} - E_f}{kT}\right], \tag{2.3}$$

$$\frac{C_{X^=}}{C_{X^0}} = \frac{\theta_{X^=}}{\theta_{X^0}} \exp\left[-\frac{E_{X^=} + E_{X^-} - 2E_f}{kT}\right], \tag{2.4}$$

$$\frac{C_{X^+}}{C_{X^0}} = \frac{\theta_{X^+}}{\theta_{X^0}} \exp\left[-\frac{E_f - E_{X^+}}{kT}\right], \tag{2.5}$$

$$\frac{C_{X^{++}}}{C_{X^0}} = \frac{\theta_{X^{++}}}{\theta_{X^0}} \exp\left[-\frac{2E_f - E_{X^{++}} - E_{X^+}}{kT}\right], \tag{2.6}$$

where E_f is the Fermi level and

$$C_{X^0} = C_L \theta_{X^0} \exp\left[\frac{S^f_{X^0}}{k}\right] \exp\left[\frac{-H^f_{X^0}}{kT}\right] \tag{2.7}$$

A comparison of above equations with Eq. 2.1 shows that formation energy of a charged defect depends on its charge state as

$$G^f_{X^-} = G^f_{X^0} + E_{X^-} - E_f. \tag{2.8}$$

In above equations we have assumed that defects exist only in five charged states denoted by $X^0, X^-, X^=, X^+, X^{++}$. We also note that whereas equilibrium concentration of neutral defect X^0 is independent of the Fermi level, the charged defect concentration depends on the Fermi level and energy level of the defect in the band gap. As a consequence the concentration of charged point defects and hence the total point defect concentration can be manipulated by doping (i.e. changing the Fermi level).

Under extrinsic doping conditions the Fermi level changes its position depending on the type and extent of doping. Assuming that Fermi level changes its values from E^i_f under intrinsic case to E^e_f under extrinsic case, a change in the concentration of charged defect X^- can be expressed as

$$\frac{(C_{X^-})}{(C_{X^-})^i} = \exp\left[\frac{E^e_f - E^i_f}{kT}\right]. \tag{2.9}$$

Using the relation $n/n_i = \exp[-(E_f^i - E_f^e)/kT]$ the above relation can be written as

$$\frac{(C_{X^-})}{(C_{X^-})^i} = \frac{n}{n_i}. \tag{2.10}$$

Here n and n_i are the electron concentration in the n-doped and intrinsic semiconductors respectively. Above argument can be applied to all possible charge states. Thus by generalising the above idea, we obtain the following equations

$$\frac{C_{X^-}}{(C_{X^-})^i} = \frac{n}{n_i}, \qquad \frac{C_{X^=}}{(C_{X^=})^i} = \left[\frac{n}{n_i}\right]^2,$$
$$\frac{C_{X^+}}{(C_{X^+})^i} = \frac{p}{n_i}, \qquad \frac{C_{X^{++}}}{(C_{X^{++}})^i} = \left[\frac{p}{n_i}\right]^2.$$

These equations show that concentrations of negatively charged point defects are higher in n-type material as compared to intrinsic material. Similarly positively charged point defect prevail in highly p-doped material. This result can be utilised to detect the charged defect involved in diffusion by changing the defect concentration and looking at its effect on diffusion of impurities. It is difficult, however, to determine which kind of point defect (vacancy or interstitial) is involved in diffusion.

Another phenomenon which affects the intrinsic carrier concentration and hence the charged defect concentration is the *band-gap narrowing*. Band-gaps of semiconductors are influenced by temperature as well as doping. The intrinsic carrier concentration, n_i, changes with the temperature as

$$n_i = \sqrt{N_C\, N_V}\, \exp\left(-\frac{E_g}{kT}\right), \tag{2.11}$$

where N_C and N_V are the density of states in the conduction and valence band respectively and E_g is the bandgap. Increase of temperature and doping reduces the bang-gap [1]. Both these factors change the intrinsic carrier concentration and hence affect the charged defect concentration according to Eq. 2.10. The effect of band-gap narrowing on charged defect concentration due to temperature (as well as doping) can be understood in terms of decrease in the gap between the defect level and Fermi level assuming that defect levels remain fixed with respect to band edges [6].

2.2 Diffusion mechanisms

The most important step in understanding diffusion is to identify the dominant diffusion mechanisms. Diffusion of self-atoms is considered relatively simple as the atoms involved are identical. Impurity atoms, on the other hand, have different sizes and electronic properties compared to the host atoms. Diffusion mechanisms have been classified as *direct* and *indirect* mechanisms [8], on the basis of whether or not they require intrinsic defects as diffusion vehicles.

2.2.1 Direct diffusion mechanisms

In the simplest case of an ideal crystal where all the lattice sites are occupied, the only way atoms can move to neighbouring sites is via an exchange of their respective positions. This mechanism is known as the *direct exchange mechanism* and is illustrated in Fig. 2.2. The direct exchange mechanism can occur for impurity atoms incorporated substitutionally in the same way as for self-atoms. This mechanism can also occur in the form of a ring exchange of atoms. Direct exchange mechanism requires a high energy due to large lattice distortion associated with it and hence is less probable.

Atoms whose equilibrium position is an interstitial site (especially small sized atoms) can jump from one interstice to the other. Such a mechanism is called an *interstitial mechanism* and is marked as process 1 in Fig. 2.2. Atoms using this mechanism diffuse fast as the probability of a jump site being empty is very high. The process requires small amount of energy.

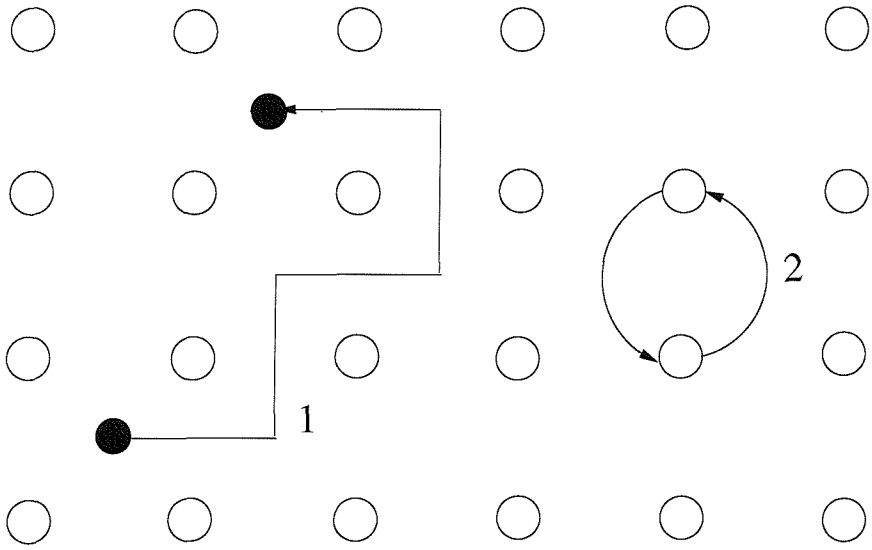

Figure 2.2: Direct diffusion mechanisms. Mechanism shown by 1 is the interstitial mechanism involving jumps of self or impurity atoms positioned at interstices. Mechanism 2 represents the direct exchange mechanism where substitutional atoms exchange positions.

2.2.2 Indirect diffusion mechanisms

Indirect diffusion of atoms requires intrinsic defects as diffusion vehicles. *Vacancy* and *interstitialcy* are the mechanisms that come in this category. The vacancy mechanism occurs as a result of a substitutional (self- or impurity) atom moving into an adjacent available vacant lattice site. A two dimensional representation of this mechanism is presented Fig. 2.3. This relatively simple mechanism is known to be responsible for self-diffusion in most closed

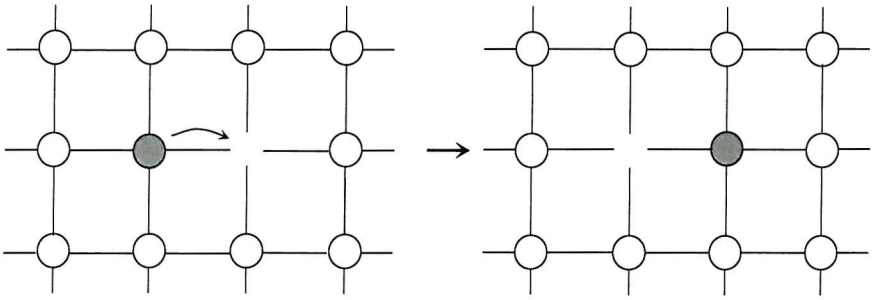

Figure 2.3: Schematic of the vacancy mediated mechanism for impurity diffusion. The open circles represent lattice atoms while the shaded circle represents impurity atom. The impurity atom makes a substitutional jump into the vacancy present at next lattice site leaving its own lattice site vacant.

packed metals. Since this mechanism involves the movement of only one atom, it is energetically favoured over the direct exchange mechanisms. In the case of impurity atom diffusion, the vacancy has to travel close to an impurity atom. If there exist sufficient binding between a dopant atom (A) and a vacancy, they may diffuse as pair (AV). For a progressive diffusion step via the vacancy mechanism in a diamond lattice, the pair has to separate and the vacancy has to move away to at least its third nearest neighbour site in order to return along a different path as shown in Fig. 2.4.

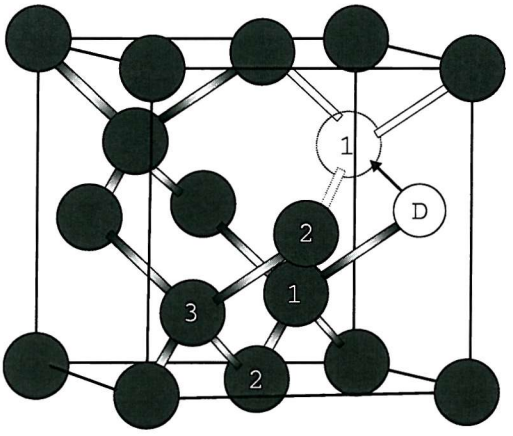

Figure 2.4: Representation of diffusion via a vacancy in diamond lattice. The dopant atom denoted by D can exchange site with a vacancy at position 1 and make a diffusion step. However if a dopant vacancy pairing exists then to make a progressive diffusion step the vacancy has to follow $1 \rightarrow 2 \rightarrow 3 \rightarrow 2' \rightarrow 1'$ to return to dopant via a different path.

The other indirect diffusion mechanism involving the self-interstitials point defects is the interstitialcy mechanism. In this mechanism, the impurity atom shares a lattice position

with self-atom and makes a diffusion jump by changing from one interstitialcy position to other as shown in the jump sequence presented in Fig. 2.5. An important difference between the interstitialcy and pure interstitial mechanism is that the latter does not involve any self-interstitials. The vacancy and the interstitialcy mechanism may even operate simultaneously in the crystal.

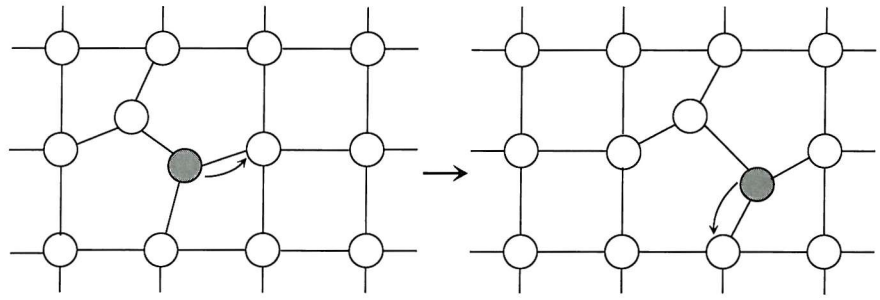

Figure 2.5: Schematic of the interstitialcy mechanism for impurity diffusion. The open and the shaded circles represent the lattice and the impurity atoms, respectively. In this mechanism the dopant-interstitialcy defect does not need to dissociate completely but a diffusion jump can still be made.

Impurity atoms can occupy either interstitial or substitutional sites in the host lattice depending on their size and solubility. They then may migrate via substitutional-interstitial mechanisms, categorised as kick-out and dissociative mechanisms. These mechanisms are represented in Fig. 2.6. An important feature of these mechanisms which distinguishes them from other direct or indirect mechanisms is that the impurity atoms migrate very fast while located at interstitial sites in the lattice and move long distances in the lattice before occupying a substitutional site. In the kick-out mechanism [9], a self-interstitial may kick-out an impurity substitutional atom into an interstitial position while the self-interstitial occupies the lattice site previously occupied by impurity atom. This mechanism can be expressed as

$$A_s + I \rightleftharpoons A_i,$$

where A_i represents the interstitial impurity atom, I the self-interstitial and A_s the substitutional atom. While in the interstitial position, impurity atom diffused by hopping from one interstitial site to another until it returns to a substitutional site by kicking-out a host atom from a lattice site and replacing its position. In the dissociative mechanism, sometimes known as the Frank-Turnbull mechanism [10] the transition between a substitutional and interstitial site involves a vacancy as

$$A_s \rightleftharpoons A_i + V.$$

The reaction represents formation of a Frenkel pair in forward and recombination in reverse direction. Once again the impurity atom diffuses fast while in the interstitial position. The

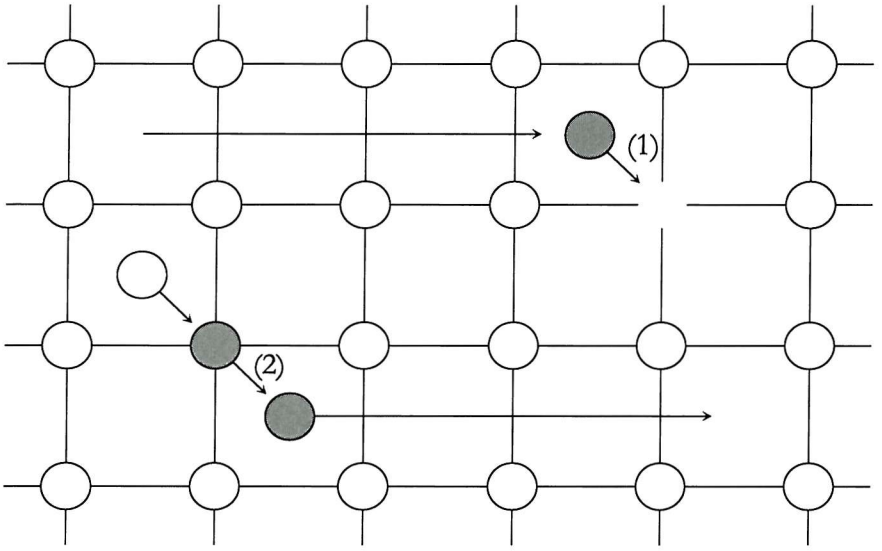

Figure 2.6: Dissociative and kick-out mechanisms are marked by (1) *and* (2) *respectively. In these mechanisms, elements diffuse interstitially in the lattice and eventually either occupy a vacant lattice site or kick-out a host atoms and become substitutional.*

difference between kick-out and dissociative mechanisms is the way in which the impurity atoms interchange between interstitial and substitutional states.

2.3 Mathematics of diffusion

Mathematical foundation on diffusion was first given by Fick. Fick's first law states that flux of a species J_x, is proportional to its concentration gradient measured normal to the area. Accordingly, under one dimensional flow, the flux can be written as

$$J_x = -D\frac{\partial C(x,t)}{\partial x}, \tag{2.12}$$

where $C(x,t)$ is the concentration of diffusing species as a function of position and time, and D, the constant of proportionality, known as the *diffusion coefficient* or *diffusivity* of the species. The negative sign in the equation indicates that the direction of flow is from high to low concentration.

Applying the law of conservation of matter, the change in concentration with time is equal to the rate of change of flux (in absence of a source or sink). Mathematically, this statement is

$$\frac{\partial C(x,t)}{\partial t} = -\frac{\partial J_x}{\partial x} = \frac{\partial}{\partial x}\left(D\frac{\partial C(x,t)}{\partial x}\right). \tag{2.13}$$

For atomic diffusion in semiconductors, the diffusivity can be considered to be independent of concentration if the semiconductor is intrinsically doped. Above equation then simplifies

to

$$\frac{\partial C(x,t)}{\partial t} = D\frac{\partial^2 C(x,t)}{\partial x^2}, \tag{2.14}$$

which is known as Fick's second law. Since it is easier to measure concentration than flux, diffusivity is extracted by solving Eq. 2.14 rather than Eq. 2.12 either analytically or numerically subjected to various initial and boundary conditions [11].

2.3.1 Atomic diffusion coefficient

Diffusion occurs as a result of random motion of atoms which are thermally activated. This makes the diffusion coefficient strongly temperature dependent. Ideally, the diffusion coefficient of an impurity species or self-atoms obeys Arrhenius law. For self-diffusion

$$D_{self} = D_0 \exp\left(-\frac{E_a}{kT}\right). \tag{2.15}$$

Here D_0 is the *pre-exponential factor* or *frequency factor* in cm^2/s, E_a the *activation energy* in eV, k the Boltzmann's constant and T the absolute temperature. D_0 is related to the atomic jumping frequency and a jumping distance of the impurity or self-atoms [12]. Assuming only one kind of defect (X: vacancy or interstitial) to be responsible for diffusion, the self-diffusion coefficient can also be expressed as

$$D_{self}\, C_L = D_X\, f\, C_X. \tag{2.16}$$

Here D_X is the defect diffusivity, f the correlation factor, C_X the defect concentration (given by Eq. 2.1), and C_L the number of available lattice sites in the crystal. The correlation factor is related to the probability of a reverse jump in the direction it has come from. It has values of 0.73 and 0.5 for self-diffusion in a diamond lattice by the interstitial and vacancy mechanism, respectively. The defect diffusivity D_X, is a microscopic quantity and can be expressed in terms of random movement of a defect:

$$D_X = g\, a_0^2\, \nu_0\, \exp\left(-\Delta G^m/kT\right) = g\, a_0^2\, \nu_0\, \exp\left(S_X^m/k\right) \exp\left(-H_X^m/kT\right), \tag{2.17}$$

where H_X^m and S_X^m represent the enthalpy and entropy of migration of the defect X, respectively, ν_0 the attempt frequency of a jump, a_0 the lattice parameter and g a geometric factor that takes the crystal structure into account. By combining Eqs 2.1, 2.16 and 2.17 we realise that the diffusion coefficient can be divided into two factors: one that takes care of defect formation terms (S_X^f, H_X^f), and the other that accounts for defect migration (S_X^m, H_X^m). However, it should be mentioned that the two parts are correlated. There is a correlation between E_a and D_0 known as the Meyer-Neldel rule [13].

The form of Eq. 2.15 suggests that a semi-logarithmic plot of diffusion coefficient D, against inverse temperature ($1/T$) should yield a straight line and therefore it is possible to calculate D_0 from its intercept and E_a from its slope. It should however be noted that

usually a large error is involved in the calculation of D_0 due to the fact that the intercept is calculated by extrapolation. This conventional way of analysis helps to recognise the nature of the defect and diffusion mechanism involved.

2.3.2 Activation energy of diffusion

For self-diffusion via one type of defect, say vacancies, the substitution of D_X and C_X from Eq. 2.17 and Eq. 2.1 in Eq. 2.15 results in the following expression for the activation energy

$$E_{aV}^{self} = H_V^f + H_V^m. \tag{2.18}$$

Hence the activation energy is the sum of formation and migration energies of the defect responsible for diffusion. This assessment is for the simplest case when self-diffusion occurs only via one kind of defect. When self-diffusion involves multiple defect species one has to improve Eq. 2.16 accordingly to include the effect of other defects. In the case of impurity diffusion, additional terms accounting for interaction between defects and impurity atoms also need to be introduced.

It is believed that the impurity atoms can diffuse when they are in one of their defect states such as impurity-vacancy pair, impurity-interstitialcy or impurity-interstitial pair. For the diffusion of an impurity A, the measured diffusivity D_A can be divided in contributions from the vacancies and interstitials as [6]

$$D_A = D_{AV} + D_{AI} = d_{AV}\,\frac{C_{AV}}{C_A} + d_{AI}\,\frac{C_{AI}}{C_A}, \tag{2.19}$$

where d_{AV}, d_{AI} represent the diffusivity of impurity-defect pair. The diffusivity of the pairs can be expressed by an equation similar to Eq. 2.17 as

$$d_{AX} = f\,g\,a_0^2\,\nu_0\,\exp\left(S_{AX}^m/k\right)\exp\left(-H_{AX}^m/kT\right), \tag{2.20}$$

where S_{AX}^m and H_{AX}^m now represent the entropy and enthalpy of migration of the impurity-defect pair. The impurity concentration C_A and the concentration of associated defects C_{AX} are associated by Eq. 2.2. However, it should be mentioned that under dilute concentration approximation the associated defect concentration (C_{AX}) would not exceed the isolated dopant concentration (C_A) [6]. Substituting Eq. 2.2 and Eq. 2.20 in Eq. 2.19, the diffusion coefficient of an impurity associated with a point defect can be written as

$$D_{AX} = D_0\,\exp\left(-\frac{E_{AX}}{kT}\right), \tag{2.21}$$

where the measured activation energy is the sum of formation and migration energies of the impurity-defect complex (AX) which is expressed as

$$E_{AX} = H_{AX}^m + H_{AX}^f. \tag{2.22}$$

According to Hu's analysis [14], the activation energy term for impurity diffusion via vacancy can be decomposed as

$$E_{AV} = \underbrace{H_V^f - E_{AV}^b}_{H_{AV}^f} + H_{AV}^m, \tag{2.23}$$

where E_{AV}^b represents the binding energy of an AV defect. The migration barrier for a vacancy associated with an impurity can be decomposed in terms of vacancy migration energy H_m^V, binding energy of impurity vacancy complex E_{AV}^b and potential energy ΔE_{AV}^3 of vacancy when the vacancy is at the third nearest neighbour site i.e.

$$H_{AV}^m = H_V^m + E_{AV}^b - \Delta E_{AV}^3. \tag{2.24}$$

Thus one finds that the difference between the activation energy for self- and impurity diffusion via the vacancy mechanism can be given by subtracting Eq. 2.23 from Eq. 2.18

$$E_{aV}^{self} - E_{AV} = \Delta E_{AV}^3, \tag{2.25}$$

where $\Delta\ E_{AV}^3$ is the potential energy difference between the vacancy being very far away and at third nearest neighbour site from the impurity atom[2].

Above equation describes the correlation between the activation energy for self- and impurity diffusion via the vacancy mechanism. One can observe that although the presence of an impurity reduces the formation energy of a defect in the vicinity of the impurity, it increases the migration energy by the same amount due to formation of a impurity vacancy complex. The above equation suggests that for self- and impurity diffusion occurring via the vacancy mechanism, the activation energy for impurity diffusion may be smaller than that for self-diffusion [14]. This analyses highlights the importance of the interaction potential. Fahey *et al.* [6] have emphasised that the strength and long or short range nature of the interaction potential must determine the dominance of vacancy mechanism for impurity diffusion.

A brief comment on the interaction between an impurity and a defect is required here. Basically two kinds of interactions exist: one is the Coulombic interaction between an ionised impurity and a charged point defect. The other is the elastic attraction due to the difference in bonding radii between the impurity and the lattice atom. Conceptually, it is difficult to speak of Coulombic interaction unless one assumes that the impurity and defects are separated by many lattice sites [6]. For elastic interactions, one can visualise that a large sized impurity may relieve the elastic stress by being closer to a vacancy than an interstitial atom. Similarly an impurity atom smaller than the host atoms would prefer to be in the vicinity of an interstitial point defect. Although the elastic interactions are highly probable, one can not explain all experimental observations on self- and dopant diffusion by appealing to such interactions alone [6].

[2]For a linear potential, a correction to this term has been suggested by Dunham *et al.* [15]

A similar analysis as above but for the case when interstitial mediated mechanism is responsible for both impurity and self-diffusion leads to the following equation for activation energy of impurity diffusion

$$E_{AI} = \underbrace{E_I^f - E_{AI}^b}_{E_{AI}^f} + E_{AI}^m. \tag{2.26}$$

We see that the presence of an impurity changes the formation energy of the defect in the impurity's vicinity. Expressing $E_{aI}^{self} = E_I^f + E_I^m$ as activation energy for self-diffusion via an interstitial mediated mechanism, one can write the difference between activation energy of self- and impurity diffusion $(E_{aI}^{self} - E_{AI})$ as

$$E_{aI}^{self} - E_{AI} = (E_I^m - E_{AI}^m) + E_{AI}^b. \tag{2.27}$$

There lies a fundamental difference in the way vacancy and interstitial mediated mechanisms operate with the help of the respective point defect: For the vacancy mechanism, the defect-impurity complex (AV) need to dissociate, at least partially, to complete a diffusion process in the forward direction as shown in Fig. 2.4. On the other hand a successful jump with the interstitialcy mechanism would not require that the defect-impurity complex (AI) must dissociate [6]. Thus there exist no relationship between the quantities E_I^m and E_{AI}^m unlike in the case of the vacancy mechanism.

On the basis of above analysis, we can draw the following conclusion: If self-diffusion occurs by the vacancy mechanism, the measured activation energy for self- and impurity diffusion should be similar (within experimental errors) for impurities diffusing by the same mechanism unless ΔE_{AV}^3 significantly differs from zero due to large Coulombic interaction or elastic forces. For the case when interstitialcy mechanism is responsible for self- and impurity diffusion, one can expect to find different values for the activation energy for different impurities unless a relationship between binding and migration energies of the impurity-defect complex exist. For the case where dopant diffusion occurs by a mechanism other than self-diffusion, the situation becomes very complex.

2.3.3 Doping effects on diffusivity

As discussed in Sec. 2.1, defects may exist in various charged states. The concentration of defects can be altered by varying the Fermi level via doping. Under extrinsic dopant diffusion conditions, not only does the defect concentration change but a drift component is also introduced due to the gradient of ionised dopant concentration. The combined effect makes the diffusion process concentration dependent.

We consider a simple case of self-diffusion occurring by the monovacancy mechanism in which the monovacancies exist in neutral, singly positive and singly negative charged state. Self-diffusivity D_{self}, for the case when neutral (V), singly charged acceptor (V^-) and singly charged donor (V^+) states of vacancy are participating in impurity diffusion in

intrinsic material is given by [16] as,

$$D^{i}_{self} = \frac{1}{2}\left(D_V[V]_i + D_{V^-}[V^-]_i + D_{V^+}[V^+]_i\right). \tag{2.28}$$

Here D_V, D_{V^-} and D_{V^+} are the diffusivities of the indicated vacancy charged states; $[V]_i$, $[V^-]_i$, and $[V^+]_i$ (i represents the intrinsic material) are the vacancy concentration in various charged states expressed as site fraction. The factor 1/2 accounts for the correlation factor for diffusion via vacancy mechanism in diamond lattice. This expression can be written in a simpler form as [16]

$$D^{i}_{self} = D^0 + D^- + D^+, \tag{2.29}$$

with

$$D^0 = \frac{1}{2}D_V[V]_i\,, \quad D^- = \frac{1}{2}D_{V^-}[V^-]_i, \qquad \text{and} \quad D^+ = \frac{1}{2}D_{V^+}[V^+]_i.$$

Doping of semiconductor will change charged vacancy concentration according to Eq. 2.11. Hence the final expression for self-diffusion in the extrinsic material takes the form

$$D_{self} = D^0 + D^-\left(\frac{n}{n_i}\right) + D^+\left(\frac{n_i}{n}\right) \tag{2.30}$$

Since vacancies and interstitials can be found in multiple charged states, above equation can be generalised as

$$D_{self} = D^0 + \sum_{r=1}^{2} D^{r-}\left(\frac{n}{n_i}\right)^r + \sum_{r=1}^{2} D^{r+}\left(\frac{n_i}{n}\right)^r \tag{2.31}$$

where r represents the charged state, and D^0, D^{r-} and D^{r+} represent the intrinsic diffusivity of self-atom interacting with a neutral point defect, an ionised acceptor point defect and an ionised donor point defect, respectively.

The above expression in its generalised form can be extended for impurity diffusion via various charges states as well where D^0, D^{r-} and D^{r+} become impurity diffusion coefficients associated with neutral, ionised acceptor and ionised donor charge state of defect involved under intrinsic conditions. Above expression is modified further when the effect of drift component of diffusion is introduced as well (see Ref. [6]).

Chapter 3

Literature review

3.1 Diffusion in silicon

3.1.1 Self-diffusion

The initial measurements of silicon self-diffusion were made using a short-lived radiotracer isotope ^{31}Si (half-life 2.6 h) deposited on sample surfaces. Concentration distributions were determined by sectioning using hand-lapping, electrochemical etching or sputtering techniques [17, 18, 19, 20]. These methods limited the studies to a narrow temperature range close to the melting point as the sectioning methods required long diffusion lengths (in μm range). Diffusing stable ^{30}Si into natural silicon [21] was a variation to this technique. After diffusion, ^{30}Si was neutron-activated to ^{31}Si and then profiled using chemical sectioning. Diffused profiles of ^{30}Si were also measured by ion sputtering and mass spectroscopy. Another kind of experiment involved ^{30}Si ion implantation. Diffusion in this case was measured by a (p,γ)-resonance technique using the reaction $^{30}\mathrm{Si}(p,\gamma)^{31}\mathrm{P}$ [22, 23]. Recently, isotope heterostructures (isotopically controlled multilayer structures) have been used for self-diffusion studies in conjunction with SIMS. The use of chemically pure and stable isotopes has allowed broader temperature ranges to be utilised and circumvent other experimental problems. As a result the accuracy of self-diffusion experiments has been much improved by these studies. Voss *et al.* [24] have reported a novel technique to measure short-lived radioisotope concentrations. They have successfully applied it in the measurement of self-diffusion in Si-Ge alloys [25].

Table 3.1 gives silicon self-diffusion parameters from different diffusion studies along with the method used and the temperature range studied. There is considerable scatter in activation energy among earlier works reported. This scatter is suggested to be caused by numerous factors such as difference in oxygen content in the Czochralski-grown and float-zone silicon wafers, different methods utilised, and measurements in different temperature range. The values for activation energy vary from about 5 eV at temperatures close to melting point to about 4 eV at lower temperatures. Similarly, a variation in pre-exponential coefficient (~10

D_0^{self} (cm^2/s)	E_a^{self} (eV)	Temperature range (°C)	Technique	Reference
1800	4.77	1200–1400	Radiotracer, hand lapping	[17]
9000	5.13	1100–1300	Radiotracer, electrochemical sectioning	[18, 19]
1460	5.02	1047–1385	Radiotracer, sectioning by sputtering	[20]
1200	4.72	1178–1300	Radiotracer, chemical sectioning	[21]
8	4.1	900–1100	Implantation, (p,γ)resonance of ^{30}Si	[22]
154	4.65	855–1175	Implantation, SIMS	[26]
20	4.4	830–1200	Implantation, (p,γ)resonance of ^{30}Si	[23]
530	4.75	855–1388	Isotope heterostructures, SIMS	[27]
560	4.76	800–1100	Isotope heterostructures, SIMS	[28]

Table 3.1: Values of pre-exponential factor D_0^{self} and activation energy E_a^{self} for silicon self-diffusion obtained from various studies. There is a large variation in the diffusion parameters resulting from different experimental conditions. Recent isotope heterostructure measurements seem to agree quite well with each other.

to $\sim 9\times10^3 \text{cm}^2/\text{s}$) is observed. Seeger *et al.* [4] explained the observed variation of activation energy at low and high temperatures on the basis that self-diffusion in silicon occurs via monovacancies at low temperature and via interstitials at higher temperature. To explain the large pre-exponential factor in silicon self-diffusion compared to those of metals, they further argued that both monovacancies and self-interstitials were spread out over several atomic volumes. Further support for their arguments came with the observed difference in diffusion behaviour of group III and group V dopants and the doping dependence of silicon self-diffusion [8].

Pre-exponential factors and activation energies derived in more recent experiments using isotope heterostructures for silicon self-diffusion [27, 29, 30] agree well with each other [see Table 3.1]. Selective defect injection studies have shown that silicon self-diffusion is enhanced by injection of both vacancies and interstitials. Ural *et al.* [30] have calculated the fractional contribution by interstitials for silicon self-diffusion in temperature range 800–1100 °C using defect injection. It has been found [30] that this fraction lies between 0.5 and 0.62 suggesting that contribution from vacancies and interstitials is almost equal. Further evidence have come from doping dependence studies. An enhancement in self-diffusivity value under extrinsic conditions (both n- and p-doping condition) [8, 31, 32, 33, 34] suggests that both the vacancy and the interstitial mechanisms operate simultaneously. Defect charge states responsible for diffusion have been partially recognised, but, the issue of the dominating mechanism at different temperatures has not been completely resolved.

In addition, using theoretical calculations, attempts have been made to estimate the activation energy and predict the diffusion path for self-diffusion in silicon. The activation

energy of interstitial mediated self-diffusion has been calculated to be ~3.5 eV using density functional theory local density approximation (DFT-LDA), and to be ~3.8 eV using the PW91 generalised gradient approximation functions [35]. These values are significantly lower than the experimental estimates (4.95 eV by Bracht *et al.* [27] for interstitial mediated self-diffusion). Calculations using diffusion quantum Monte Carlo methods have predicted the sum of formation and migration energy to be about 5 eV which lie closer to the experimental values [36].

3.1.2 Diffusion of group III and V elements

Due to the technological importance, diffusion of group III and V dopants in silicon has been evaluated for various dopant source conditions. We shall not go into detail of these studies but try to present a brief picture of the current understanding. The mean values of activation energies for these dopants are shown in Table 3.2. These values have been reproduced from the review article by Fahey *et al.* [6] but they do not represent the overall picture especially in the case of the vastly studied dopant boron.

The activation energy values of group V dopants, which are slightly higher than those of group III dopants, are closer to the activation energy of self-diffusion given in Table 3.1. Higher activation energy values for group V dopants (close to self-diffusion activation energy) than group III dopants suggests that the diffusion coefficients of group V elements lie closer to self-diffusion and are lower than those of group III elements.

Donor	Activation energy (eV)	Acceptor	Activation energy (eV)
P	3.51–3.67	B	3.25–3.86
As	4.05–4.34	Al	3.36
Sb	3.89–4.05	Ga	3.75
		In	3.60

Table 3.2: Activation energies of group III and V dopants in silicon from Ref. [6]. Group III dopants possess lower activation energies as compared to group V dopants and hence show faster difusion.

In the case of boron diffusion in silicon, recent careful measurements which were conducted in a relatively lower temperature range using samples protected by surface coatings, have revealed a small activation energy ~2.68 eV [37] as compared to previously believed value 3.46 eV [38]. Other reports have also shown activation energies comparable to those of Zangenberg [39, 40]. It should be noted however that despite the broad range of experiments performed, an agreement on activation energy is still lacking.

However, on the issue of mechanisms responsible for diffusion, recent defect injection studies in silicon have a provided further understanding. Quantitatively, the mechanism

of dopant diffusion is expressed in terms of an interstitial fraction f_{AI} [6]. For dopants of commercial importance the dictated limits obtained from various studies are:

$$0.8 \leq f_{BI} \leq 1, \quad \text{[8, 41] at 850 °C} \tag{3.1}$$

$$0.98 \leq f_{BI} \leq 1, \quad \text{[28] at 1000 °C, [42] at 800 °C} \tag{3.2}$$

$$0.94 \leq f_{PI} \leq 1, \quad \text{[6] at 1100 °C, [28] at 1000 °C} \tag{3.3}$$

$$0.35 \leq f_{AsI} \leq 0.55, \quad \text{[28] at 1000 °C} \tag{3.4}$$

$$0 \leq f_{SbI} < 0.22, \quad \text{[6] at 1100 °C, [28] at 1000 °C, [42] at 800°C} \tag{3.5}$$

Conventionally, the occurrence of one kind of mechanism in preference to the other is explained in terms of the covalent radii of the impurity atom. There seems to exist a correlation between covalent radii and f_{AI} at least for the group V and IV elements as shown by Frank *et al.* [8]. As the dopant covalent radius increases, f_{AI} appears to decrease, a fact which makes intuitive sense as there can be elastic attraction between an oversized impurity atom and a vacancy as well as repulsion with self-interstitial. The preference for the interstitial mechanism by group HI elements, however, is explained in terms of the Coulombic attraction between negatively charged acceptors and positively charged interstitials.

In summary, there exists a large scatter in diffusion parameter for self- and dopant diffusion in Si. The defect injection studies have been successful in identifying the dominating point defect responsible for self- and dopant diffusion and in some cases quantitative measurements have been made. However, more careful investigation is still required to pinpoint the defect charge states and their individual contribution to diffusion.

3.2 Diffusion in germanium

3.2.1 Self- and group IV elements

Interest in self-diffusion studies in germanium has mainly been scientific. The availability of the germanium radioisotope ^{71}Ge with a half life of 11.2 days, has added to the success of self-diffusivity measurement over a wide temperature range. Initially, conventional methods such as sectioning by grinding were used [43, 44] which limited the temperature range studied. Later, using ion beam sputtering for sectioning, diffusion temperature have been extended to small temperatures as well [45, 46]. Recently, isotope heterostructures studies in conjunction with SIMS have provided high precision measurements [47].

The activation energy and pre-exponential factor of self-diffusion in germanium from various studies are given in Table 3.3. Compared to self-diffusion in silicon, more agreement in the diffusion parameters can be seen. In various studies, activation energies vary from 2.95 to 3.14 eV and pre-exponential factors range from 7.8 to 44 cm^2/s.

D_0^{self} (cm^2/s)	E_a^{self} (eV)	Temperature range (°C)	Technique	Reference
7.8	2.95	766–928	Sectioning by grinding	[43]
32	3.1	750–870	Sectioning by grinding	[44]
44	3.12	731–915	Steigmann's method	[48]
10.8	2.99	731–915	Gruzin's absorption method	[48]
24.8	3.14	549–891	Sectioning by sputtering	[45]
13.6	3.09	535–904	Sectioning by sputtering	[46]
12	3.05	543–690	SIMS	[47, 49]

Table 3.3: Values of pre-exponential factor D_0^{self} and activation energy E_a^{self} for germanium self-diffusion from various studies. There exist a better agreement in self-diffusion parameters for germanium than for silicon. Spread out monovacancy is believed to be dominant defect responsible for self-diffusion in germanium.

The self-diffusion parameters in germanium are well represented by a single Arrhenius line in the whole temperature range studied. This led Seeger *et al.* [4] to argue that germanium self-diffusion can be explained using only one type of intrinsic defect. The doping dependence of self-diffusion in germanium was also explainable by assuming a monovacancy mediated process. The large pre-exponential factor compared to metals (by a factor of $\sim 10^3$) was suggested to be due to a large entropy term which was related to the spreading out of a vacancy over several atoms volumes.

We digress here a little from the current discussion and draw attention to remarks made by Seeger *et al.* [4] on the relative contributions by interstitial and vacancy defects to self-diffusion in germanium and silicon. Using the idea of the *extended defect* Seeger *et al.* [4] were able to account for the high pre-exponential factor observed in the case of self-diffusion in both silicon and germanium. Self-diffusion data of silicon at high temperature were successfully accounted for by the extended interstitial model. Realising that both silicon and germanium contract on melting, they expanded the same idea to self-diffusion in germanium and estimated the energy and entropy of formation of such a defect in the germanium lattice. The contribution to the diffusion coefficient of germanium at the melting point from extended self-interstitials was found to be negligible compared with the extrapolated experimental value. Hence they disregarded the extended interstitial mechanism for germanium self-diffusion due to a very high formation energy and formation entropy of such a defect. Fig. 3.1 taken from Ref. [4] represent the relative contributions of interstitials and vacancies in self-diffusion in silicon and germanium as estimated by Seeger *et al.* Note that plot presented in Fig. 3.1 is only a schematic reproduction of the plot presented in Ref. [4] and does not contain experimental data. We note that there is a cross-over for self-diffusion coefficient for diffusion via interstitial and vacancy mechanisms in the case of silicon whereas for the case of

germanium self-diffusion, the contribution due to the interstitial mechanism is consistently lower than for the vacancy mechanism at all temperatures. Based on the concepts developed in Sec. 2.3.2 we may state that an element diffusing via self-interstitials in germanium should show a behaviour similar to that of self-diffusion via the interstitialcy mechanism i.e. the diffusivity values should be smaller than measured self-diffusion in germanium.

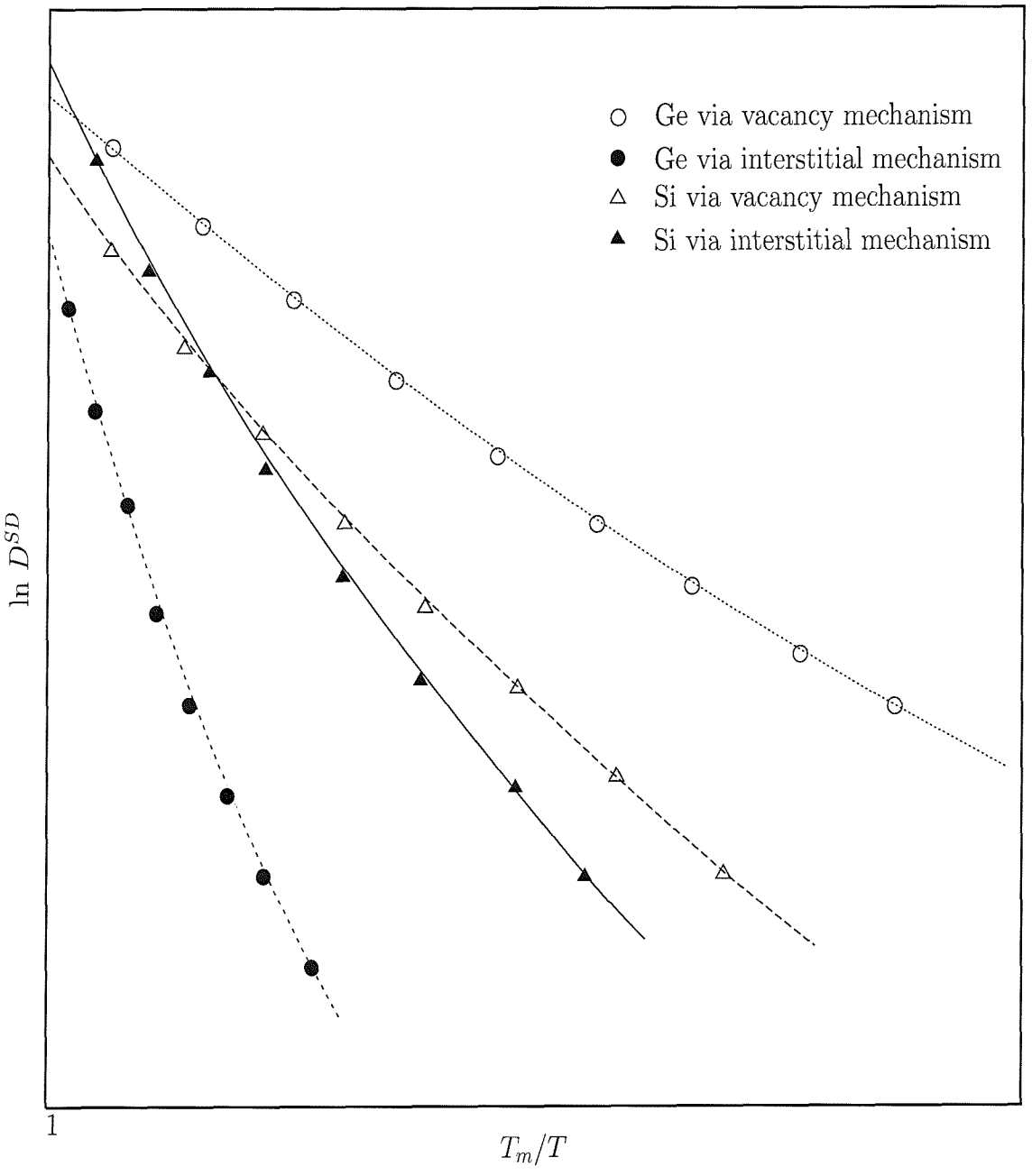

Figure 3.1: Contribution to silicon and germanium self-diffusion coefficient by vacancy and interstitial mechanisms as predicted by Seeger et al. [4]. The graph is reproduced from Ref. [4] and does not contain the experimental data. Note that the axis on the scale has not been provided in the original article and reason for the curvature in the lines is not clear.

We continue our discussion on self-diffusion in germanium. Doping effects on self-diffusion in germanium have also been studied [44, 45, 46]. It was concluded in all studies that n-doping increases self-diffusivity while p-doping reduces it. Assuming that self-diffusion in germanium occurs by monovacancies and that the vacancy in germanium exist in a neutral and negatively charged or acceptor state, the observed result of enhancement(retardation) of the self-diffusion coefficient by n(p) doping can be easily explained [8]. Shaw [16] analysed the data of doping dependence of germanium from Valenta *et al.* [44] along with the isotope effect measurement on germanium (^{71}Ge,^{77}Ge at 900 °C by Campbell [50]) and calculated a value of 0.5 for the correlation factor which corresponds to self-diffusion in diamond lattice by the monovacancy mechanism. The argument of Hu [14] that for diffusion via the vacancy mechanism, decrease in diffusivity should be observed with increasing pressure was also confirmed in the studies of Werner *et al.* [46].

Studies involving Cu [51], Ni and Zn [52] and Au [53, 54] in germanium have provided indirect evidence on diffusion parameters for self-diffusion in germanium and are in good agreement with literature values obtained using direct measurements. Thus it is noted that there exists a strong evidence for monovacancies to be the dominant defect for self-diffusion in germanium. It should be emphasised in the light of remarks made by Seeger *et al.* [4] that an interstitial component of self-diffusion may also exist but it is bound to be smaller than the vacancy component at all temperatures. Therefore the interstitial component has not been observed in self-diffusion experiments.

Theoretical studies on self-diffusion in germanium have been limited. Density functional theory calculations for self-diffusion in germanium via vacancies, using the plane wave (PW) functional of the density functional theory have estimated an activation energy of ~2.4 eV which is about 1 eV below the experimental values [55]. A correction procedure based on the B3LYP functional was employed to improve the calculations. Although a better agreement with experimental values for the activation energy was observed, the agreement with cohesive energy was found to be far from acceptable [56]. Theoretical calculations on formation and migration energies of the defects in silicon as well as germanium can also be found in early literature [4, 16]. The sum of the formation and migration energy of vacancies is in reasonable agreement with experimental values of activation energy for germanium self-diffusion. However, the reliability of these early theoretical results is questionable.

Among other group IV elements, we postpone the discussion on silicon diffusion in germanium until a later section (Sec. 3.3) and instead consider another isovalent impurity, i.e. Sn. From literature, the activation energy for Sn diffusion in germanium seems to vary between 2.68–3.26 eV [57, 58, 59, 60]. Within experimental uncertainties these values are in good agreement with those for self-diffusion in germanium. On the basis of similar activation energies, it has been argued that Sn diffusion in germanium occurs by the same mechanism as self-diffusion.

3.2.2 Group III elements

Due to lack of commercial interest in germanium, diffusion studies of group III dopants have not been enthusiastically followed. Among group III elements, we discuss the results of Al, Ga and In diffusion in germanium and postpone discussing boron diffusion to later in the section.

Table 3.4 gives an overview of the diffusion parameters available for group III elements in germanium. We notice a variation of more than 1 eV in activation energies for Al and In. We find larger variations in the pre-exponential factors which can be expected due to D_0 being calculated by extrapolating the Arrhenius line. However, one is obviously concerned about the reliability of the data due to such variations in measured activation energies. Due to the difficulties of annealing germanium at high temperatures and also the material's vulnerability to oxidation and contamination it is no surprise that large variations in diffusion parameters are seen.

Acceptor	Activation energy (eV)	Pre-exponential factor (cm^2/s)
Al	2.2–3.45	9.8×10^{-4}–1×10^{3}
Ga	3.0–3.31	10–1.4×10^{2}
In	2.47–3.63	10–1.8×10^{4}

Table 3.4: Values of pre-exponential factor D_0^{self} and activation energy E_a^{imp} of group III dopants in germanium. Values are taken from Ref. [57].

Södervall *et al.* [61] also studied the isotope effect of Ga diffusion in germanium and argued that the observed isotope effect for self-diffusion in germanium can also be brought in agreement by assuming diffusion via relaxed interstitials. However, their measurements of the isotope effect of Ga, although slightly lower than that of self-diffusion, can be reconciled with the relaxed vacancy model for impurity diffusion. It should be mentioned that group III elements in germanium are believed to diffuse by the vacancy mechanism [8] although no direct evidence has been observed as e.g. by defect injection.

Let us now move to literature data on boron diffusion in germanium. In the diffusion measurements performed by Dunlap [62] boron was pyrolytically deposited on germanium samples which were then heated to diffusion temperatures in ampoules filled with argon. No mention of any surface damage or oxidation has been made. For boron diffusion an anomalously high activation energy was obtained as compared to other dopants studied. This was attributed to the fact that boron does not alloy easily with germanium and thus the deposited boron film does not make good contact with the underlying crystal. Poor adhesion has made boron diffuse slowly at lower temperature thus giving a higher value of activation energy. In the second study by Meer *et al.* [63], intrinsic germanium samples were sealed in

ampoules containing germanium powder doped with boron. Due to difficulties in the preparation of boron doped germanium powder a surface concentration of only 5×10^{18} atoms/cm^3 was obtained. However, an important feature of this study was the successful application of SiO_2 and Si_3N_4 films as diffusion masks for germanium.

Dunlap [62] used the pn-junction method to measure bulk diffusion whereas Meer *et al.* [63] used incremental sheet resistance via four-point probe method. The diffusion parameters have not been provided in the original articles but have been calculated by Stolwijk [57] and are listed in Table 3.5.

D_0 (cm^2/s)	E_a (eV)	Temperature range (°C)	D (800 °C) (cm^2/s)	Experimental technique	Reference
6×10^{8}	4.5	700–900	4.4×10^{-13}	pn-junction	[62]
9.5×10^{6}	4.5	760–850	6.9×10^{-15}	Incr. sheet resistance	[63]

Table 3.5: Pre-exponential factor D_0, and activation energy E_a values for boron diffusion in germanium. The method of study and the temperature range of the diffusion experiment are also provided. Note a difference of two orders of magnitude in diffusion coefficient at 800 °C. *The data has been calculated from the Arrhenius curve in original articles by Stolwijk [57].*

We find disagreement in the diffusivity at 800 °C which is greater than 2 orders of magnitude. This difference in diffusivity comes mainly due to the difference in the pre-exponential factors since surprisingly the same value of activation energy has been calculated. However, this value is about ~1.5 eV higher than the measured self-diffusion activation energy for germanium and lies close to that of self-diffusion in silicon.

On the mechanism front, we have noted that there exist some direct as well as indirect evidence for self-atoms in germanium to diffuse primarily via vacancies. For group IV elements tin(Sn) and silicon, and group IH elements it has been argued on the basis of similarity between activation energy for impurity and self-diffusion that diffusion occurs primarily via the vacancy mechanism. Since the activation energy for boron is higher that other group III elements or self-diffusion, doubt on the dominance of the vacancy mechanism for boron diffusion in germanium can be casted. Due to this anomaly of boron diffusion with other group III elements as well as differences observed in previous studies, an investigation with a better measurement technique is highly desirable.

3.2.3 Group V elements

Major work on P, As and Sb diffusion in germanium has been performed mainly using electrical methods. Table 3.6 gives the range of activation energy and pre-exponential factor for diffusion of group V elements in germanium as given by Stolwijk [57]. Mention should

Acceptor	Activation energy (eV)	Pre-exponential factor (cm^2/s)
P	2.1–3.1	9×10^{-2}– 3.3×10^{2}
As	2.2–2.5	$0.71 - 1.5\times10^{2}$
Sb	2.08–2.9	$0.22 - 5\times10^{2}$

Table 3.6: Values of pre-exponential factor D_0^{self}, and activation energy E_a^{imp} for group V dopants in germanium. The values are taken from Ref. [57].

also be made on limited but recent studies on these dopants in germanium. Phosphorus diffusion in germanium has shown a concentration dependent diffusion [64, 65] as in the case of silicon. Recent arsenic diffusion measurement using a GaAs overlayer has also shown a concentration dependence [66] and this study held vacancies in neutral and doubly negative charge state responsible for arsenic migration in germanium. This argument was further confirmed by a limited temperature (450–550°C) measurement using implanted sources [67].

In another investigation on pressure effect on arsenic diffusion in germanium by Mitha *et al.* [68], it was concluded on the basis of small negative activation volume calculated from pressure dependence of arsenic diffusion in germanium that its diffusion is not entirely mediated by vacancies. It was argued that if arsenic diffusion in germanium occurs via vacancy mechanism only then either the vacancy formation volume is unexpectedly low or the vacancy migration energy is quite high. They further speculated on the possibility of an interstitialcy mechanism for arsenic diffusion bringing into doubt the view that diffusion of group III, IV or V elements in germanium is entirely vacancy dominated.

Doping dependence of group V impurities have been studied by Valenta *et al.* [69]. It has been reported that for arsenic and antimony diffusion in germanium, the doping dependence is similar to that for germanium self-diffusion i.e. n-doping enhances and p-doping reduces the diffusion of arsenic and antimony in germanium. This observation has been at least qualitatively explained by invoking a vacancy based diffusion model [4, 16]. It should be noted that similar doping dependence has been observed for a group III element indium in germanium. However for other group III elements the doping dependence has not been characterised.

On a broader scale we note that the diffusion rate of donor impurities is higher than acceptor impurities in germanium as shown in Fig. 3.2. This observation has been also been explained using a monovacancy mechanism. Since vacancies in germanium are believed to be in acceptor state (negatively charged), they attract the positively ionised group V donor atoms. In addition to the elastic attraction of large group V elements towards vacancies, this Coulombic attraction increases the likelihood of a vacancy to be found in the neighbourhood of a donor atoms and thus increases the diffusion coefficient. The elastic component of attraction towards vacancies exists for large group III elements as well but since these

elements suffer a Coulombic repulsion from vacancies, the diffusion coefficients for group III elements are found to be lower than for group V elements.

3.3 Diffusion in Si-Ge alloys

The inspiration for this work came from the ever growing interest in Si-Ge alloys and the absence of data at the high germanium end. We will briefly review the self-diffusion studies in Si-Ge alloys first and then try to understand dopant diffusion in Si-Ge especially B and Sb diffusion which is largely studied.

3.3.1 Self-diffusion

3.3.1.1 Diffusion of germanium in silicon

Since self-diffusion is the simplest form of diffusion, its understanding is a key to model dopant diffusion. Let us consider germanium diffusion in pure silicon. Due to the suggestion of McVay *et al.* [70] that germanium diffusion in silicon might be similar to silicon self-diffusion there has been considerable interest in germanium diffusion in silicon owing to the possibility of using a relatively long lived germanium radiotracer isotope (11.2 days) as an alternative to its silicon counterpart (2.5 h) for self-diffusion in silicon. The measurement techniques used vary from radiotracer deposition/implantation and characterisation using sectioning by grinding or ion beam sputtering, to growing epitaxial layers using Molecular Beam Epitaxy (MBE) and profile analysis using SIMS. Table 3.7 gives the diffusion parameters obtained in various studies for germanium diffusion in silicon.

D_0 (cm^2/s)	E_a (eV)	Temperature range (°C)	Technique	Reference
1.5×10^3	4.7	1200–1380	Radiotracer, mechanical sectioning	[70]
2.5×10^3	4.97	1030–1302	Radiotracer, sectioning by sputtering	[71]
3.5×10^{-1}	3.93	850–1000	Radiotracer, sectioning by sputtering	[71]
7.55×10^3	5.08	1100–1300	Deposition, SIMS	[72]
1.38×10^5	5.39	1000–1200	Implantation, SIMS	[73]
1.03×10^5	5.33	876–1388	Deposition, SIMS	[74]
2.44×10^3	4.92	850–1100	Epitaxial layer, SIMS	[75]
3.1×10^2	4.66	925–1050	Epitaxial layer, SIMS	[76]
2.1×10^3	4.88	1062–1214	Radiotracer, ion beam sectioning	[25]

Table 3.7: Values of pre-exponential factor D_0, and activation energy E_a, for germanium diffusion in silicon. A large scatter in diffusion parameter similar to that of self-diffusion in silicon can be seen. Similar to self-diffusion, germanium diffusion in silicon is believed to occur via both vacancy and interstitial mechanisms.

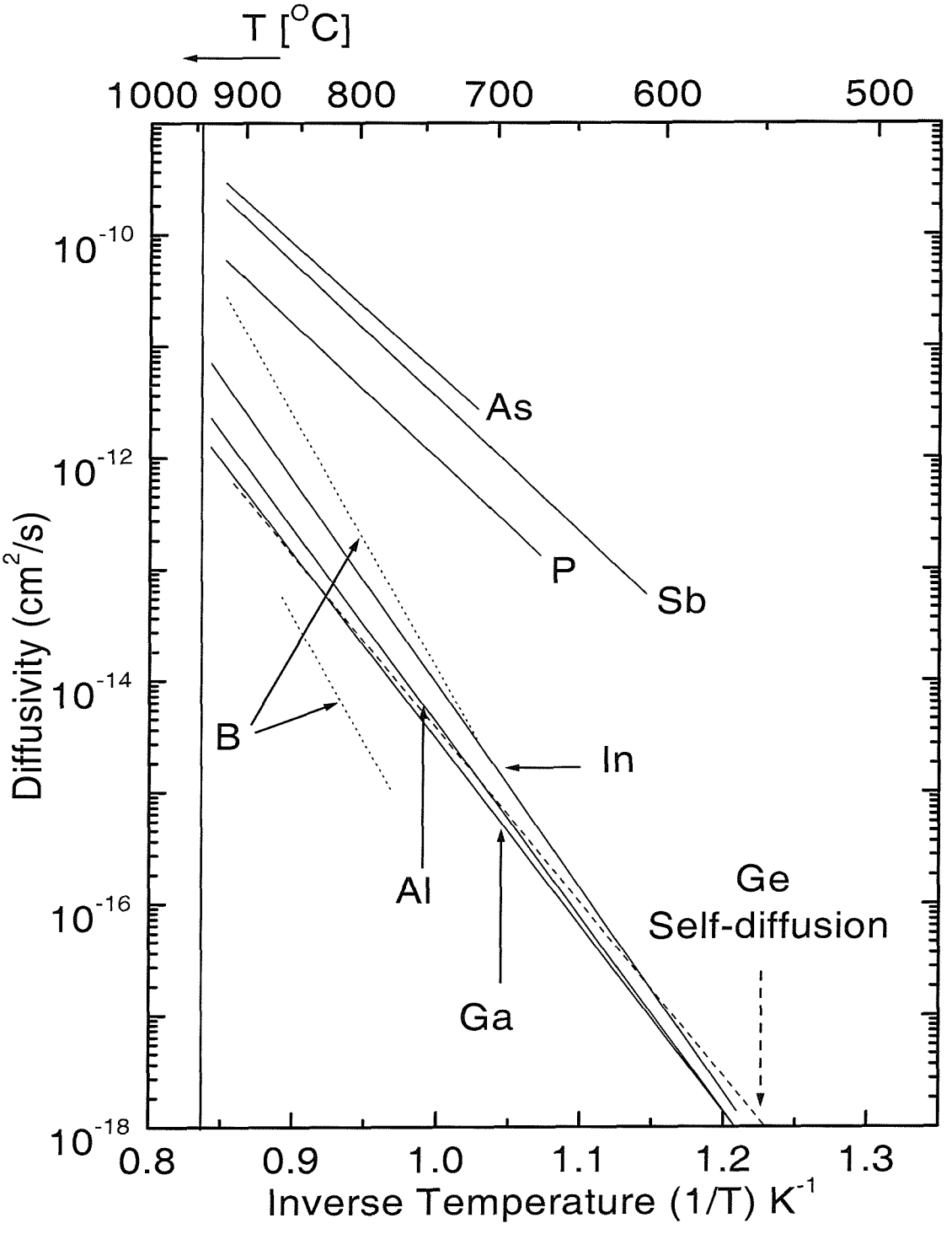

Figure 3.2: Self-diffusion and diffusion of group III and V elements in germanium. The values of diffusion coefficient at various temperatures have been calculated using the data provided by Stolwijk [57] in their actual temperature range. Result of both previous studies in boron diffusion are also shown.

Owing to the similar bonding radius of germanium and silicon, it has been suggested that the two elements exhibit similar diffusion behaviour. This is visible in the non-Arrhenius behaviour of germanium [71] diffusion in silicon and silicon self-diffusion [23]. Recent silicon self-diffusion studies using isotope heterostructure [27, 28] can be compared with the latest germanium diffusion experiments in silicon [25, 76] and we see that their activation energies and pre-exponential factors agree quite well.

Using defect injection experiments it has also been shown explicitly that germanium diffusion in silicon involves both vacancy and interstitial defects [75, 77] as in the case of silicon self-diffusion [31]. Results obtained from one such defect injection studies for germanium diffusion in silicon is shown in Fig. 3.3. Germanium diffusion is enhanced under both conditions of vacancy and interstitial injection. In contrast, antimony diffusion is enhanced only during vacancy injection while it is retarded during interstitial injection. This suggests the dominance of vacancies in antimony diffusion. A comparison of the behaviours of the two elements under similar defect injection conditions reveals that germanium diffusion in silicon is mediated by interstitials as well as vacancies. It should however be noted that the vacancy contribution for germanium diffusion in silicon (60–70%) [75] is higher than for silicon self-diffusion (40–50%) [30].

3.3.1.2 Diffusion of silicon in germanium

Moving on to silicon diffusion in germanium, once again we find only a few studies available in literature. Räisänen *et al.* [78] implanted 40 keV ^{30}Si ions with various fluence in germanium and analysed the profile broadening after annealing using (p, γ) resonance broadening method. In these measurements, silicon was found to diffuse slower than self-diffusing germanium. They also reported on an anomalous concentration peak of silicon close to the surface after annealing (see Fig. 6.14). Doping dependence of silicon diffusion in germanium was also examined using lightly n- and p-doped germanium. The slight enhancement of silicon diffusion in p-doped samples over n-doped ones was attributed to the strain in the lattice caused by the presence of holes in the valence band. In another work by Södervall *et al.* [65], silicon was sputter deposited on germanium surface and subjected to thermal treatment under vacuum. Diffusion profiles were measured using SIMS. It was concluded that silicon is another element other than boron which diffuses slower than germanium in self-diffusion. Although a higher value of activation energy and pre-exponential factor than those of germanium self-diffusion were observed, the straight line in the Arrhenius line was taken as an indication of a single migration mechanism for silicon diffusion in germanium. Strohm *et al.* [25] also studied silicon diffusion in germanium as part of their work on self-diffusion in Si-Ge alloys using radiotracer implantation and ion beam sectioning. The values of the diffusion parameters obtained in the study are given in Table 3.8 along with those from other workers. They found slightly larger silicon diffusivity values in germanium than the

literature values. Nevertheless, their values of silicon diffusion in germanium were smaller than their germanium self-diffusion values which suggests that silicon diffusion is slower than germanium self-diffusion.

It should also be noted that based on the argument of similar activation energy, silicon diffusion in germanium is believed to be mediated by vacancies as for self-diffusion in germanium. With a note in our mind that silicon diffusion in germanium is slower than germanium self-diffusion and that vacancy contribution of germanium diffusion in silicon is slightly larger than silicon self-diffusion, we may conclude that the diffusion behaviour of the two elements is quite similar both in germanium and silicon. Fig. 3.4 presents diffusion coefficients for silicon and germanium self-diffusion as well as germanium diffusion in silicon and vice-versa.

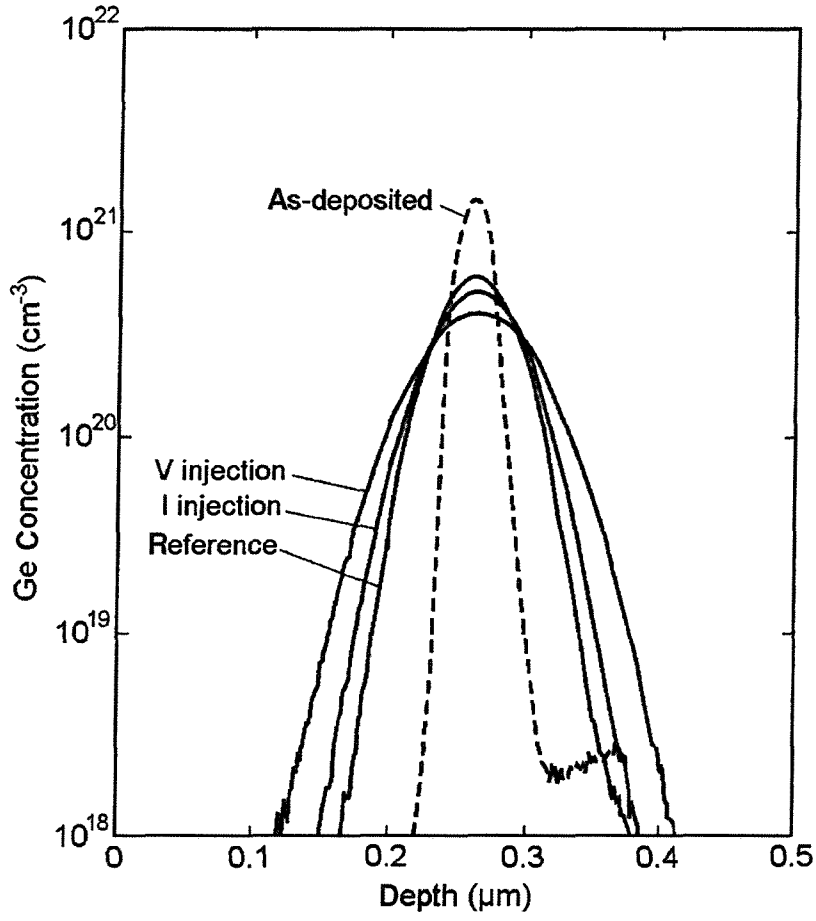

Figure 3.3: Germanium concentration profile in silicon after inert annealing (labelled as reference) and under the conditions of selective point defect injection [77]. Germanium diffusion in silicon is seen to increase under vacancy and interstitial injection conditions suggesting a vacancy and interstitial contribution for germanium diffusion in silicon. Reproduced by the permission of MRS Bulletin

D_0 (cm^2/s)	E_a (eV)	Temperature range (°C)	Technique	Reference
2.4×10^{-1}	2.9	650–900	Implantation, (p,γ) resonance	[78]
1.4×10^{2}	3.47	650–930	Deposition, SIMS	[65]
4.3×10^{1}	3.19	843–903	Radiotracer, ion beam sectioning	[25]

Table 3.8: Values of pre-exponential factor D_0, and activation energy E_a for silicon diffusion in germanium. Based on similar activation energy for silicon diffusion in germanium and germanium self-diffusion, it is believed that silicon diffusion occurs mainly via vacancy mechanism in germanium.

3.3.1.3 Germanium diffusion in Si-Ge alloys

In Si-Ge alloys, McVay and DuCharme [80] studied germanium diffusion in poly-crystalline $Si_{1-x}Ge_x$ with x up to 77% using ^{71}Ge radio-isotope deposition and mechanical sectioning. They found an increasing diffusivity with the germanium content. The activation energy and pre-exponential factor however showed a break at approx. 35% germanium. The activation energy was found to level off to the germanium self-diffusion activation energy of ~3 eV at this composition after decreasing from its value in silicon at 4.7 eV. On the other hand, the pre-exponential factor reduced up to 35% and then increased towards higher germanium content thereby increasing the total diffusivity. This behaviour was explained in terms of the change-over in the type of defect associated with diffusion.

Another recent study on germanium diffusion in Si-Ge alloys using radiotracer and a modified ion beam sectioning technique has reported a similar break in activation energy and pre-exponential factor at almost the same composition [25]. The results were explained in terms of the entropy factor which determines the dominating defect responsible for self-diffusion. It has been argued that the break originates due to a transition from the interstitialcy mechanism at low germanium content to a vacancy mechanism at high germanium content [71].

In another investigation by Zangenberg *et al.* [76] germanium was diffused in Si-Ge using isotopically enriched ^{72}Ge, in MBE grown epitaxial layers with germanium content up 50%. Concentration-depth analysis was performed by SIMS. The effect of strain and germanium content on diffusion was carefully isolated by growing compressive, tensile and relaxed layers. The diffusion coefficient was found to increase with germanium content but the values were smaller than those of McVay *et al.* [70] possibly due to the use of poly-crystalline material in the latter investigation. It was found that the activation energy and pre-exponential constant decrease with the germanium content. In this study at about 50% germanium content, the activation energy attained a value almost equal to that of germanium self-diffusion. This behaviour was explained in terms of germanium atoms favouring a vacancy mediated path for

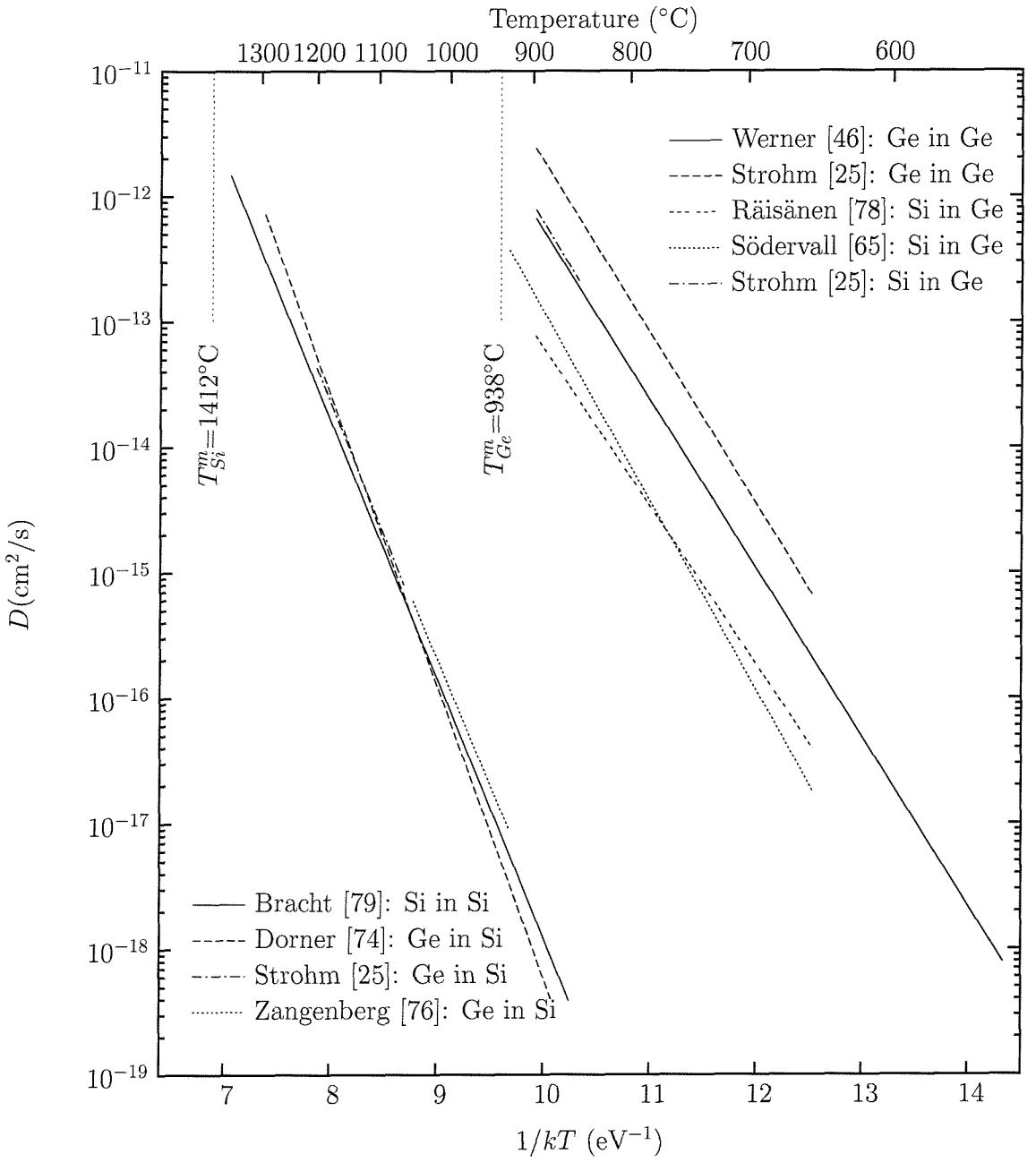

Figure 3.4: Self-diffusion in Si-Ge alloys. Recent studies of self-diffusion and germanium diffusion in silicon match closely. However, diffusion of silicon in germanium is relatively slower than self-diffusion in germanium.

diffusion in Si-Ge matrix. The activation energy reduction was thought to be occurring due to the decrease in the vacancy formation energy from silicon (3.5–4.0 eV) towards germanium (1.7–2.3 eV) with increase in germanium nearest neighbour atoms. However, one expects a discontinuity in the pre-exponential factor for germanium diffusion at germanium contents >50% in Si-Ge alloys from their study to match the diffusion coefficient values in germanium self-diffusion similar to one observed in literature. This break in pre-exponential factor, however, remains unexplained.

A theoretical calculation by Venezuela *et al.* [81] which was based on the density functional theory with local density approximation seem to predict the decrease in activation energy observed by Zangenberg's [37]. The authors in Ref. [81] found that the vacancy formation energy decreases linearly with the number of germanium nearest neighbour atoms in $Si_{0.5}Ge_{0.5}$ implying that a vacancy is preferred in proximity of germanium atom as compared to a silicon atom in the alloy.

Silicon diffusion in Si-Ge alloys can be studied using isotope heterostructures but to author's knowledge such attempts have not been made thus far.

3.3.2 Group III and V elements

Among group III elements, boron has been extensively studied due to its use as a p-type dopant. As has been highlighted in the previous sections of this chapter, in silicon boron is believed to diffuse predominantly via interstitials. From the literature we do not find conclusive evidence about the mechanism governing boron diffusion in germanium though it is regarded at par with other group III and V elements i.e. diffuse by the vacancy mechanism.

Surprisingly though, one finds convincing reports in the literature that on addition of germanium to silicon (at least up to 40%), boron diffusion is retarded as compared to that in pure silicon. Kuo *et al.* [39] performed experiments on relaxed Si-Ge alloys with germanium contents up to 55% and concluded that boron diffusion decreases rapidly in Si-Ge alloys with germanium content up to 40% after which it seems to increase. At lower germanium content, it has been suggested that the reduction in diffusivity is caused by a B-Ge pairing mechanism [39]. In other studies, usually a comparison of strained Si-Ge with silicon is made and a retardation in diffusivity is reported [41, 82]. In recent studies of Zangenberg [37], no reduction in boron diffusivity with germanium content in Si-rich relaxed Si-Ge alloys was observed. It was suggested that the enhancement due to a chemical effect could be counterbalanced by a retardation due to pairing. However, the strain effect on boron diffusion in this study was found to be similar to that of Kuo *et al.* [83]. Our present understanding of boron diffusion in Si-Ge alloys as a function of germanium content is given in Fig. 3.5.

To explain the reduction of diffusivity with germanium content, Moriya *et al.* [85] and Chen *et al.* [86] attributed bandgap narrowing effect as causing a change in charged defect concentration. Though a pronounced reduction of diffusivity in Si-Ge alloys at higher boron concentration is reported [39, 87, 88], Cowern *et al.* [88] argue that this effect is not large enough to explain the observed reduction. Cowern *et al.* [88], however, proposed that boron diffusivity reduction was due to a decrease in self-interstitial concentration caused by the long-range strain in the Si-Ge layer. Fang *et al.* [89] rejected this idea and attributed the phenomenon to be caused by a decrease in mobile boron diffusivity rather than the self-interstitial concentration. Defect injection studies have confirmed that boron diffusion in silicon and strained Si-Ge alloys with germanium content up to 20% is largely interstitial

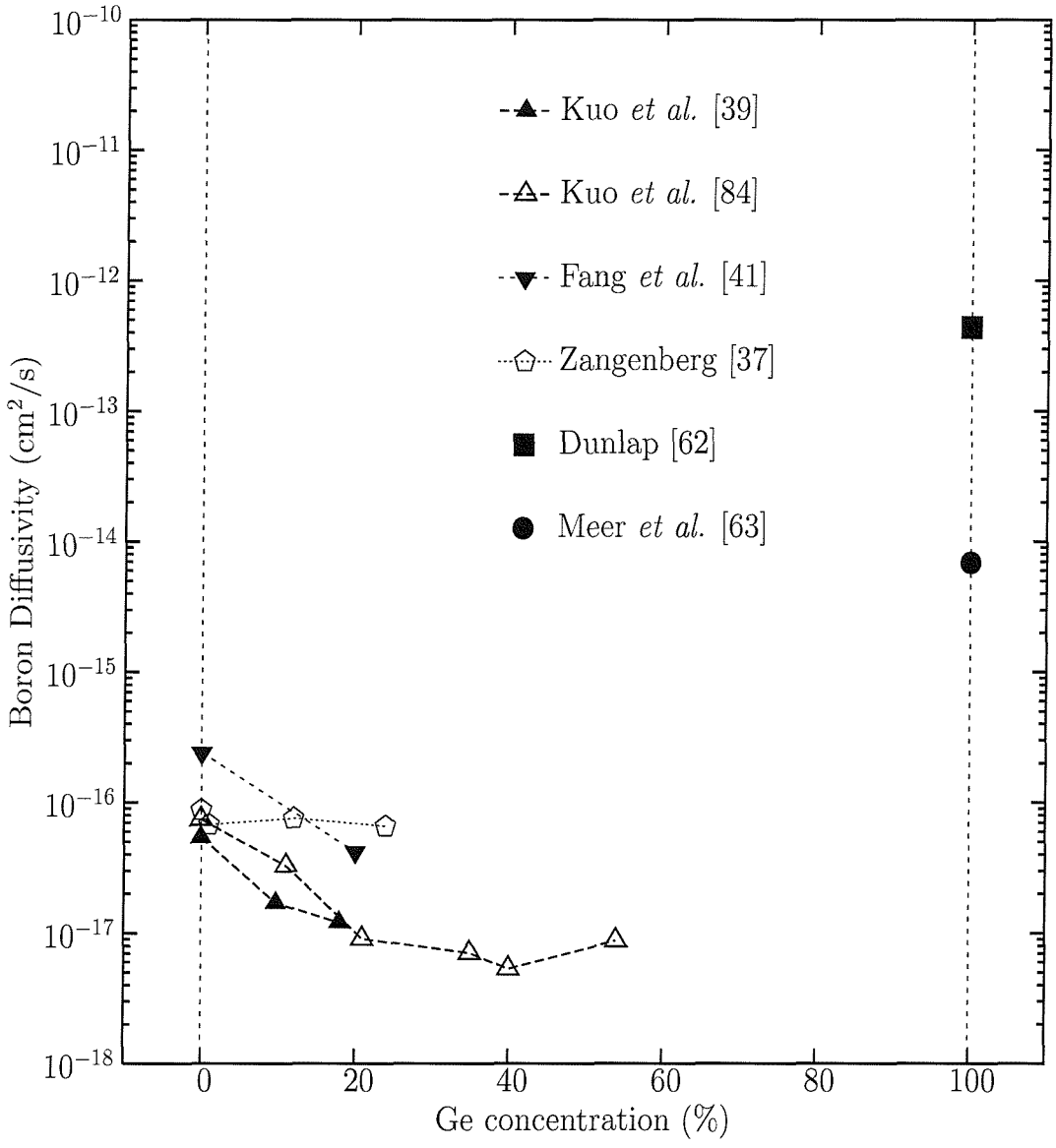

Figure 3.5: Boron diffusion in Si-Ge alloys as studied by various authors. Kuo et al. [84]: in strained Si-Ge, measured at 860 °C*; Kuo et al. [39]: in relaxed Si-Ge, measured at* 800 °C*; Fang et al. [41]: in strained Si-Ge, measured at* 860 °C*; Zangenberg [37]: in relaxed Si-Ge, measured at* 800 °C*. Values in germanium are at* 800 °C*.*

mediated [41, 90]. From the measurement of enhancement and retardation of boron diffusion in strained $Si_{0.8}Ge_{0.2}$, Fang *et al.* [41] rejected the idea that a reduction in interstitial component of boron was responsible for lower boron diffusivity in Si-Ge alloys as compared to silicon.

Among group III and V elements, antimony is the only element believed to diffuse mainly via the vacancy mechanism in both silicon and germanium and possibly this behaviour applies to the whole Si-Ge alloys spectrum. Kringhøj *et al.* [91] have studied antimony diffusion in strained as well as relaxed Si-Ge alloys. They found that diffusivity of antimony in relaxed

Si-Ge alloys with up to 50% germanium increases with the germanium content. In an attempt to exclude any alloy effect from macroscopic strain effects, they also compared diffusion in relaxed as well as compressive and tensile strained material and discovered that compressive strain enhances the diffusivity whereas tensile strain retards it. Note that this behaviour of antimony towards strain is opposite to that shown by boron and therefore can be taken as further confirmation that different types of defects are responsible for their diffusion in Si-Ge alloys. This result is in agreement with the prediction by Cowern *et al.* [88] who argued that tensile strain has the opposite effect of retarding(enhancing) the vacancy(interstitial) mediated components respectively. Paine [92] has also studied antimony diffusion in (compressively) strained Si-Ge layers and found a similar trend of increasing diffusivity with germanium content. Recently, defect injection technique has been successfully applied to investigate the kinds of defects responsible for diffusion of antimony in silicon and Si-Ge alloys (~10% germanium content) [93]. From the diffusion enhancement during vacancy injection and retardation during interstitial injection, it has been concluded that antimony diffusion in silicon and $Si_{0.9}Ge_{0.1}$ is primarily dominated by the vacancy mechanism.

Studies of phosphorus and arsenic diffusion in Si-Ge alloys have been very limited. Kuznetsov *et al.* [94] have shown an increase in diffusion coefficient of phosphorus in compressively strained $Si_{0.87}Ge_{0.13}$ as compared to silicon. Using interstitial injection by oxidation of a silicon cap on Si-Ge layer, they found an interstitial fraction of 0.87 for $Si_{0.9}Ge_{0.1}$. Christensen *et al.* [95] have found only a small increase in diffusion coefficient of phosphorus in strained Si-Ge alloys with germanium content (up to 22%). The results have been interpreted in terms of a compensating effect of composition and strain (similar to that suggested for boron diffusion in Si-Ge by Zangenberg [37]) resulting in a Si-like concentration of interstitials and hence not a large increase in diffusion coefficient. Recent studies of Zangenberg [37] also show an increase in phosphorus diffusivity in relaxed Si-Ge layers (up to 40% germanium) under intrinsic conditions.

There are reports in the literature suggesting an enhanced diffusion of arsenic in Si-Ge alloys as compared to silicon [96, 97] though the diffusion coefficient was not quantified. A value of 2.7($\pm$0.7) eV has been assigned as activation energy for arsenic diffusion in Si-Ge for all compositions up to 50% germanium [96]. Eguchi *et al.* [98] have implanted phosphorus and arsenic in silicon and $Si_{0.8}Ge_{0.2}$ up to extrinsic level. They reported a 7 fold increase for arsenic and a 2 fold increase for phosphorus diffusivity in $Si_{0.8}Ge_{0.2}$ as compared to silicon. Interestingly, they have observed a retarded diffusion under transient conditions which is also shown for Si-Ge, synthesised using ion beam [99].

In summary, from literature we clearly find that the diffusion coefficient of antimony, phosphorus and arsenic is enhanced with the addition of germanium in silicon. It should be noted that in silicon, antimony is believed to diffuse almost exclusively via the vacancy mechanism whereas phosphorus shows a very high interstitial component [6]. For arsenic diffusion in silicon, a contribution from both interstitials as well as vacancies exists. It has

been found that enhancement of its diffusivity on addition of germanium is higher than that of phosphorus. For boron, a reduction of diffusivity in silicon rich Si-Ge alloys compared to silicon has been reported but the observation is not fully explained.

3.4 Defects in germanium

It is a well know fact that interstitials and vacancies are equilibrium defects present in silicon [4]. Also, from diffusion experiments, it is believed that at high temperatures interstitial defects dominate where as at lower temperatures a vacancy dominance exists [100]. Defect properties measured with the help of experiments involving hybrid elements suggest a similar picture [100].

In germanium, metal diffusion experiments analogous to those for silicon have been performed to obtain information about equilibrium properties of defects. It has been shown that Cu and Ni diffuse in germanium via a vacancy controlled dissociative mechanism. This provides evidence that Ge-self diffusion mainly occurs via vacancies [51, 101, 102]. Au, on the other hand, is understood to diffuse via an Au_i (Au interstitial) controlled dissociative mechanism [53, 54]. It should also be noted that in $Si_{1-x}Ge_x$ ($0 \leq x \leq 0.24$) epi-layers, diffusion of Au is slower than that of silicon or germanium and it is argued to occur via a self-interstitial or a Au_i-controlled kick-out mechanism [103].

Thus we see strong evidence that vacancies are the dominant defects present in germanium at thermal equilibrium. But are there any interstitials observed in germanium as well? Attention is drawn to Fig. 3.1, in which an indication of a very low concentration of self-interstitials in germanium is present as suggested by Seeger *et al.* [4]. It is believed though that their contribution to self- or impurity diffusion is very small. Saito *et al.* [104] have performed irradiation experiments on pure germanium samples and found that a large fraction of interstitial do not recover to lattice sites even after annealing at 400 °C. Quite recently, theoretical and experimental consideration has been given to native defects in germanium. Theoretical calculations based on density functional theory with local density approximation suggest the presence of both vacancy and self-interstitial defects [105]. For an interstitial in germanium, a dumbbell configuration is found to more stable than hexagonal or tetrahedral configuration [106]. It is also reported that the formation energy of a germanium interstitial is higher than that of a vacancy. The results may be taken as an indication as to why only vacancies are seen to contribute to germanium self-diffusion. Irradiation experiments using Perturbed Angular Correlations Spectroscopy and Moessbauer spectroscopy have identified vacancies and self-interstitials at low temperatures [107, 108]. Some agreement in theoretical calculations and experiments on the presence of germanium interstitial has been reached with the assumption of an extended self-interstitial defect in the germanium lattice.

3.5 Implantation in germanium

We briefly review literature on boron implantation in germanium. Herzer *et al.* [109] studied electrical properties of B, Ga, P and As in germanium after implantation at low energies (4–30 keV) using Hall effect and sheet resistance methods. They found that unlike other dopants boron was electrically active in the as-implanted state. Concentration profiles measured for these elements were found to penetrate deeper than predicted by the LSS theory [110] and in the case of boron this effect was attributed to radiation enhanced diffusion. It should, however, be noted that the incident beams were not misoriented with respect to the wafer normal in their case. Ponpon *et al.* [111, 112] studied the behaviour of implanted boron as p type contacts for high purity germanium detectors. Important observations made were a) annealing of the damaged layer created by 15 keV boron ions implanted to a dose of 10^{15} ions/cm^2 at temperature of 170 °C and b) the presence of electrically active boron in the as-implanted state. The observed deep distribution of boron atoms as compared to theoretical calculations was hypothesised to be caused by acceptor centers (vacancies) produced by the ion implantation process. Gusev *et al.* [113] studied the electrical properties of boron implanted germanium in the dose range 6×10^{13}– 6×10^{17} ions/cm^2 at 30 keV. During room temperature implant they also found that boron penetrates deeper than that suggested by theory and attributed the extended tails to the channelling effect. In this study, the damaged layer resulting from the high dose 6×10^{16} ions/cm^2 boron implant was shown to anneal out at about 600 °C. However, during a high temperature implant, a radiation-enhanced diffusion was also observed by other workers [114].

MacDonald and Palmer [115] implanted carbon and boron in germanium to the same dose and energy (60 keV, 10^{15} ions/cm^2) in order to study lattice disorder caused by implantation. They found a lower lattice disorder as a result of boron implantation compared to carbon implantation. The disorder in boron implanted layers was found to anneal completely at 150 °C. Also the acceptor behaviour observed after carbon implantation was attributed to the lattice defects produced during implantation whereas for boron it was due to electrically active boron. Jones *et al.* [116] studied electrical activation of boron in germanium in comparison to carbon and BF_3 implants. They found boron to be electrically active in entire implanted dose and energy ranges studied (25–100 keV, 5×10^{11}–1×10^{14} ions/cm^2). The hole traps observed using Deep Level Transient Spectroscopy were found to anneal out at a thermal budget of 350 °C for 30 min leaving boron at substitutional sites.

An important observation of Metzger's [117] study using implantation doping of germanium using boron was the formation of GeO_2 at the interface between germanium and deposited SiO_2 layer on annealing at temperatures higher than 650 °C. We also note another observation of Axmann *et al.* [118] who studied diffusion of donor impurities in germanium by implantation doping. They found that the measured diffusion coefficients for samples covered with a protective SiO_2 layer were smaller compared to samples annealed without

the layer. This is an important observation since similar protective layers have been used in this study. It should be realised though that this effect is not very large since the absolute values of the diffusion coefficients reported were within experimental errors.

Chapter 4

Experimental techniques

4.1 Ion implantation

Ion implantation is a well developed technique used to introduce energetic, charged particles into a target material. When applied to semiconductors, it is a process by which the desired impurity/dopant atoms can be introduced into the substrate material to change its electronic properties. The process consists of extracting impurity ions from a source, purification and accelerating them with high velocity towards the target. Ion implantation is widely used in semiconductor doping and is preferred over conventional doping methods. Some of the unique characteristics of ion implantation are:

- A precise amount of almost any impurity atom can be introduced in a variety of substrates.
- The doping profile can be tailored by controlling the energy, current and position of the ion beam.
- Reproducible and well controlled profiles from a single or multiple implants of the same or different impurities can be achieved.
- Since it is a non-equilibrium process, concentrations beyond solubility limit can be obtained.

Implantation process has some disadvantages as well. Other than being an expensive technique, it causes damage in the target wafer. Mostly, the implanted atoms are left electrically inactive. A thermal treatment is generally required to electrically activate the impurities introduced by implantation. Implantation damage can result in anomalous diffusion effects such as transient enhanced diffusion during annealing.

Implantation energies range from a few hundred eV to a few MeV with average depths ranging from 100 Å to 10 μm. The typical dose range is 10^{12} to 10^{18} ions/cm^2.

4.1.1 Mathematical model for ion implantation

As an energetic ion enters the target surface it undergoes a series of collisions with the target atoms. With each collision the ion loses some amount of its energy before eventually coming to rest by losing all its energy. The energy transfer from incident ions to the target atoms takes place in two ways. One is via the elastic collisions with nuclei of target atoms. This may cause deflection of impinged ions and the target nuclei may also be dislodged from its original lattice positions. These kinds of collisions are significant for higher mass ions at low energies. These nuclear collisions cause physical damage to the target and may result in point or line defects. The second process by which the incident ions loose their energy is by interacting with free and bound electrons. This results in excitation of the electrons. Only a very small amount of energy is lost during such collisions. The two processes can be characterised by *nuclear stopping power* S_n and *electronic stopping power* S_e. The average rate of energy loss with distance is given by

$$\frac{dE}{dx} = N[S_n(E) + S_e(E)], \tag{4.1}$$

where N is the number of target atoms per unit volume of the semiconductor. The average distance travelled by the ion before coming to rest, R, can be calculated by

$$R = \int_0^R dx = \frac{1}{N}\int_0^{E_0} \frac{dE}{S_n(E) + S_e(E)}, \tag{4.2}$$

where E_0 is the initial ion energy. Practically, it is very difficult to measure the range R since not all ions suffer the same collisions. The quantity of more interest is the projection of this range along the direction of incident ions. Due to the statistical nature of the process, the ion distribution after implantation is characterised by an average depth called *projected range*, R_p, and by a standard deviation, ΔR_p, known as *straggle* along the direction of incident ions. The widely accepted theory for the calculation of these parameters is given by Lindhart *et al.* [110]. According to this theory for an amorphous target, the range distribution $N(x)$, can be approximated by a Gaussian distribution. For the one dimensional case,

$$N(x) = N_{max}\ \exp\left[-\frac{1}{2}\left(\frac{x - R_p}{\Delta R_p}\right)^2\right], \tag{4.3}$$

where N_{max} is the maximum concentration occurring at R_p. The area under the ion distribution curve is the total implanted dose. Denoted by Φ, this can be calculated as

$$\Phi = \int_0^\infty N(x)\, dx. \tag{4.4}$$

Substituting for $N(x)$ gives an expression for the maximum concentration, N_{max}, as

$$N_{max} = \frac{\Phi}{\sqrt{2\pi}\,\Delta R_p} \approx \frac{0.4\,\Phi}{\Delta R_p}. \tag{4.5}$$

The total dose can be calculated by measuring the beam current and integrating it over the time of implantation. Thus the final distribution in terms of parameters which can be either calculated or measured, takes the following form:

$$N(x) = \frac{\Phi}{\sqrt{2\pi}\,\Delta R_p} \exp\left[-\frac{1}{2}\left(\frac{x - R_p}{\Delta R_p}\right)^2\right]. \tag{4.6}$$

The Gaussian profile as given by Eq. 4.6 may only be an approximation to the true profile. Usually the experimental profile is asymmetrical and we require higher spatial moments to accurately describe the ion distribution. An arbitrary normalised distribution, $f(u)$, can be characterised in terms of its moments defined as

$$R_p = \int_{-\infty}^{\infty} u f(u) du \qquad \text{(Range)} \tag{4.7}$$

$$\Delta R_p (= \sigma) = \sqrt{\int_{-\infty}^{\infty} (u - R_p)^2 f(u) du} \qquad \text{(Straggle)} \tag{4.8}$$

$$\gamma = \frac{\int_{-\infty}^{\infty} (u - R_p)^3 f(u) du}{\sigma^3} \qquad \text{(Skewness)} \tag{4.9}$$

$$\beta = \frac{\int_{-\infty}^{\infty} (u - R_p)^4 f(u) du}{\sigma^4} \qquad \text{(Kurtosis)} \tag{4.10}$$

Parameters skewness (γ) and kurtosis (β) measure the asymmetry and flatness (at the top of distribution) of the ion distribution, respectively. A Gaussian distribution has a skewness of 0 and a kurtosis of 3. The Pearson distribution which makes use of above mentioned four moments can be used to describe the concentration profiles more accurately than simple Gaussian distribution. The Pearson distribution is based on the solution of the differential equation

$$\frac{df(u)}{du} = \frac{(u - a) f(u)}{b_0 + b_1 u + b_2 u^2}, \tag{4.11}$$

where $u = x - R_p$. The Pearson coefficients (a, b_0, b_1,b_2) can be written in terms of the four moments of distribution as

$$a = -\frac{\sigma\gamma(\beta + 3)}{A}, \tag{4.12}$$

$$b_0 = -\frac{\sigma^2(4\beta - 3\gamma^2)}{A}, \tag{4.13}$$

$$b_1 = a, \tag{4.14}$$

$$b_2 = -\frac{(2\beta - 3\gamma^2 - 6)}{A}, \tag{4.15}$$

where A is

$$A = 10\beta - 12\gamma^2 - 18. \tag{4.16}$$

Out of different solutions available for Pearson's equation, Pearson IV is generally used for ion implantation profiles. The solution has a maximum at $x = R_p + a$ and decays smoothly to zero on both sides of the peak.

4.1.2 Implantation effects

Mostly an implantation profile can be represented by a Gaussian or Pearson distribution as discussed in Sec. 4.1.1. However there could be some anomalous effects which may affect the final distribution of the implanted ions. A few of them are discussed below.

4.1.2.1 Channelling

An energetic ion loses its energy in a series of collisions with target atoms. For an amorphous target where no regular arrangement of atoms exists, impinged ions make random collisions and come to rest in a very short distance inside the target. When the target is crystalline with regular arrangement of atoms, atoms rows or planes line up to leave long-range open spaces which act like channels in which implanted ions may travel. The ions incident along a major crystallographic direction may suffer glancing collisions with atom rows or planes and are steered deep into the lattice before coming to rest. The phenomenon is known as *channelling*. A one dimensional representation of channelling phenomenon is shown in Fig. 4.1. The overall result of channelling is to add a tail to the implanted distribution.

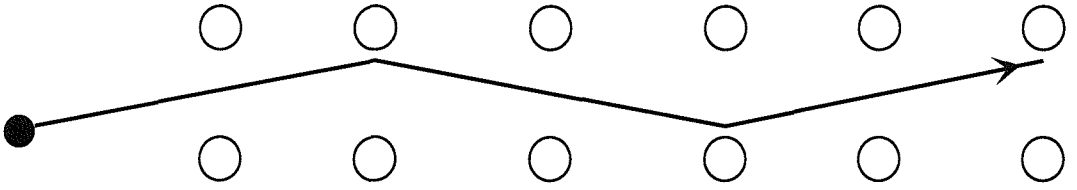

Figure 4.1: A two dimensional representation of Channelling phenomenon. The incident atom represented by dark circle makes inelastic collision with lattice atoms shown by open circle and gets deflected by small angles. It may travel deep distances guided by aligned rows or planes of a crystal lattice

Channelling is characterised by critical angle Ψ given by [119]

$$\Psi = \sqrt{\frac{2Z_1 Z_2 e^2}{4\pi\epsilon_0 E d}} \approx 9.73\sqrt{\frac{Z_1 Z_2}{E d}} \tag{4.17}$$

where Z_1 and Z_2 are atomic number of ion and target respectively, E is the incident ion energy in keV and d is the atomic spacing along the ion direction (in Å). For boron atoms in germanium incident at 20 keV along <111> direction this angle is $\sim 5^\circ$ [119]. The critical angle represents the maximum angle at which an ion can enter a channel without leaving it.

Channelling primarily depends on 1) the critical angle of approach 2) the temperature of the implant and 3) the degree of crystallinity. We note from Eq. 4.17 that critical angle increases for heavier ions and lower energies. Thus channelling would be dominant for heavy ions at lower energies. It also depends on the orientation of the target through the atomic spacing d. As the temperature of a crystal is increased the lattice vibrations increase. Thus

the probability of large angle collisions with incident ions increases and hence the channelling is reduced. For an amorphous target the lattice atoms are distributed randomly and no long range order exists. For implantation in such a target channelling is totally eliminated. Also the presence of defects and dislocations in the crystal reduces channelling.

In practice channelling is desirably avoided since the channelled implanted profile depends on a large number of factors and is very sensitive to target conditions. Channelling can be substantially reduced by tilting the target by an angle larger than the critical angle for implantation. Channelling is also limited by the crystallinity of the target. Sometimes the damage caused by nuclear stopping of non-channelled ions is sufficient to eliminate channelling. In other cases, the target can be pre-amorphised to destroy the crystal structure to avoid channelling completely. Another possible means to avoid channelling is to implant through an amorphous layer deposited on the target.

4.1.2.2 Implantation damage

While travelling through the target lattice, the impinged ions pass their energy via collisions to the target atoms. The binding energy of lattice atoms is generally small as compared to the implantation energy and so the target atoms may get easily dislocated. These lattice atoms can have sufficient energy to work as projectiles for other target atoms displacing them from lattice locations. Thus a single implanted atom may cause displacement of many lattice atoms and a collision cascade results. By the increase in the number of implanted atoms, an initially crystalline target may be changed to a highly disordered state. Light ions transfer a small amount of energy in each collision and get deflected by large angles. The target atoms receiving this energy may not be able to cause a collision cascade. A heavy ion, however, imparts more energy to the target atom in a head-on collision which may then become capable of dismantling other lattice atoms. Thus lattice damage occurs but in a smaller volume as compared to that because of the light ions. Increasing the dose causes isolated disordered regions to overlap which may leave the target amorphous. For a light ion more dose is required to create an amorphous layer than for heavy atoms at the same energy.

The disordered region consists of vacancies, divacancies, self- and impurity interstitials, Frenkel pairs etc. At high temperatures the displaced atoms, vacancies and interstitials can move and repair the damage. If during implantation, the temperature of the substrate is high, self-annealing might occur. Therefore only a little damage is left behind even in the case of heavy ions.

4.1.2.3 Enhanced diffusion

The tail in the implanted profile is generally caused by channelling but it may also be due to a rapid interstitial diffusion process. The implanted atoms which are left in interstitial

positions, specially in the deeper regions of the target (beyond R_p), may diffuse interstitially until they find a suitable trapping center. The point defects created during implantation can also assist the atoms to diffuse, enhancing the defect-assisted diffusion. This process may occur during the implantation time even at room temperature [120].

4.1.2.4 Damage annealing

The annealing of the implanted layer is usually performed to either relocate the implanted ions on substitutional sites in order to achieve electrical activation or to regrow the amorphous layer produced by the implantation process. Conventionally, furnace annealing is used for an appropriate time and at sufficiently high temperatures to achieve the desired results. This time and temperature combination is mainly dictated by the dose, energy and implanted species. Furnace annealing used to recover damage may also lead to significant diffusion. Therefore processes such as rapid thermal annealing (RTA) or laser annealing which involve very short annealing times are used. However processes such as transient enhanced diffusion during RTA may become significant and lead to anomalous diffusion profiles.

4.2 Secondary Ion Mass Spectroscopy (SIMS)

4.2.1 Principle

Secondary ion mass spectroscopy (SIMS) is an analytical technique used to characterise the composition at the surface or near surface region. Conceptually, the process is very simple. An energetic beam of ions bombards a surface. The incident particle energy is transferred to the target atoms. A cascade of collisions occurs among the atoms of the target; some collisions return atoms to the surface which results in the emission of atoms and/or atom clusters. Some of these species get ionised while leaving the target surface which are collected electrostatically and can be analysed for their mass using a mass spectrometer.

There are two modes of SIMS: *dynamic* and *static* SIMS. The two are distinguished by the primary ion dose used during analysis. Static SIMS, which uses a low primary ion flux, finds its usage in surface analysis whereas dynamic SIMS has applications in chemical analysis of semiconductor materials by using a relatively high primary ion dose.

4.2.2 Depth profiling using SIMS

For detecting trace elements using SIMS, a steady state condition of erosion rate is required. The primary ion dose is so chosen as to remove many layers from the target rapidly, thereby increasing the secondary ion flux so that even a low concentration of elements present can be detected. On reaching a steady state, the sputtered atom/ion yield reflects the relative concentration of components.

In carrying out a depth profile analysis, the primary ion beam is rastered over a defined area on the wafer surface. Each scan erodes a certain depth generating secondary ions which are collected by mass analyser. The edges of the eroded region are carefully excluded from the analysis electronically. This ensures that the secondary ions collected originate from the crater bottom. A secondary ion count of selected elements as a function of time is obtained by collecting the secondary ions, from which a concentration-depth profile can be obtained.

4.2.2.1 Quantification

A typical SIMS profile is expressed as a plot of concentration of element of interest (in atoms/cm^3) vs depth. Each data point in this profile is obtained by counting the secondary ions of the element of interest, whilst the primary ions sputter a finite depth of the sample in a finite time. The relationship between secondary ion current (I_{i+}, positive ions of element i say) and the concentration of element i in the specimen is given by

$$I_{i+} = I_p \, S \, \gamma_{i+} \, N_i \, \eta \tag{4.18}$$

where I_p is the primary ion beam current, S is the sputter yield, γ_i^+ is the ionisation efficiency for i^+, N_i is the atomic fraction of i, and η is an instrumental factor which includes effects due to collection, transmission, and detection efficiency. The quantitative analysis includes effects due to specimen matrix (via S, γ_i), and its electronic properties (via γ_i) in addition to the concentration of the element of interest in the specimen. Hence a quantitative SIMS analysis would require prior knowledge of sputtering rate and a calibration of the secondary ions using standards whose matrix and surface electronic properties match those of the sample under analysis. The accuracy depends on matching of analysis conditions for the standards and the specimens.

Ion-implanted samples with known doses are most commonly used as standards. In the implanted samples, the implantation dose (total number of implanted atoms per unit area) can be controlled and measured with good accuracy. Thus, provided that none of the implanted dose is lost during annealing and precipitation/segregation effects do not occur, a linear relation between the SIMS signal and the element concentration can be assumed. That is, the product of I_p, S, γ_i , and η is assumed to be constant for the standard and the specimen. The secondary ion signal integrated over the entire profile measured for the standard can be related to the total number of implanted atoms contained in the specimen as

$$\int_0^z I_{i+}(z)dz = K \int_0^z C_i(z) \, dz, \tag{4.19}$$

where z is the depth of analysis, and K is the calibration factor used for converting secondary ion signal measured over a small depth dz into an average concentration C_i in atoms/cm^3. If the analysis depth exceeds or equals the maximum extent of implantation in the standard, the integration of C_i over the whole area equals the known fluence F (in atoms or ions/cm^2)

i.e.

$$\int_0^z C_i(z)\,dz = F. \tag{4.20}$$

Thus the calibration factor can be obtained by integrating the secondary ions signal over the depth z.

Since the secondary ions signal is measured over short interval dt, an independent measure of sputtering rate is required. The sputtering rate can be calculated by measuring the crater depth using a profilometer and dividing it by the total time taken to create the crater. It is assumed that the sputtering rate of the sample is constant in time which is generally a good approximation. The calibration factor K can be written as

$$K = \frac{1}{F}\frac{dz}{dt}\int_0^t I_{i^+}(t)dt, \tag{4.21}$$

where t is the total time over which the profile is integrated. The calibration constant K can now be used to convert the measured secondary ion signal into absolute concentration by:

$$C_i = \frac{1}{K} I_{i^+}. \tag{4.22}$$

The accuracy of above analysis depends on identical nature of the element to be analysed in unknown and standard specimen and also on identical analysis conditions for the standard and the unknown. Ideally the standard is analysed along with the unknowns. Implanted specimens can work as self-standards provided the implanted dose is known. The integrated profile in this case provides the calibration factor that can be used to convert instantaneous secondary ion signal to the concentration.

4.2.2.2 Operating conditions

For a depth profile analysis using SIMS, three instrument parameters are of importance: *the primary beam species, the primary beam energy and the primary angle of incidence.* These parameters are optimised for detection limit of the impurity element within the matrix and the depth resolution.

Primary beam species: The most widely used primary beam species for depth profile analysis for semiconductor materials are O_2^+ and Cs^+. The choice depends on the matrix and the secondary ion yield for the element being analysed i.e. positive or negative ion yield is favoured for the impurity under analysis. In case of boron and silicon in germanium matrix, positive ions are favoured and the use of O_2^+ ions can provide a high secondary ion yield and is therefore used in this study.

Primary beam energy: The sputtering and secondary ion yield increase with primary beam energy for all species but such gains are offset by unwanted effects such as *implant damage* and *enhanced diffusion* making the analysis less accurate. On the other hand for high resolution a lower beam energy is preferred but the lower the beam energy, the slower

is the sputtering rate. Therefore usually 0.5–10 keV beam energy is used for analysis. For profiles used in this work 500 eV and 1 keV ion beams have been used.

Primary angle of incidence: Sputtering yield increases with the angle of incidence[1] whereas the secondary ion yield decreases. For optimum depth resolution, a high angle of incidence is generally required. However, the oblique incidence causes less roughening of the crater. For high sputtering rate and depth resolution, a compromise for incidence angle is made. For this study an angle of 25°–45°or a normal incidence has been used.

We note that depth profiling is governed by a range of parameters which are optimised to obtain a good dynamic range and depth resolution. For further reading on the subject the reader is referred to Ref. [121].

4.3 Development of annealing schedule

One of the difficulties faced in this project was the surface damage endured by germanium during high temperature annealing. The germanium surface is more prone to oxidation damage specially at high temperatures. Unlike silicon oxide, germanium oxide is unstable at high temperature and therefore can not act as a diffusion mask or protection against contamination. Thus it is advisable not to rely on its own oxide for protection of germanium surface. A 200 nm SiO_2 layer as suggested in literature [122] was deposited as a barrier to oxidation, thermal etching and out-diffusion of dopant during annealing. Surprisingly, open boat annealing of these protected samples in flowing argon resulted in severe surface damage. Due to a high etch pit density the samples became practically unusable for SIMS. Subsequently, a reducing forming gas atmosphere was attempted with a view to avoid oxygen reacting with the germanium surface but with little success. At high temperature and long anneal times surface damage continued to prevail. An example of such surface damage is shown in Fig. 4.2. For the sample shown in the figure, the annealing was carried out at 800 °C for 24 h in forming gas ambient. Since the size of etch pits on sample surfaces was of the order of crater dimensions of SIMS, quantitative SIMS became impossible with these samples.

An alternative solution considered was to deposit a poly-crystalline germanium (or silicon) instead of the oxide layer. However, such a process could have caused diffusion of implanted species into surface layer via grain boundaries. Additionally, location of the original surface in SIMS analysis could have been difficult. One could suggest the deposition of a thicker oxide layer as a solution but such a layer could be unstable and would have lead to additional strain [122] that may affect diffusion. In order to avoid the thermal etching of the sample surfaces, the possibility of depositing an unreactive silicon-nitride layer on top of oxide was also explored. According to literature such a combination of oxide and nitride layers provides inert annealing conditions in the case of silicon [6]. Each layer was ~200 nm

[1]Normal incidence of ion beam is zero degrees.

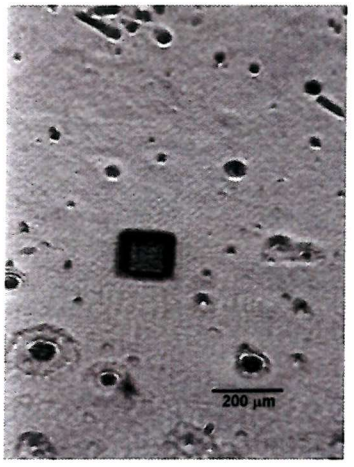

Figure 4.2: Optical micrograph of a sample annealed at high temperature in forming gas atmosphere without protective silicon-dioxide layer. The etch pits were of the order of the size of SIMS crater (also shown in the figure). With such surface damage SIMS quantification becomes very difficult.

thick and was deposited using Plasma Enhanced Chemical Vapor Deposition (PECVD) at ~300 °C. It seemed that the oxide and nitride layers did not adhere very well to the germanium substrate and therefore surface damage could not be fully prevented.

In order to circumvent the problems with sample surfaces, it was considered important to maintain an unreactive atmoshphere throughout the annealing time. The samples were therefore sealed in evacuated ampoules prior to annealing. High purity argon (99.999%) gas was purged through the ampoules 3–5 times before finally sealing them under vacuum ($\sim 4 \times 10^{-6}$ torr). The surface damage was significantly lessened at least for short annealing times. A comparison of the surface quality for annealing with and without the use of ampoule is given in Fig. 4.3.

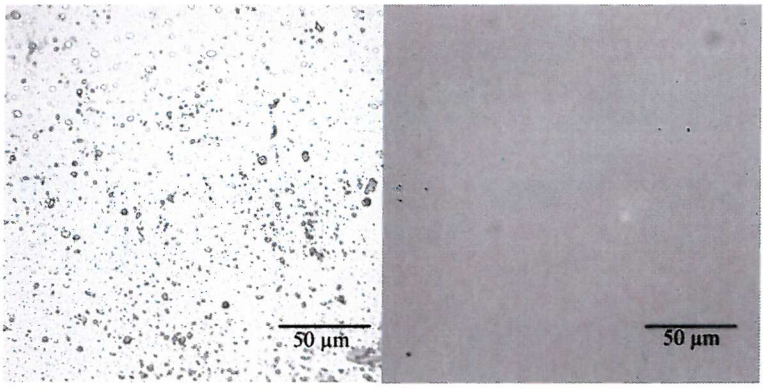

Figure 4.3: Optical micrograph of sample surfaces annealed in open boat environment under flowing forming gas ambient (left) and in evacuated ampoules (right). The samples shown here were annealed at 750 °C *for* 5 h.

The samples with and without oxide and nitride layers were also annealed in evacuated ampoules. Exposing samples coated with such layers to high temperatures caused the protective layer to crack on the sample surface possibly due to lattice mismatch/strain. An example of such cracking of silicon nitride layer is shown in Fig. 4.4. It was also observed that introducing the samples with such layers to high temperature in a short time sometimes leads to evaporation of the films. To avoid such problems samples need to be exposed to high temperature slowly.

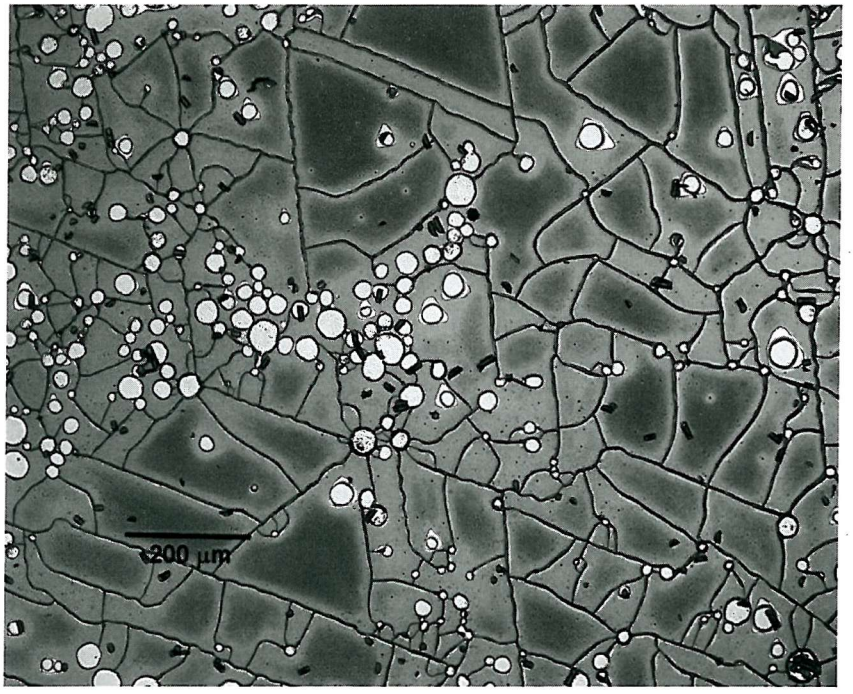

Figure 4.4: Cracking of the protective film of silicon nitride during diffusion anneal. A 200 nm *silicon nitride film was deposited on a* ~200 nm *thick silicon dioxide layer already deposited on germanium surface. Cracks in the nitride film occurred after subjecting the sample to high temperatures.*

Removal of the nitride layer after deposition also caused some concern. During high temperature annealing the nitride layer tends to achieve stoichiometry. It was observed that the etch rate of nitride layers annealed at high temperature was much slower than that of as deposited ones. The use of hydro-phosphoric acid at 160 °C (with reflux system), recommended as etching solution for silicon nitride layer, was also found inadequate. Instead concentrated HF acid (48%) was successfully used to remove both nitride and oxide layers from sample surfaces.

4.4 Sample details

The central aim of the experiments described in this work was to measure the boron and silicon diffusivity in germanium using modern techniques. Increased precision of the boron diffusivity data obtainable using such techniques was expected to give more insight into the behaviour boron in Si-Ge alloy system.

To this end boron and silicon species were implanted in bulk germanium and heat treated for a variety of times and temperatures using furnace annealing. Samples used for the implantation study are tabulated in Table 4.1. Table 4.2 gives details of the samples used in the study of boron diffusion in germanium. Processing details of samples used in silicon diffusion studies are given in Table 4.3.

Sample number	Substrate specification	Boron implantation	SIMS Characterization
I1	<111>, n-Ge	$1\times10^{14}\,cm^{-2}$, 20 keV	1 keV, Normal incidence
I2	<111>, n-Ge	$6\times10^{14}\,cm^{-2}$, 20 keV	500 eV, Normal incidence
I3	<100>, n-Ge	$6\times10^{14}\,cm^{-2}$, 20 keV	500 eV, Normal incidence
I4	<111>, n-Ge	$3\times10^{13}\,cm^{-2}$, 5 keV	500 eV, Normal incidence
I5	<111>, PA with ^{72}Ge	$6\times10^{14}\,cm^{-2}$, 20 keV	500 eV, Normal incidence
	$2\times10^{15}\,cm^{-2}$, 400 keV		500 eV, Normal incidence

Table 4.1: Details of the samples used for boron (^{11}B) implantation study in germanium. PA stands for pre-amorphised. An O_2^+ primary beam has been used for SIMS analysis in all samples.

Sample number	Substrate specification	Boron implantation	Anneal conditions	Protective surface layer	SIMS Characterization
D0	<111>, n-Ge	$5\times10^{14}\,cm^{-2}$, 20 keV	As implanted	—	1 keV, Normal incidence
D1	<111>, n-Ge	$5\times10^{14}\,cm^{-2}$, 20 keV	725 °C, 1/2 h, Ar	SiO_2	1 keV, Normal incidence
D2	<100>, n-Ge	$5\times10^{14}\,cm^{-2}$, 20 keV	800 °C, 3 h, Forming gas	SiO_2	1 keV, 25° to the normal
D3	<111>, n-Ge	$6\times10^{14}\,cm^{-2}$, 20 keV	850 °C, 24 h, Forming gas	SiO_2	500 eV, Normal incidence
D4	<111>, n-Ge	$6\times10^{14}\,cm^{-2}$, 20 keV	900 °C, 8 h, Ampoule	SiO_2+Si_3N_4	500 eV, Normal incidence
D5	<111>, n-Ge	$3\times10^{13}\,cm^{-2}$, 5 keV	As implanted	—	500 eV, Normal incidence
D6	<111>, n-Ge	$3\times10^{13}\,cm^{-2}$, 5 keV	800 °C, 24 h, Ampoule	SiO_2+Si_3N_4	500 eV, Normal incidence
D7	<111>, n-Ge	$3\times10^{13}\,cm^{-2}$, 5 keV	875 °C, 12 h, Ampoule	None	500 eV, Normal incidence
D8	<100>, Epitaxial Ge	Delta layer Peak B$\sim5\times10^{18}$at./cm^3	875 °C, 12 h, Ampoule	None	500 eV, Normal incidence

Table 4.2: Description of the samples used for boron diffusion study in germanium. The resistivity of all n-Ge samples was $\leq 0.4\,\Omega$cm *which corresponds to a doping concentration of* $\sim10^{14}$ atoms/cm^3. *An* O_2^+ *primary beam has been used for SIMS analysis for all samples.*

Sample number	Anneal conditions	Protective surface layer
S0	As implanted	—
S1	750 °C, 360 min, Forming gas	none
S2	800 °C, 30 min, Ampoule	SiO_2+Si_3N_4
S3	825 °C, 180 min, Ampoule	none
S4	850 °C, 30 min, Ampoule	none
S5	860 °C, 60 min, Ampoule	none
S6	875 °C, 50 min, Ampoule	none

Table 4.3: Description of the samples used in the study of silicon diffusion in germanium. The samples were obtained from <111> oriented n-Ge ($\rho \leq 0.4\,\Omega$cm) and were implanted with ^{28}Si to a dose of 5×10^{14} ions/cm^2 with 50 keV. A 500 eV O_2^+ primary beam has been used in SIMS analysis of all samples.

Chapter 5

Ion implantation: results and discussion

5.1 Implantation

Single crystal germanium wafers (about 300 μm thick) with a nominal dislocation density less than 5000 cm^{-2} were obtained from EaglePicher Inc. (USA). The pre-polished wafers were either undoped ($\rho > 30\,\Omega$cm) or lightly n-doped with antimony ($\rho \leq 0.4\,\Omega$cm).

The wafers were cleaved in half with the aid of a diamond-tipped tool (special care had to be taken during this step due to the extra brittleness of the material). The wafer pieces were then cleaned by dipping in fuming nitric acid for 3–5 min, rinsing in de-ionised water and drying using nitrogen blow.

5.1.1 Implantation of boron

The half-wafers were implanted with boron using doses varying from 5×10^{13} to 6×10^{14} cm^{-2}. ^{11}B ions were implanted at an energy of 20 keV. Such shallow implant would make diffusion more significant. A higher energy would drive boron deeper into germanium lattice. The implants were carried out at the University of Southampton ion beam accelerator. Boron implantation was performed in <100> and <111> oriented wafers. For these room temperature implants, the incoming ion beam was misoriented by 7° to the normal of the wafer surface to avoid possible channelling. A constant dose across the wafer was ensured by keeping the beam stationary and moving the wafer holder such that the beam rastered the wafer.

Theoretical calculations using SUSPRE [123] show that a boron dose of more than 3.5×10^{15} cm^{-2} at 20 keV is required to fully amorphise the implanted region of germanium lattice. The doses chosen in this study were below this threshold and therefore we expect that the implanted region is not left amorphised after boron implantation although some damage to the lattice can be anticipated. Prompted by the initial diffusion results

revealed in Chap. 6, a further set of experiments was planned at a lower implantation dose of $3\times10^{13}\text{cm}^{-2}$ at 5 keV.

5.1.2 Implantation of silicon

To obtain silicon concetration peak almost at the same depth as in the case of boron, ^{28}Si ions were implanted with 50 keV and to a dose of $5\times10^{14}\,\text{cm}^{-2}$. This implantation was carried out at room temperature with the ion beam misoriented by 7° to the normal in a <111> oriented wafer. The germanium wafer was implanted at the Surrey Center for Research in Ion Beam Applications (SCRIBA). The silicon implantation dose is close to the theoretically predicted amorphisation dose $7.5\times10^{14}\text{cm}^{-2}$ calculated at 50 keV using SUSPRE [123].

5.2 Simulation of implantation process

As the first step toward predicting the implantation behaviour, theoretical profiles were generated by computer simulation. Implantation parameters such as projected-range, straggle required as input for the calculation were obtained from literature [124, 125]. As mentioned in Chap. 2, a theoretical Gaussian profile could be generated using Eq. 4.6 using the parameters given by LSS theory. Finally, a Monte Carlo model popularly known as SRIM [126], which describes the stopping and range of ions into matter using a quantum mechanical treatment of ion-atom collisions, was also used to predict the implantation profiles. Fig. 5.1 shows results of the simulations performed for boron implanted at 20 keV to a dose $6\times10^{14}\text{cm}^{-2}$. The values of the parameters used are given in Table 5.1.

One should note from the table that the values predicted by various calculations are in close agreement. A basic assumption made during theoretical calculations is that the implantation target is amorphous. As mentioned earlier, for boron implantation the wafers were tilted by 7°. In such a direction the atomic density of the diamond lattice seen by the ion beam is higher than that along a crystallographic orientation direction, say <100> (see Fig. 5.6(b)). The assumption of the amorphous target is therefore fulfilled, at least partially. Hence, unless some other phenomenon is present, one expects the experimental boron profile

Simulation method	Projected range R_p (nm)	Straggle ΔR_p (nm)	Reference
SUSPRE	48.7	38.5	[123]
LSS calculations	47.4	35.3	[124]
SRIM calculations	50.0	40.8	[126]

Table 5.1: Values of the implantation parameters for boron in germanium at 20 keV *from theoretical calculations. The parameters from different calculations agree with each other.*

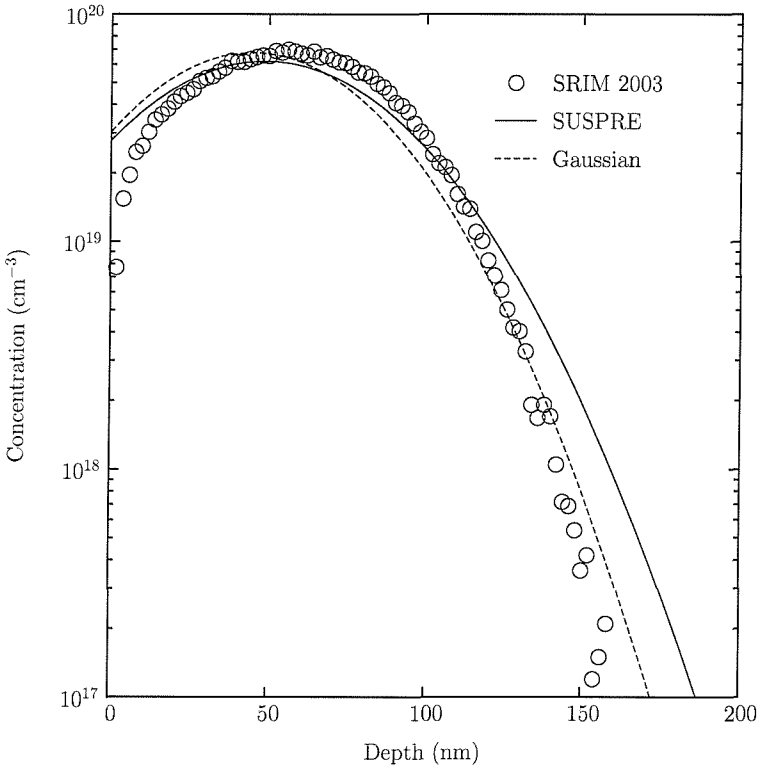

Figure 5.1: Theoretical profile of boron implantation in germanium at 20 keV *and* 5×10^{14}cm^{-2} *dose, calculated using SRIM [126] and SUSPRE [123]. Gaussian profile based on Eq. 4.6, calculated using the parameters given by LSS theory [124] is also shown for comparison.*

to match those presented in Fig. 5.1.

5.3 Results of boron implantation

Experimentally obtained boron concentration profiles are depicted in Fig. 5.2. The figure presents results obtained for 5 and 20 keV implants for different doses. One can notice that concentration peaks for 20 keV profiles occur at nearly the same depth for the two different dose values. Incidently, these two profiles also show long tails rather than falling abruptly to low concentrations. Note that the profile for 5 keV has been given a lower dose of 3×10^{13}cm^{-2}. A possible explanation for the tail is that the high energy incident ion beam used during SIMS analysis might have pushed some atoms deeper into the sample. By using a low energy incident beam in SIMS profiling, the effect of this ion beam mixing can be minimised [121]. A primary O_2^+ beam at 500 eV has been used during SIMS analysis for most of the profiles except for the sample subjected to the 20 keV implant with 1×10^{14}cm^{-2} dose where a 1 keV O_2^+ beam has been used. The effects of ion beam mixing in these profiles can thus assumed to be minimal and this presumption is justified by the graphs with the observation of similar profiles for different primary ion beam energies.

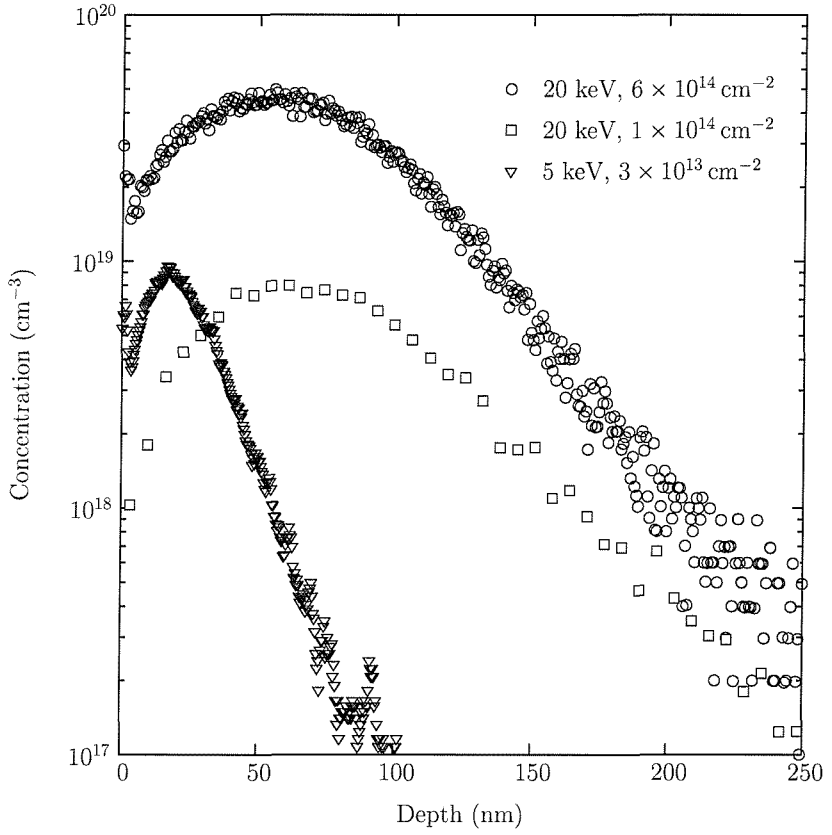

Figure 5.2: Experimental concentration profile of boron implanted with different dose and energy (sample no. I1, I2, I4) obtained using low energy high resolutions SIMS. Note that for 20 keV, $1\times10^{14}\text{cm}^{-2}$ *implant a* 1 keV O_2^+ *ion beam has been used during SIMS analysis. For other profiles shown a* 500 eV O_2^+ *beam was used.*

The next step was to compare the predicted profiles with those from experiments. This comparison is shown in Fig. 5.3 for a 20 keV, $6\times10^{14}\text{cm}^{-2}$ dose boron implant in germanium. One observes a significant difference between the theoretical and the experimental curves. Experimental profiles show a long tail which diminishes more gradually than the tail in the theoretical profile.

A possible reason is the non-uniform sputtering of germanium during SIMS that could have caused the roughening of the crater. This affect might have lead to a false concentration tail. In an attempt to verify if roughening indeed has taken place, the crater bottom was profiled using atomic force microscopy (AFM). It was observed that ripples at the bottom of crater were negligible (~1–2 nm only). Thus by AFM profiling we could rule out the possibility of the observed tail to have caused by non-uniform sputtering during SIMS analysis. The AFM image of the crater bottom is shown Fig. B.3 in Appendix B. The use of low energy SIMS and absence of ripples at the crater bottom point to the fact that the observed tail is due to a real effect and not an artifact of SIMS.

This effect therefore was further investigated by implanting boron in two wafers with

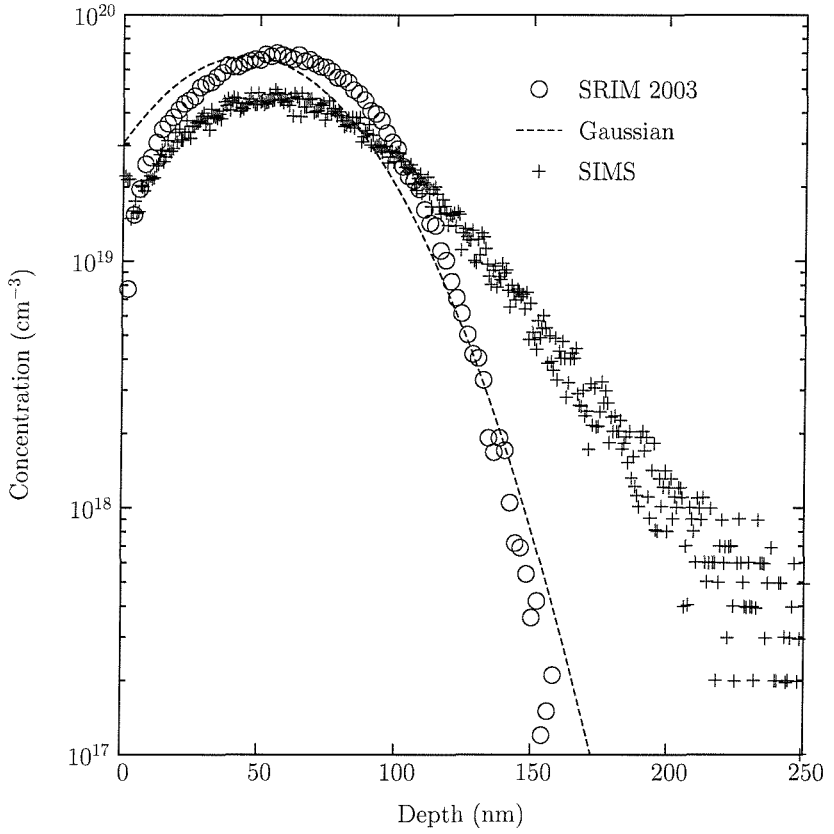

Figure 5.3: Comparison of theoretical and experimental concentration profile of boron implanted in germanium with 20 keV *to* 6×10^{14}cm^{-2} *dose in* <111> *oriented samples (sample no. I2). A deeper penetration of boron as compared to theoretically calculated profile is observed.*

different orientations <111> and <100>, the implantation conditions being the same for both wafers. SIMS profiles of these implants are presented in Fig. 5.4 along with the theoretical Gaussian profile based on parameters given by LSS calculations and calculated using the same dose and energy used as for the experiments. The tails observed in experimental profiles appear similar regardless of the orientation.

We have already noted that the observed tails, which should be absent theoretically, are not thought to be caused by SIMS profiling. However, it is important to bear in mind that probably the basic assumption of an amorphous target is not met adequately, even by 7° misorientation of the crystalline target.

5.4 Discussion on boron implantation

We noted that the experimental profile for implanted boron in germanium is different from the ones predicted by theory. Also the implantation tails in wafers with two different orientation were quite similar. The possibility of SIMS profiling technique being responsible for

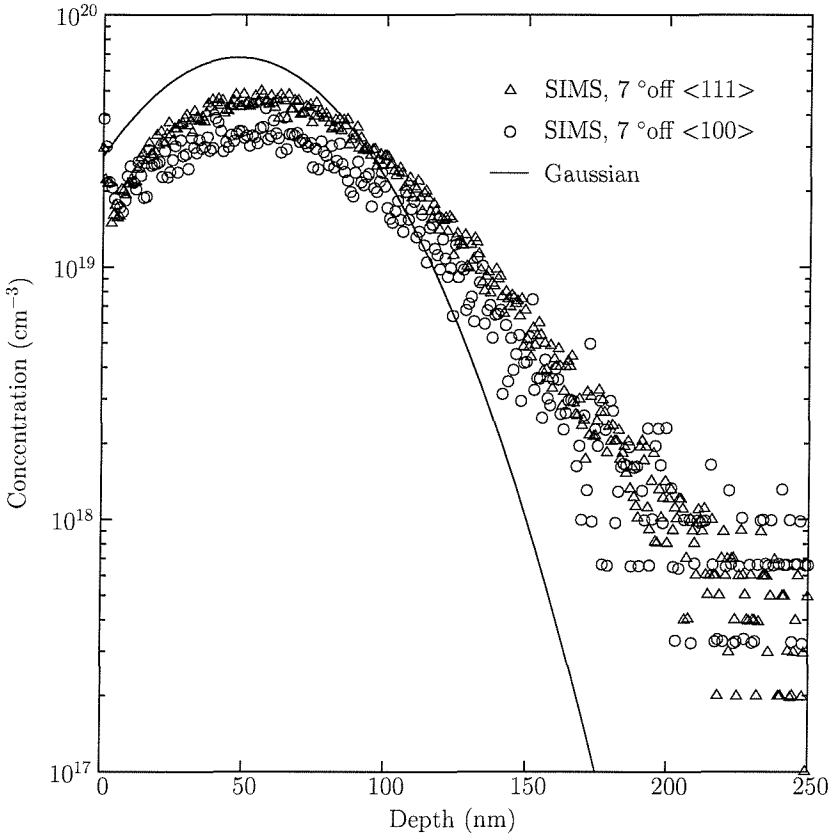

Figure 5.4: Boron concentration profiles for implantation in two directions (samples I2 and I3, dose: $6\times10^{14}\mathrm{cm}^{-2}$*, energy:* 20 keV*). The observed tails are very similar suggesting almost no effect due to orientation. For comparison a theoretically predicted profile is also shown. Note that dose calibration has not been performed for the profiles shown.*

these tails has been ruled out. This leaves only two possibilities (a) enhanced diffusion during implantation (b) channelling. Looking at the profiles closely, one is tempted to attribute the tails more to channelling effects since similar profiles have been obtained for boron in silicon in other studies (see Chap. 2 and 4 in Ref. [38]). It has been shown that in case of implanted boron in silicon, the tails are caused by channelling rather than enhanced diffusion. However, if one attributes the implantation tail to channelling, one should expect a difference in the amount of channelling for implantation in the two different orientations. Hence a difference in experimentally obtained profiles can be expected. Previous studies suggest the presence of radiation enhanced diffusion as a possible cause for tails during implantation at room temperature [109] as well as at high temperatures [114, 127]. Enhanced interstitial diffusion during phosphorus implantation in germanium has also been reported [128]. Gusev *et al.* [113] also observed boron implantation profiles to penetrate deeper than predicted by theory but attributed the observation to channelling. Since in the previous studies boron was not analysed using SIMS, it is not possible to compare our results directly with theirs.

Due to the contradictory nature of reported results in literature, it is also difficult to remark conclusively on the observed effects.

In a highly damaged/amorphised crystal, long range order is absent. Thus the incident ions do not find open passages to penetrate deep into the material. Instead, they collide randomly with target atoms and loose most of their energy by nuclear scattering due to such collisions. This process results in very small or no channelling of implanted ions in the target. Keeping this fact in mind an experiment was designed to amorphise germanium prior to boron implantation in order to destroy the lattice order and eliminate the presence of open channels. In this experiment, germanium wafer was pre-amorphised with 400 keV ^{72}Ge ions to a $2\times10^{15}cm^{-2}$ dose. Thereafter boron was implanted to the same dose and energy i.e. 20 keV, $6\times10^{14}cm^{-2}$ as used for implantation in crystalline germanium. The results of this experiment are shown in Fig. 5.5. For a comparison the profiles forecast on the basis of theoretical calculations (LSS, SRIM) and the experimental profiles from implantation in crystalline target are also shown in the same plot. Strong evidence of de-channelling of implanted boron in pre-amorphised germanium is present since the profile in this case agrees well with the theoretical profile calculated on the basis of an amorphous target. Radiation-enhanced diffusion during implantation is expected to occur irrespective of the fact that the target material is amorphous.

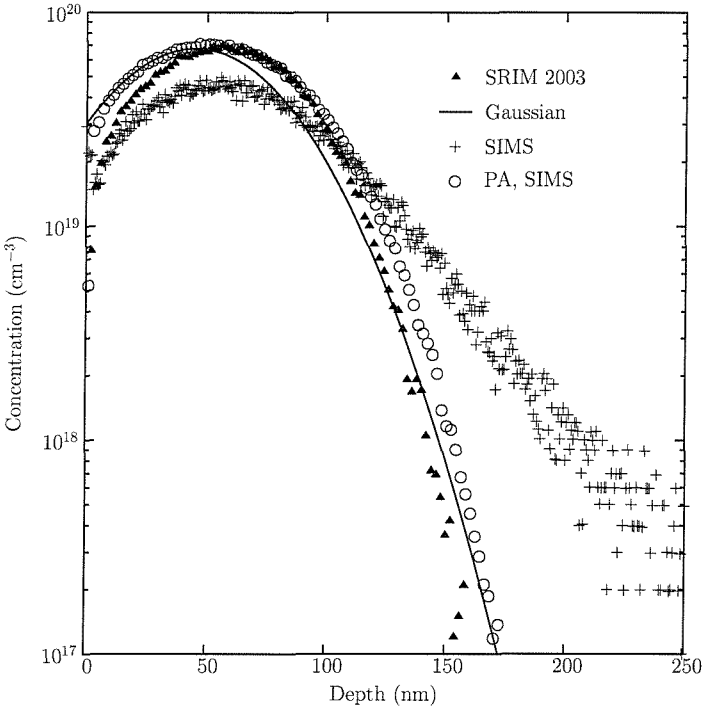

Figure 5.5: Comparison of as-implanted boron profiles in crystalline (sample I2) and pre-amorphised (PA) germanium (sample I5). The theoretical profile matches well with the experimental profile for the amorphised germanium indicating the presence of channelling in crystalline germanium.

It still remains to explain as to why channelling is observed even when the implantation is carried out 7 ° off the crystallographic axis and why does it produce similar tails in the two different orientations tested. In order to explain this, let us look at the diamond lattice from <100> direction as shown in Fig. 5.6(a). One can see the presence of open spaces between the atoms the size of which is of the order of $0.3a_{Ge}$ (=1.695 Å), where a_{Ge} (=5.658Å) is the lattice constant of germanium. Boron is a relatively small atom with an atomic radius=1.17Å. An energetic boron ion can travel in the open spaces in germanium without being deflected by a large angle and penetrate deep.

A model of germanium lattice which is rotated by 7 ° from the <100> direction, is shown in Fig. 5.6(b). A similar model can be drawn for <111> direction. When the target is misaligned, the incident ions loose their energy in a large number of random collisions. The implantation direction was chosen to be misaligned by 7 ° in order to avoid directing the ion beam to the barrels of open space between the crystallographic axes shown in Fig. 5.6(a). We also note that the critical angle Ψ for 20 keV boron ions incident along <111> direction is calculated to be ~5 °. Although the atomic density in a direction 7 ° off the <100> axis is higher than that along the axis, channelling may still take place to some extent. After the initial scattering by the densely packed atoms, the ions may be deflected to the open

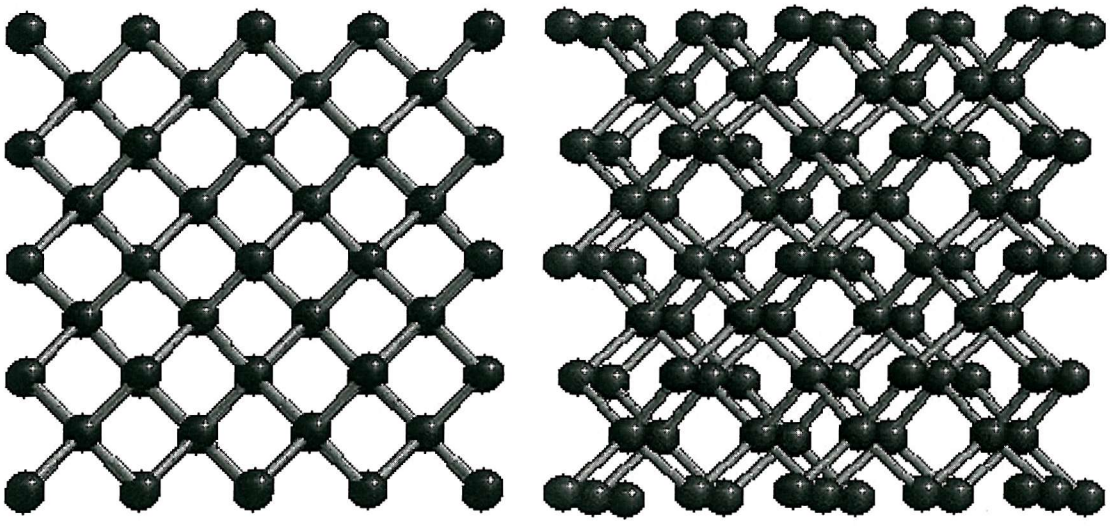

(a) (b)

Figure 5.6: Model of a germanium lattice shown along <100> direction. Illustration (a) shows the atomic arrangement on viewing the lattice along <100> direction. The open channels are seen to be present. The atomic density is higher in a direction 7 ° off from <100> axis as shown in (b). Small boron atoms can fall into the channels after initial collisions and migrate long distances.

channels in which they will lose very little energy by the electronic stopping process and

therefore penetrate deep into the material. This explains why channelling could be observed in boron implanted germanium even though the implantation beam was misoriented with respect to the crystal direction.

The germanium lattice as seen 7° off from <111> direction appears relatively denser than from <100> direction. The channelling critical angle for the two directions is very similar. The width of the channels along these two directions does not differ very much. Also the atomic packing in the diamond lattice is loose, the packing fraction being 0.34 only. This openness also helps the energetic but small boron atoms to travel far distances and produce the observed tails. However, by amorphisation long range channels can be completely destroyed. Implantation in such materials should not produce channelling tails. Had the implantation tails in the crystalline target been due to radiation enhanced diffusion, we would have expected a similar or even longer tails produced by the long-range migration of defects which are produced during pre-amorphisation.

We also note that if the incident ions are channelled, the energy loss via nuclear stopping should decrease causing less damage to the lattice. The observation of channelled profiles and the fact that the maximum implantation dose used in this study is about 6 times smaller than estimated amorphisation dose indicate that it is unlikely that an amorphous region could have been produced by boron implantation in crystalline germanium.

5.5 Results and discussion on silicon implantation in germanium

The theoretical values of implant parameters for silicon diffusion in germanium were also obtained from literature [125]. The values calculated using SRIM and SUSPRE are presented in Table 5.2. It should be noted that the theoretical calculations are based on the assumption amorphous implantation target though in this work silicon ions were implanted in crystalline germanium.

The results from silicon implantation in germanium are shown in Fig. 5.7. The plot compares the experimental implanted profile with one predicted by SRIM calculation. Contrary to the case of boron, experimental implanted profile is in much closer agreement to the theo-

Simulation method	Projected range R_p (nm)	Straggle ΔR_p (nm)	Reference
SUSPRE	49.7	33.3	[123]
LSS calculations	45.0	32.0	[125]
SRIM calculations	48.0	31.8	[126]

Table 5.2: Values of the implantation parameters for silicon in germanium at 50 keV *from theoretical calculations.*

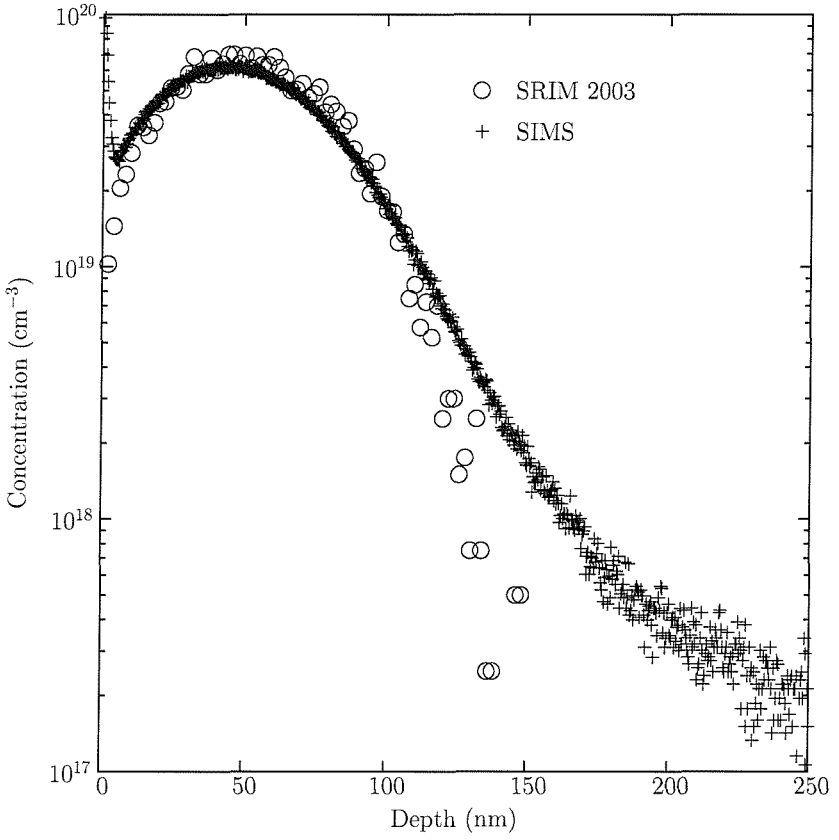

Figure 5.7: Theoretical and experimental concentration profiles of silicon implanted in germanium at 50 keV *to* 5×10^{14}cm^{-2} *dose. The agreement of the two profiles at high concentration regions is suggestive of a highly damaged/amorphised surface region caused by silicon ions.*

retical predictions, although one observes a departure at low concentrations. It is to be noted that the implantation dose used here (5×10^{14}cm^{-2}) is quite close to the amorphisation dose (7.5×10^{14}cm^{-2}, calculated using SUSPRE) for silicon in germanium at 50 keV. It should also be noted that the size of silicon atoms is also higher than the size of boron atoms. Thus the probability of silicon ions being steered into channels like in the case of boron is quite low since the incident energy is lost mainly due to nuclear stopping. The close agreement between the theoretical profile calculated on the assumption of an amorphous target and the experimental profile suggests that at the dose and energy studied, the implanted region of germanium may have suffered high levels of damage. The disagreement in the two profiles at low concentrations suggests presence of some amount of channelling.

5.6 Conclusions

For boron implantation in crystalline germanium, implantation tails in the concentration profiles have been observed. No significant difference in the concentration profile tails is

found for implantation in <100> and <111> oriented wafers. The implantation tails disappear when the target is pre-amorphised. Thus, it can be concluded that the tails in the concentration profiles are due to channelling phenomenon. We can also speculate that for the implantation dose and energy range studied, the implanted region largely remains crystalline. For silicon implantation in crystalline germanium the absence of similar implantation tails as observed in the case of boron implantation suggests that channelling plays a less important role in determining implantation profiles of silicon in germanium at the dose and energy studied. Also, we suspect that silicon implantation causes considerable damage to the germanium lattice which may have influenced subsequent diffusion as will be shown in next chapter.

Chapter 6

Diffusion: results and discussion

6.1 Experimental programme

6.1.1 Masking

Following the introduction of dopant, the samples were subjected to high temperature in protective atmosphere for the purpose of diffusion. As a requirement of SIMS, it was necessary to keep sample surfaces smooth. Furthermore, in order to avoid contamination and out-diffusion of implanted species, it was important to deposit a masking layer before the thermal treatment. To achieve this, following the implant the wafers were dipped in fuming nitric acid for 2–3 min and then rinsed in deionised water. A silicon-dioxide layer which has been proposed in literature as an effective diffusion mask for impurities in germanium [122], was deposited on the implanted side of the wafer using Plasma Enhanced Chemical Vapor Deposition (PECVD) at ~300 °C. This layer (~200 nm) was expected to protect samples from surface damage by reducing evaporation of the material.

Guided by the observations made after the initial diffusion anneals during which the sample surfaces were damaged as outlined in Sec. 4.3, the requirement for additional surface protection was felt. To this aim a relatively unreactive silicon-nitride layer was further deposited on the existing silicon-dioxide layer. This layer was ~200 nm thick and was deposited using PECVD at ~300 °C. Due to the deposition being on silicon-dioxide layer, the nitride layer was not expected to cause interfacial stresses in the underlying germanium.

In the latter part of the project, the technique for annealing was improved by sealing the samples in evacuated quartz tubes under vacuum. Semiconductor grade quartz tubes (HSQ300) obtained from Heraeus Quartz Ltd. were used for ampoule making. Following was the sequence of steps used for ampoule and sample cleaning:

Ampoule cleaning

- Rinsing in De-ionised (DI) water

- HF (48%) dip for 7-10 min
- DI water rinse
- Rinse in Acetone
- Rinse in Methanol (2 times)

Sample cleaning

- Rinsing in DI water
- Ultrasonic clean in DI water, Acetone and Methanol
- DI water rinse
- HF dip (30 s-1 min)
- DI water rinse
- Rinse in Acetone
- Rinse in Methanol (2 times)

Note that the samples with silicon-dioxide and/or nitride deposited layer were not given an HF dip. Following the above steps the ampoules were purged with high purity argon 4-5 times and sealed under vacuum ($\sim 4\times10^{-6}$ torr). Before annealing the ampoules were dipped in fuming nitric acid for 2-3 min followed by rinsing in DI water. The sealed ampoule size varied between 8 and 12 mm.

6.1.2 Annealing

For the annealing a three zone furnace with a constant temperature zone of ~10 cm was used. One end of the quartz tube used inside the furnace was connected to the gas source while the other was used for exchanging of samples in and out of the tube. The furnace had been calibrated for the desired annealing temperature range with a Pt-Rh thermocouple. During the diffusion anneal, the variation in temperature measurement was estimated to ± 3 °C. The quartz tube and the boat used to transport samples were cleaned with dilute HF and acetone. The annealing was performed in a temperature range from 675 to 900 °C for various time periods. The annealing ambient was a reducing atmosphere of a forming gas (mixture of H_2 (5%) and N_2) flowing at a rate of 1–2 l/min. Samples were also annealed in argon and oxygen free nitrogen atmosphere. A quartz sample carrier boat containing the samples or ampoules was manually pushed into (and pulled out of) the furnace slowly to avoid thermal shock. The time uncertainty in the annealing schedules was estimated to be (~ 5–7 min) on the basis of sample insertion/removal lead times. The time variable used

to calculate diffusion coefficients was corrected by accounting for this uncertainty. However, the necessary correction was minute even compared to the shortest anneal time of 8 h for boron diffusion in germanium. For silicon diffusion experiments on the other hand where the annealing times were relatively short, samples were inserted and pulled out of the furnace relatively quickly. After annealing the ampoules were broken open. The silicon-dioxide and nitride layer could be satisfactorily removed using concentrated HF (48%) solution before SIMS analysis.

6.2 Boron diffusion in germanium

6.2.1 Initial diffusion simulations

To design a set of diffusion experiments, initial simulations were carried out using diffusivity values for boron obtained from literature (see Table 3.5). To generate a theoretical implanted profile in the simplest form, given in Eq. 4.3, parameters given in Table 5.1 were used. During annealing, implanted atoms diffuse deeper into the wafer depending upon the diffusion coefficient at temperature and time of annealing. Let D be the diffusion coefficient and t be the time for the diffusion anneal. We further assume that the substrate into which the impurity diffuses is infinitely thick and also that there is no out-diffusion from the sample surface. Under these assumptions concentration profiles will retain its Gaussian shape at the end of diffusion process [120]. After high temperature annealing, the ion distribution takes the following form [129]

$$N(x) = \frac{\Phi}{(2\pi)^{1/2}(\Delta {R_p}^2 + 2Dt)^{1/2}} \exp\left[-\frac{1}{2}\left(\frac{x - R_p}{(\Delta {R_p}^2 + 2Dt)}\right)^2\right]. \tag{6.1}$$

Eq. 4.6 was used for predicting the as implanted profile in simulations whereas Eq. 6.1 was used to estimate profile broadening after diffusion anneal. A MATLAB function routine based on above mentioned equations was written for the purpose. The diffused profiles were calculated for a thermal budget of 800 °C, 60 min.

Figure 6.1 shows the results of initial simulations. These simulations worked as starting points for the design of experiments. Based upon the diffusivity values available in literature for boron and silicon in germanium, the time and temperature variables for the annealing process were derived. Unlike profile characterisation by electrical methods, which require very large diffusion lengths (μm) to have occurred, by SIMS smaller diffusion depths can be analysed. Owing to the surface degradation of germanium during high temperature/long time annealing, the possibility of measuring small diffusion lengths accurately is a very important factor. In these experiments, diffusion depths of about 20–100 nm were expected. To resolve such fine length scales, the expertise of the SIMS analysis group at University of Warwick was solicited.

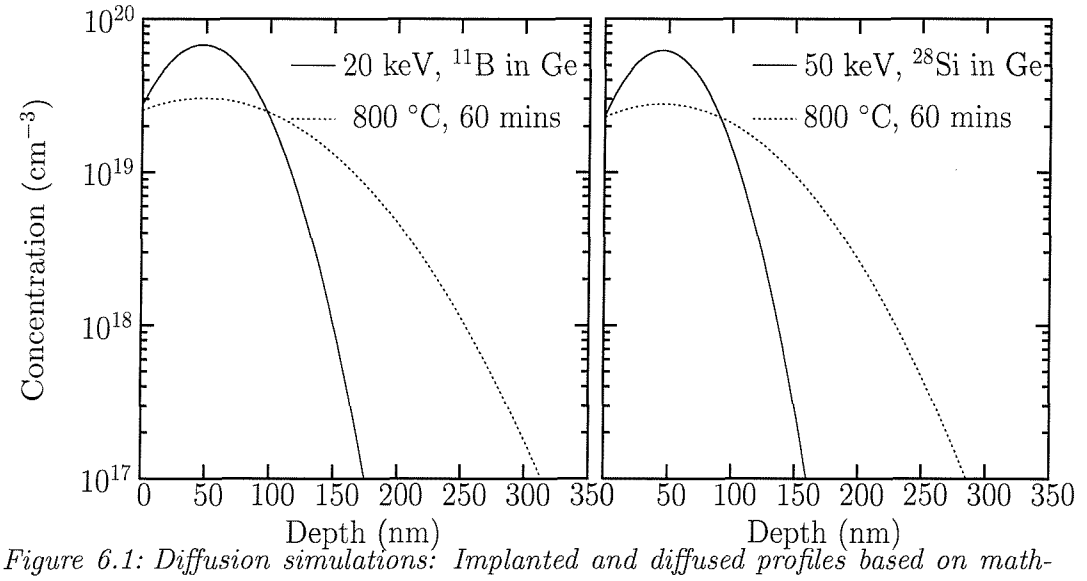

Figure 6.1: Diffusion simulations: Implanted and diffused profiles based on mathematical equations Eq. 4.6 *and* 6.1. *The as implanted profiles are for fluence* $6\times10^{14}\text{cm}^{-2}$ *in both figures. The values for implantation [124] and diffusion parameters are taken from literature [62, 78].*

6.2.2 Results

The initial set of annealing experiments carried out at temperatures 675, 700 and 725 °C for 80, 60 and 30 min (according to temperatures and times derived by simulations), respectively, did not show any profile broadening due to diffusion. Therefore the thermal budget was increased by raising the temperature to 800 °C and the annealing time to 3 h. Raising the temperature by $\sim$ 100 °C however did not produce a profile with measurable diffusion. The results for these anneals are represented in Fig. 6.2. Note that these samples had a protective silicon dioxide coating and were annealed under flowing argon. Assuming the smallest value of diffusivity of boron in germanium [62] given in literature, one expects to observe some amount of profile broadening at 800 °C after an anneal for 3 h. However, such broadening was not visible in the annealed profile. Thus it became apparent that the values given in literature have been possibly overestimated. A discussion on this issue is deferred until Sec. 6.2.3 in this chapter.

In another test experiment, the ambient for annealing was varied from argon to forming gas. The annealed profiles obtained in each case was similar indicating that the different ambient used here had no or very little effect on diffusion at 675 °C. Since subsequent annealing at higher temperatures was carried out in evacuated ampoules, no further investigation on the influence of ambient could be made.

In the next step of experiments, the temperature for annealing was increased to 850°C while annealing time was increased to 24 h. The result is presented in Fig. 6.3. One observes a very small broadening of the profile towards the tail part of the implanted profile. The diffused profile also shows a reduction in the surface concentration and an apparent increase

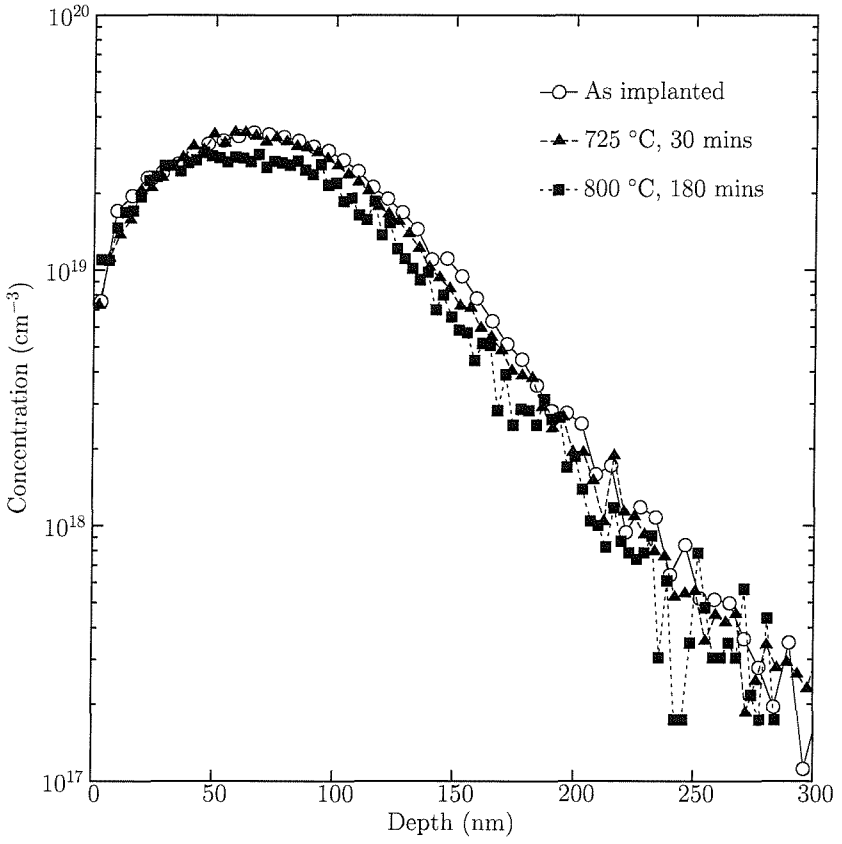

Figure 6.2: Results of experiments for diffusion anneals at temperatures up to 800 °C *for samples D0, D1 and D2 under forming gas ambient. The as implanted profile is with fluence* $5\times10^{14}\text{cm}^{-2}$ *at* 20 keV. *The annealed concentration profiles do not seem to change for annealing budgets shown in legend suggesting a much slower diffusion than literature values.*

in the peak concentration. Note that the diffused profile is normalised for constant dose and this possibly has contributed to the observed difference in peak concentration. It should also be noted that at 850 °C, we are within 100 °C of the melting point of germanium (938 °C). At such high temperatures, only a limited movement of the implanted profile would have been needed to justify the speculation that previous reports on boron diffusion in germanium had overestimated the diffusivity values.

Another sample implanted with the same dose and energy but obtained from an <100> oriented germanium wafer was subjected to the same thermal budget of 850 °C, 24 h. This sample was also coated with a ~200 nm silicon dioxide protective layer and its annealing ambient was flowing forming gas. The sample also showed a limited diffusion in the tail region. The diffusion coefficient which was quantified using the standard procedure described later in this section and is presented in Table 6.1. We note from the Table 6.1 that the two diffusivity values calculated are in good agreement within experimental error. Thus we may conclude that boron diffusion in germanium does not strongly depend on the orientation of

Temperature (°C)	Energy and dose (keV, cm^{-2})	Wafer orientation	Diffusivity (cm^2/s)
850	20 keV, 6×10^{14}	<111>	2.07×10^{-16}
850	20 keV, 6×10^{14}	<100>	1.67×10^{-16}

Table 6.1: Comparison of the diffusion coefficients as calculated from the annealed profiles for samples from different wafer orientations. The values were obtained by fitting the annealed profiles using TSUPREM.

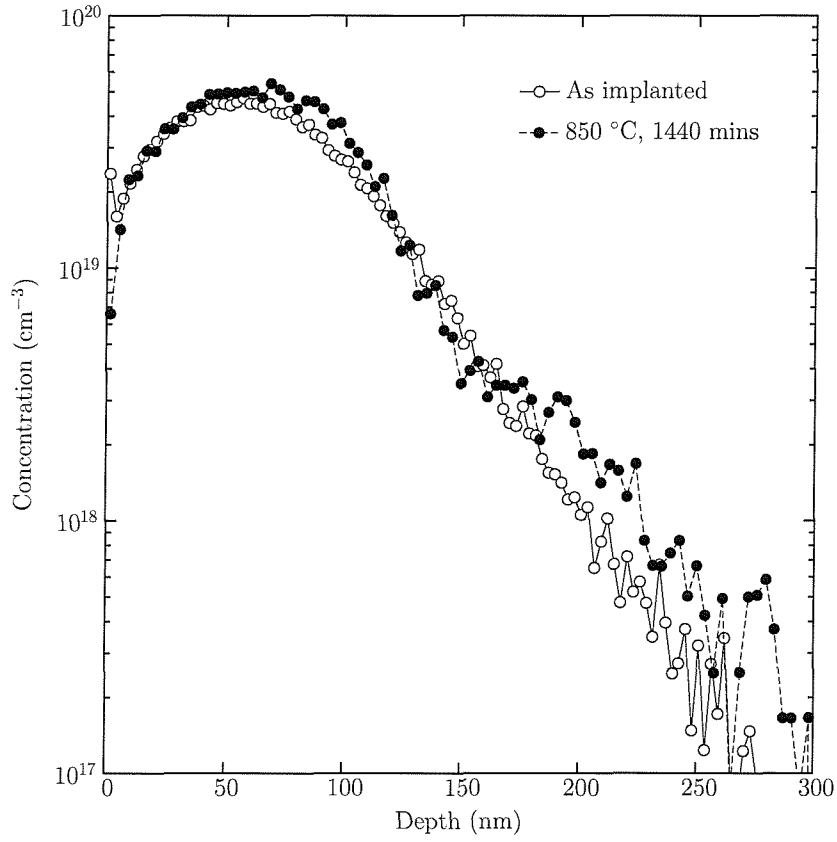

Figure 6.3: SIMS concentration profiles of sample D3 with boron implanted to $6\times10^{14}cm^{-2}$ *dose at* 20 keV. *A limited diffusion towards the tail of the implanted profile is observed. The sample had a protective silicon dioxide coating and was annealed in Forming gas ambient.*

the wafer as one would expect in cubic structures. During subsequent annealing with higher thermal budgets the samples suffered surface damage as mentioned in Sec. 4.3. Therefore, the anneals at higher temperatures were forced to be carried out in evacuated quartz tubes.

The diffusion profiles obtained from samples implanted with a higher dose and energy (20 keV, $6\times10^{14}cm^{-2}$) and subjected to different thermal budgets are presented in Fig. 6.4. Once again, one observes a lower surface concentration and an apparent increase in the peak concentration for the sample annealed at 900 °C, 8 h. Fortunately, extraction of diffusion

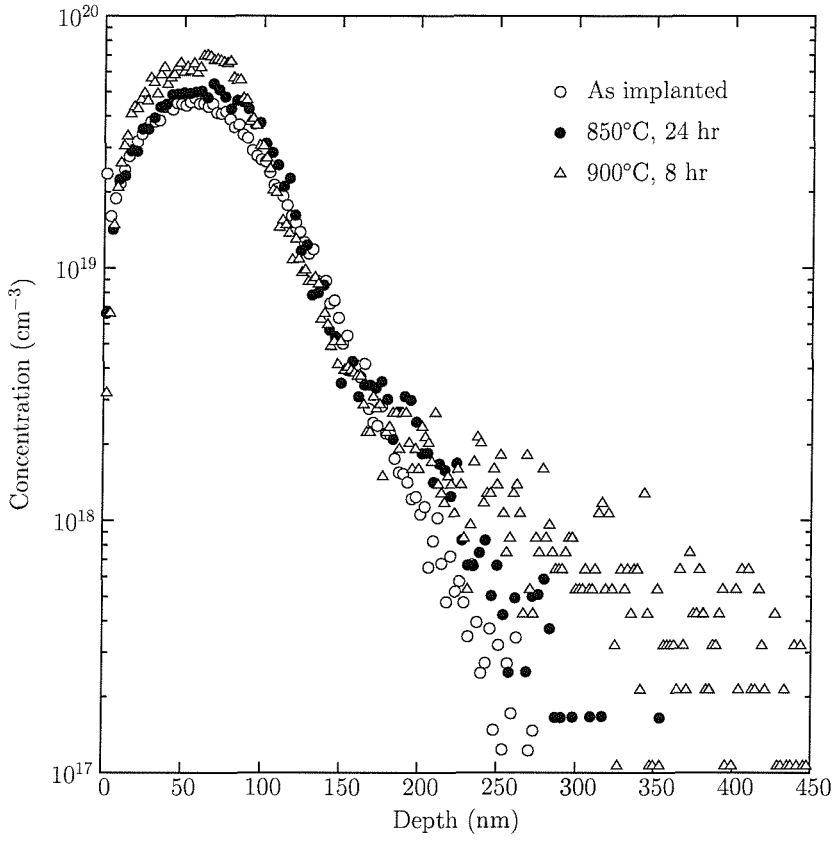

Figure 6.4: As implanted and diffused profiles for samples D0, D3, and D4 for which boron was implanted with 20 keV *energy,* $6 \times 10^{14}\text{cm}^{-2}$ *fluence and subjected to thermal budgets shown in the figure. Dose calibration has been performed for diffused profiles. Samples D3 and D4 were coated with* SiO_2 *protective layer and annealing was performed in forming gas and in ampoule, respectively.*

coefficients from both diffused profiles was possible using methods discussed later in this section. It is striking that the profiles show noticeable diffusion only in the tail region of the implanted profile. The whole of the peak appears to be immobile at such high temperatures. The peak in this sample can be associated with the immobility of boron above its solid solubility limit in germanium. The immobility of the peak could also be due to precipitation or clustering of boron at higher concentrations.

Diffusion anneals have also been carried out on samples which received a smaller dose at a lower energy, i.e. $3\times10^{13}\text{cm}^{-2}$ at 5 keV. As depicted in Fig. 5.2 such an implantation can give a narrow boron profile compared to a high energy implant. A shallow implant provides a relatively narrower initial profile which helps to distinguish even a small movement in the diffused profiles. A lower implant energy not only offers a shallow profile but also causes less damage to the target. A lower dose would also bring the peak boron concentration closer to the solid solubility limit of boron which is cited to be around $\sim10^{18}\text{atoms/cm}^3$ [57, 129]. One should note though that shallower implants are more susceptible to surface effects due

to their proximity to the surface. For such implants a higher degree of surface protection is required, a factor which led to the consideration of an inert protective layer made of silicon dioxide and silicon nitride.

The as implanted and diffused profiles for shallow implant (for sample No. D5, D6, D7) are shown in Fig. 6.5. Note that the annealing for these samples was carried out in ampoules. Sample D6 had a coating of silicon nitride on top of silicon dioxide whereas sample D7 had no protective coating. The relatively noisy SIMS data is due to the detection limit of boron in germanium. Consistent with the previous diffusion anneals limited diffusion and movement of the tail region of the implanted profile can be observed.

The concentration-depth profiles from as-implanted and annealed samples were analysed using a commercially available process simulator TSUPREM [130]. A Pearson distribution based on four moments described in Eqs. 4.7–4.10 can be used to describe the as-implanted profile. Using a dual-Pearson distribution, in which the primary Pearson function models the non-channelled portion of the implant and the secondary Pearson function models the channelled implant, the as-implanted profile can be well described [131]. However, such approach is not required when the annealed profiles are analysed for diffusivity calculation since the as-implanted profile can be loaded straight as input in the simulator. To simulate diffusion, the as-implanted input profile is allowed to diffuse with appropriate model and under boundary conditions matching those of experimental conditions. The experimental diffused profiles acts as target for the optimisation procedure of the simulator. The input parameters are varied to minimise the root mean square (rms) error between the simulated and the target profile and the best fit parameters are given out.

To simulate annealed boron profiles, the as-implanted profiles were loaded to the simulator. A solid solubility model was chosen for the present simulations since all the diffused profiles showed an immobile peak which is believed to be originating due to the solid solubility limit of boron in germanium. The parameters which are responsible for surface conditions such as segregation and transport coefficients were varied but not included in the optimisation procedure. This approach is justified since the aim of the simulation was to calculate diffusion coefficients by fitting the diffused part of the profiles. It should be noted that substantial uncertainties can result if a large number of parameters are chosen for variation. No electric field effect on diffusion is considered since the doping concentration due to boron is always smaller than intrinsic carrier concentration at the annealing temperatures. Point defect concentrations were assumed to be at the thermal equilibrium by choosing the PD.FERMI parameter [130].

In the solid solubility model used for analysis of annealed profiles, boron concentration above that specified by a variable parameter (SS.CONC) at the diffusion temperature is considered immobile while the rest is allowed to diffuse. To keep the simulations simple the parameters describing diffusivity by association of a charged point defect were turned off. Diffusion of boron with neutral defect (vacancy or interstitial) was assumed. Thus for each

temperature, parameters corresponding to boron diffusivity i.e. DIX.0 (with DIX.E=0) and solid solubility (SS.LIMIT) were chosen as variable parameters in the optimisation procedure of the simulator. An example of the input file to the simulator is given in Appendix A.

Attempts were made to fit only the diffused region of the annealed profile. For samples annealed without surface cap layer some does loss can be expected due to out-diffusion, but this hardly effects the deep region of the profile. Hence the diffusion coefficients obtained from fitting of the annealed profiles were found to be relatively independent of the surface boundary conditions. The result of such a fitting for the case of 875 °C, 12 h anneal is shown in Fig 6.6. Appropriate values of uncertainty in the measurement of diffusivity are given as error bars in the Fig. 6.7.

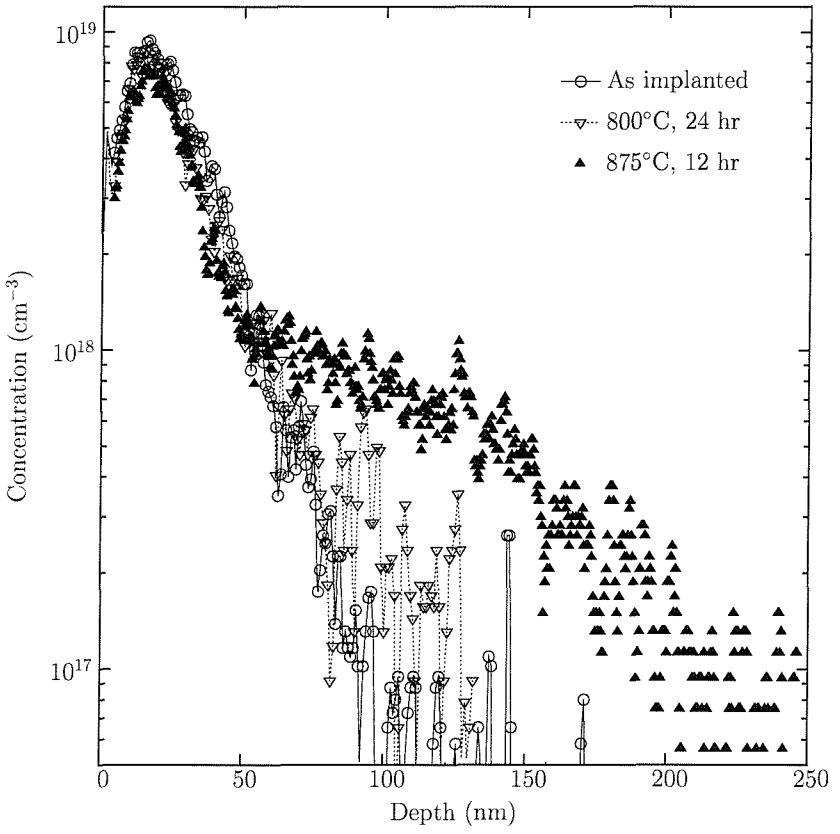

Figure 6.5: SIMS profile of boron implanted samples D5, D6, and D7 with lower dose ($3 \times 10^{13}\mathrm{cm}^{-2}$) *and energy* (5 keV) *and subjected to thermal budgets shown in the figure. A magnification of diffusion profile could be achieved using a narrow initial profile by utilising a lower dose and energy.*

Important information can be extracted by examining the peculiar shape of the diffused profiles more closely. The profile obtained for the 875 °C, 12 h anneal can be used to estimate the solid solubility of boron in germanium at this temperature by extrapolating the profile to the surface. The concentration value $2\times10^{18}\mathrm{atoms/cm}^3$ obtained this way for boron solid solubility in germanium corresponds closely with the reported values in literature [129, 57].

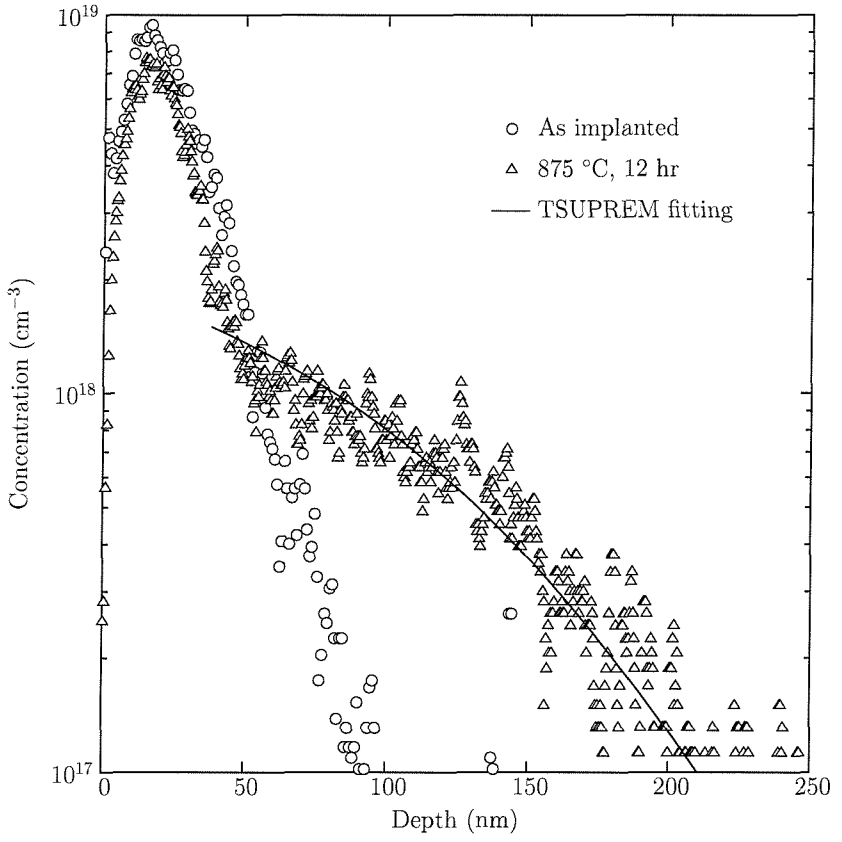

Figure 6.6: Quantification of diffusion coefficient using fitting. A fitting to the diffused SIMS profile is achieved with TSUPREM using solid solubility and diffusion coefficient as parameters.

Fig. 6.7 displays the Arrhenius plots of diffusivities extracted using the TSUPREM fitting procedure explained previously. Previously published diffusivity values for boron in germanium are also shown for the temperature range studied. It is clear that the diffusivity values calculated in this work differ by two to four orders of magnitude. This is a substantial difference even after accounting for possible experimental errors. The values of activation energy and pre-exponential coefficient for boron diffusion in germanium calculated from the plots in this study are listed in Table 6.2 along with the values from literature. One observes that the activation energy calculated in this work does not differ much from the literature values. This implies that in our case the low values of diffusivity is mainly due to the lower pre-exponential factors.

6.2.3 Discussion

The comparison of diffusivity values shown in Fig. 6.7 is interesting especially when one realises that the activation energy does not differ much from the values quoted in the literature. It is surprising to observe that this is also the case when we compare the previous measurements with each other which differed in diffusion coefficients by two orders of magnitude. In

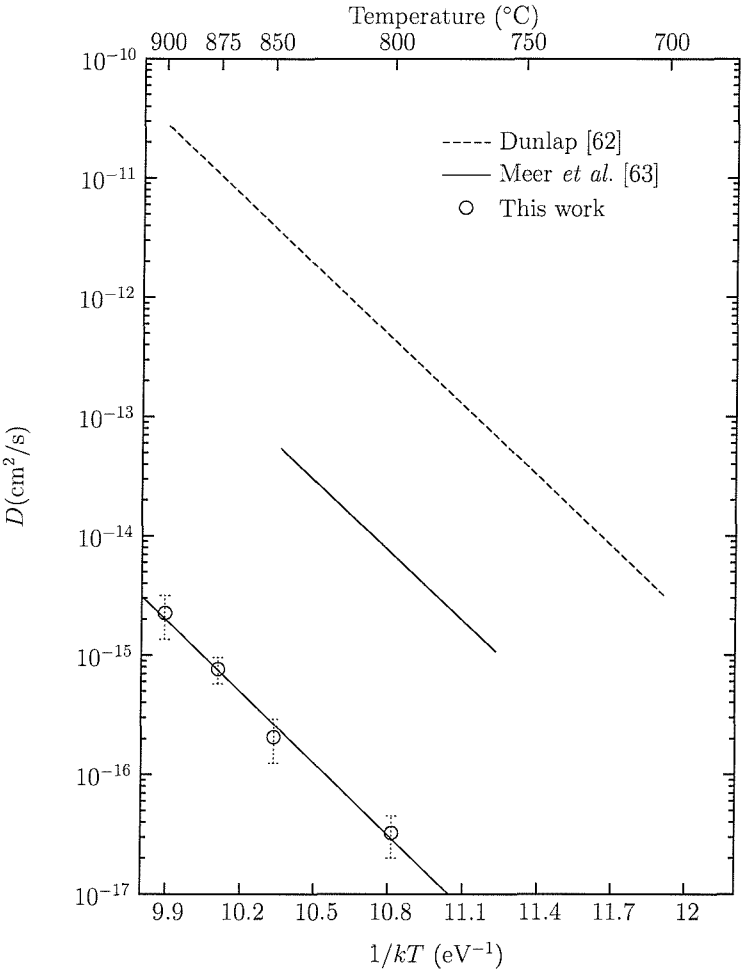

Figure 6.7: Arrhenius curve of boron diffusivity in germanium. A comparison with similar curves from literature indicates that diffusion coefficients calculated this study differ by at least two orders of magnitude.

order to explain the difference in diffusivity values, one must carefully study the differences in the experimental conditions used in different studies. Dunlap [62] reports depositing a boron film on germanium samples and annealing in ampoules filled with argon. Anomalous behaviour of boron compared to other dopants was observed in the study. The anomaly in activation energy was attributed to boron not alloying easily with germanium. According to Dunlap, this prevented boron film from making good contact with the germanium crystal and the diffusivity observed at lower temperatures was slow. This, however, is not the case in the present study as boron was introduced in germanium by implantation before diffusion annealing was carried out. In Dunlap's study, no mention was found about any surface damage suffered by germanium at high temperatures either. The other boron diffusion study in germanium carried out by Meer *et al.* [63] made use of boron doped germanium powder to introduce boron in intrinsic germanium samples. In this study as well, boron showed a slower diffusion as compared to other dopants investigated. Another important observation was that surface concentration reached a maximum of 5×10^{18} atoms/cm^3. Notably the two

D_o (cm^2/s)	E_a (eV)	Temperature range (°C)	Experimental technique	Reference
6×10^8	4.5	700–900	pn-junction	[62]
9.5×10^6	4.5	760–850	Incremental sheet resistance	[63]
1.2×10^5	4.6 (± 0.3)	800–900	SIMS profiling	This study

Table 6.2: Comparison of pre-exponential factor and activation energy values from literature and the present work. Literature values are taken from Ref. [57].

studies differed in magnitude of diffusion coefficient by two orders of magnitude.

From an experimental aspect, there exist another important difference between earlier studies and the present work: the characterisation technique. In Dunlap's study a pn-junction method was used and Meer *et al.* [63] have measured boron diffusivity using incremental sheet resistance. The electrical methods used in above mentioned studies measured the depth distribution of the charge carriers associated with electrically active dopant only. But the charge carrier distribution may not only be due to the dopant under diffusion study but also to unfortunate contamination. Hence the charge distribution may not be identical with the depth distribution of the dopant. However, we measured the depth profile of implanted and subsequently diffused boron using SIMS in this study. Therefore we can be confident that the actual elemental boron profile was measured in this study.

An example of the difference in concentration profiles measured using electrical methods and SIMS is shown in Fig. 6.8. The figures compare the concentration profile of as implanted boron measured using Hall effect & sheet resistivity [109] and SIMS [this work]. For both these profiles boron has been implanted in <111> oriented wafers at (20 keV) to a $6\times10^{14}\,cm^{-2}$ dose. It should be noted however that Herzer *et al.* [109] implanted boron in <111> direction whereas in this study the wafer was tilted by 7 °. We note that the peak concentration and its position is different in the two cases. Also the electrically measured profile is much deeper than the profile measured using SIMS. Depth profiling using electrically active profile may be influenced by the defect ionisation in the samples. However, this comparison suggests that the concentration profiles measured using electrical methods could be significantly different from the elemental profile.

We now try and understand our results in greater detail. One can argue that implantation induced defects/damage may have affected diffusion. At a microscopic level the implantation process introduces both interstitials as well as vacancies into the lattice. Hence it may actually enhance the diffusion process rather than retard it. A higher energy/dose implant is expected to introduce significantly more point defects and hence influence diffusion more strongly than in a low energy/dose case. But we observe comparable values of diffusivity even after implantation energy is increased by a factor of 4 and the dose values by more than an order of magnitude. Also, as mentioned in Chap. 3, a low temperature anneal (T~350 °C)

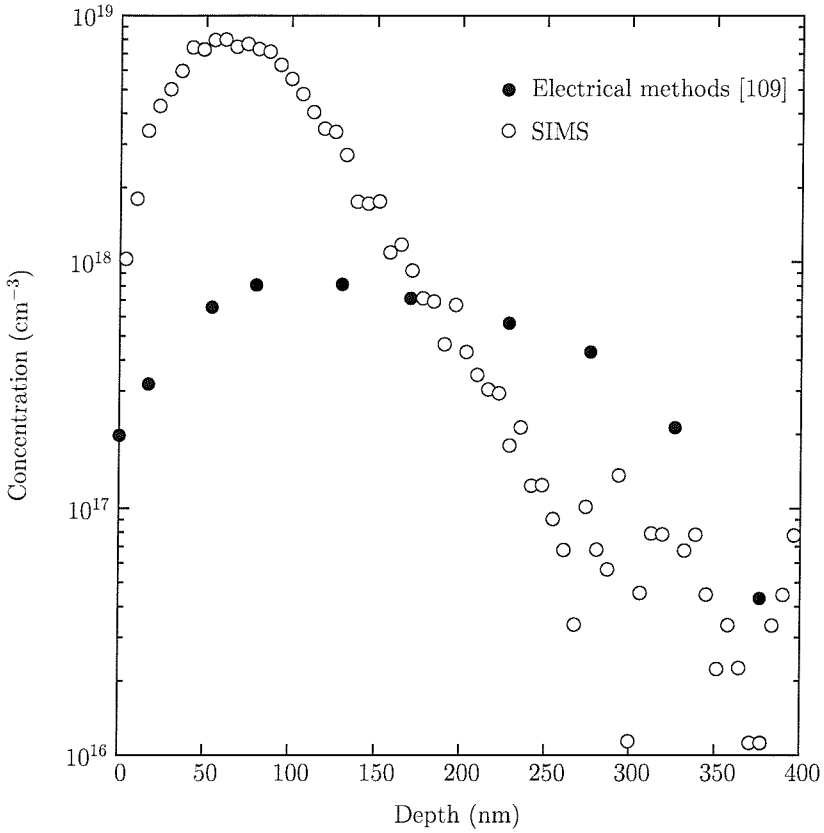

Figure 6.8: Comparison of boron concentration profile measured using electrical methods as described in Ref. [109] and SIMS used in this study. In both studies boron has been implanted in <111> oriented wafers with (20 keV) *for* $6\times10^{14}\,\mathrm{cm}^{-2}$ *dose. Note that in the study of Herzer* et al. *[109] the wafer was not tilted against the implantation beam.*

was sufficient to remove the damage caused by boron implantation in germanium. It should be noted that the annealing times and temperatures used in this study were substantially higher than that required for recovering implantation damage. However the possibility of the formation of immobile boron-defect complexes can not be ruled out.

One of the independent ways to examine whether the implantation has affected diffusion is to carry out diffusion experiments on an epitaxial layer of germanium which has a boron spike. There is a two fold advantage: (i) there will be no lattice damage due to implantation process and (ii) the dopant diffusion will be relatively free from surface effects. Such an epitaxial layer of germanium with boron peak was grown using Molecular Beam Epitaxy at the University of Warwick. The growth scheme is sketched in Fig. 6.9. The growth quality of the epitaxial germanium was checked using Nomarski imaging and Transmission Electron Microscopy. The results are described in Appendix C.

A peak boron concentration of 5×10^{18} atoms/cm^3 was chosen so that the estimated solid solubility limit of boron in germanium [129] was not exceeded. A specimen from the center

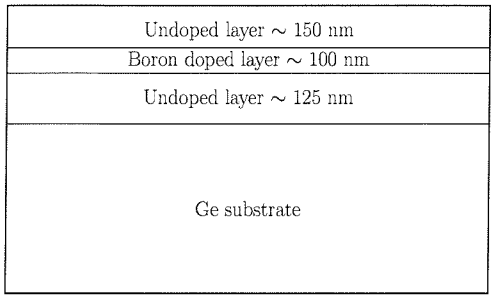

Figure 6.9: Growth structure for epitaxial germanium containing a boron doped layer. The epitaxial layer is grown at a temperature of 275 °C *using Molecular Beam Epitaxy. Peak boron concentration was* $5 \times 10^{18} atoms/cm^3$.

of the wafer was cleaned and sealed in an evacuated ampoule using the method described in Chap. 5 and this sample was subjected to a diffusion anneal of 875 °C for 12 h.

The SIMS profile obtained from the as grown and annealed sample is shown in Fig. 6.10. In order to calculate the diffusion coefficient, the as grown profile was used as input to TSUPREM and fitting to the experimental profile was achieved using the optimisation procedure described earlier in this chapter. The extracted value of diffusivity ($4.7\times10^{-16}cm^2/s$) is lower approximately by a factor of two than the value extracted from the implanted sample ($7.7\times10^{-16}cm^2/s$) which was subjected to the same thermal budget. The diffusivity value calculated using the epitaxial film is shown in Fig. 6.11 along with the values measured using implanted sources. The small variation, however, can be considered to lie within experimental errors. The proximity of the result not only provides a confirmation that the diffusion of boron is indeed slower than values published in literature but also rules out the possibility that implantation damage may have strongly affected boron diffusion.

Below, we discuss other factors that may have affected boron diffusion in germanium. An obvious consideration when studying diffusion in MBE grown layers is the effect of grown in defects. We note here that the growth of the epitaxial layer has been performed at a very low temperature of 275 °C. Using Nomarski imaging the defect density in these layers has been estimated to be $\sim10^7cm^{-2}$, however, TEM images suggest a higher value. Defect densities of this order can be expected to influence diffusion though not very strongly. In fact the grown in defects should accelerate diffusion rather than slowing it down. Hence the defects introduced during the growth of epitaxial layer are not expected to have influenced the measured diffusion coefficient significantly.

Both implanted and epitaxial samples had to be annealed in evacuated ampoules as an inevitable consequence of the high vulnerability of the germanium surface to oxidation. However, self-diffusion studies in germanium elsewhere have shown a reduction in the diffusion coefficient with pressure [46]. Thus an enhancement in diffusivity can be expected by annealing under vacuum as also shown by Räisänen *et al.* [78] for the case of silicon diffusion

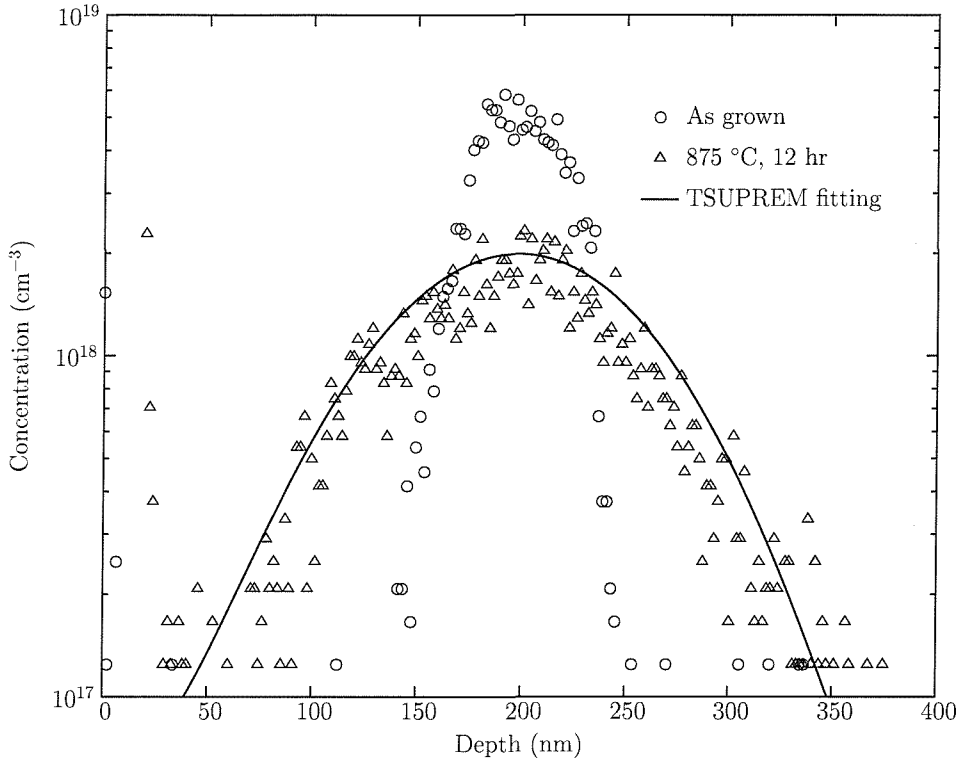

Figure 6.10: As grown and annealed boron SIMS profiles (sample D8) in epitaxial germanium. The fitting to the annealed profile is obtained using TSUPREM with as grown profile as input. The value of diffusion coefficient so calculated is consistent with that measured for implanted boron in germanium.

in germanium. If such is the case boron diffusivity values calculated in this study should present upper limits.

Another important factor affecting diffusion in this work could have been the effect of the protective layer. It has been reported that diffusion annealing under a silicon dioxide layer caused Sb to diffuse slower in germanium [118]. However this reduction is shown to be quite small and can be considered to lie within experimental error. Also the cause for this apparent retardation is not clear. Although the possibility of the silicon dioxide/nitride layer causing a retardation in diffusivity in our study can not be ruled out, it is highly unlikely that a strong retardation can be explained on this basis. It should also be noted that in epitaxially grown sample no protective layer has been deposited but still a diffusivity value comparable to that obtained from implanted samples has been calculated. It is proposed that a systematic study is required to fully characterise the effect of protective layers on dopant and self-diffusion in germanium.

Using a germanium epitaxial layer having a boron delta layer peak concentration below solid solubility, we have tried to eliminate the possibility of precipitation or formation of boron clusters which may as well retard diffusion. However further experiments using implanted sources and doped epitaxial layer in conjunction with Transmission Electron Mi-

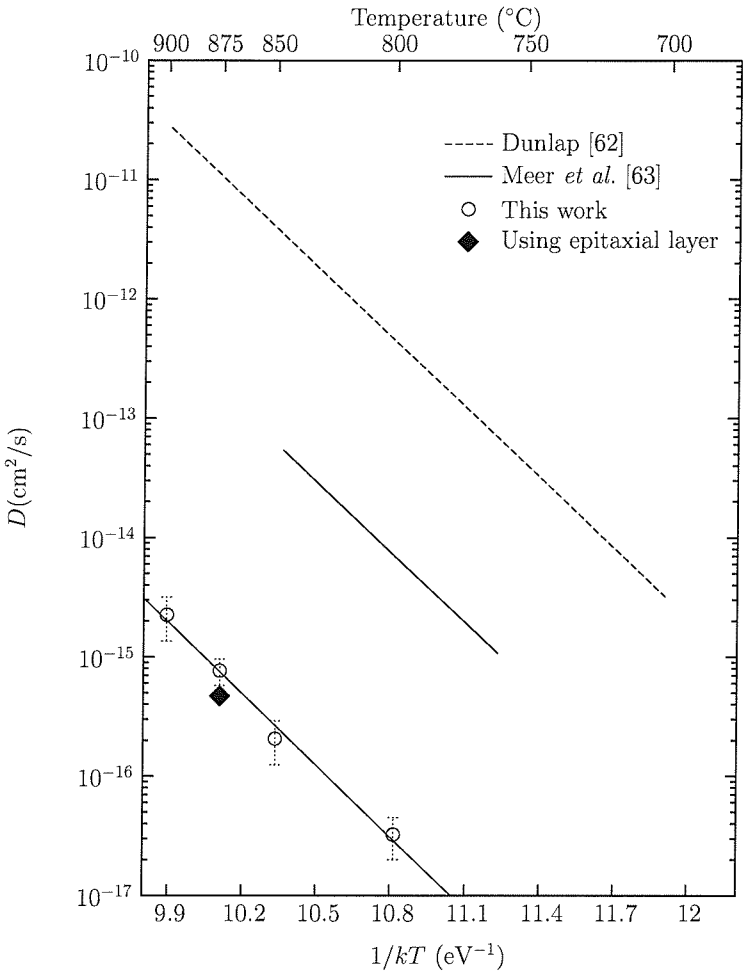

Figure 6.11: Arrhenius curve of boron diffusivity in germanium. The result of diffusivity calculated from boron doped epitaxial layer is depicted and is within error limits of the value calculated using implanted sources.

croscopy can shed more light on the issue of precipitation/cluster formation.

We note from the discussion in Chap. 3 and Fig. 3.2 that the activation energies for group V dopants and self-diffusion in germanium are reported to be smaller than those of group III elements (see also Table 6.4). Accordingly the diffusivity values for group V elements are higher than those for self- and group III elements (see Fig. 3.2). Applying Hu's analysis [14] on self- and dopant diffusion in germanium, we expect that if group III dopants diffuse via the same mechanism as self-diffusion in germanium then the activation energy for dopant diffusion should be similar or smaller than that for self-diffusion. As mentioned in Sec. 2.3.2, Hu modelled the lowering of activation energy barrier for impurity diffusion from self-diffusion to be of the order of interaction potential as:

$$E_{aV}^{self} - E_{AV} = \Delta E_{AV}^{3}. \tag{6.2}$$

We note that although the observed activation energy for group V elements is lower than the self-diffusion activation energy, this is not the case for group III dopants. Even among

group III elements boron shows a peculiar behaviour of possessing the highest value of activation energy and pre-exponential factor. This fact can be taken as an indication that diffusion of group III elements include a contribution from a mechanism other than vacancy which is believed to be responsible for self-diffusion in germanium. In silicon, successful defect injection studies have confirmed the dominating defect responsible for dopants and self-diffusion. However, such injection studies are not available for germanium.

Looking at the above equation, it can also be argued on the basis of negative interaction potential ($\Delta E^3 < 0$ i.e. repulsion) between the boron atom and vacancy that a higher activation energy for boron diffusion than self-diffusion activation energy in germanium is feasible. However, the measured difference of $\sim$1.5 eV in activation energies can not be explained purely on the basis of Coloumbic repulsion. Similarly, an elastic interaction between small boron atoms and vacancy can not account for such difference in activation energies.

In literature one finds evidence for a vacancy mediated self-diffusion process in germanium [4, 16], but for dopant diffusion, especially for group III elements, similar evidences such as doping dependence are missing (see Sec. 3.2.3). The similarity between self-diffusion and diffusion of other group III and V dopants and the characterisation of vacancy as dominant defect in germanium in thermal equilibrium from metal diffusion experiments has lead to the prevailing belief that the vacancy mechanism dominates the self- and dopant diffusion in germanium. Accordingly, the observed differences between boron and self-diffusion in germanium in the form of high value of activation energy and pre-exponential factor would indicate a diffusion mechanism other than the vacancy mechanism. Also, vacancies in germanium are believed to behave as acceptors [44]. Thus there exists a Coloumbic repulsion between substitutional boron atoms and vacancies. This effect makes diffusion via vacancies more improbable. A pure interstitial based diffusion for boron in germanium can be ruled out since we observe a much slower diffusion of boron as compared to that of Li which is a very fast interstitial diffuser [8]. If boron was to diffuse in germanium via a dissociative mechanism, involving either vacancies (e.g. Ni and Cu [102]) or impurity interstitials (e.g. Au [53, 132]), then a similarity in the diffused concentration profiles of boron and these metals highlighting high diffusivity should be obvious. In germanium, no element is yet known to diffuse via kick-out mechanism and hence a comparison to boron diffusion can not be made. It is unlikely though that such slow boron diffusion could be explained only on the basis of the kick-out mechanism. This leaves us with the possibility of an interstitialcy diffusion mechanism for boron in germanium.

In fact, indication of such a mechanism could be obtained on a close inspection of Fig. 3.1 given by Seeger *et al.* [4]. We noted from the figure that for germanium an interstitial contribution to the self-diffusion lies well below the vacancy contribution. A high value of activation energy of (6.45 eV) has been estimated for self-diffusion involving interstitials. There is no surprise that such a contribution does not show in dopant or self-diffusion experiments. A theoretical estimate for activation energy of self-diffusion via interstitials

using density functional theory with the PW91 functional is suggested to be >3.77 eV [56]. If we assume that a contribution from self-interstitials for self-diffusion exists it would explain the observed higher activation energy for boron diffusion in germanium via an interstitialcy mechanism. It could then be argued that since a thermal equilibrium concentration of self-interstitials in germanium is small, diffusion of boron which occurs with the help of self-interstitials is slower than the experimentally observed vacancy dominated self-diffusion.

To account for the high activation energy for boron diffusion in germanium, arguments similar to those presented by Nelson *et al.* [133] can be invoked. On the basis of a high exchange barrier, calculated by density functional theory, Nelson *et al.* have ruled out the vacancy as diffusion vehicle for boron diffusion in *silicon*. Following their calculation of a large exchange barrier energy between boron and vacancy, the observed high activation energy of boron diffusion in *germanium* can be accounted for. However, for the case of boron diffusion in *silicon* a high exchange barrier is more consistent with the interstitialcy mechanism than the vacancy mechanism as argued by Nelson *et al.*. This relates to the fact that the activation energy for the interstitialcy mechanism in silicon is comparatively low. Theoretical calculations similar to those of Nelson *et al.* [133] are required to establish a high first exchange barrier for boron diffusion in germanium. Depending on the activation energy for the interstitialcy mechanism this may explain the dominance of the interstitial contribution over the vacancy contribution in germanium.

However, activation energy could only act as indication of diffusion mechanism and can not be taken as a conclusive evidence. For example, experiments involving pressure effects on arsenic diffusion in germanium have shown a higher activation volume than expected on the basis of vacancy mechanism suggesting a different mechanism than self-diffusion although the activation energy for its diffusion lies well below the value of self-diffusion. In summary, although diffusion of boron via the vacancy mechanism can not be ruled out completely, the observation of a high activation energy and slower diffusion as compared to other dopants and self-diffusion brings in doubt the prevailing thought of vacancy mediated diffusion and suggests that interstitial contribution should also be considered.

We briefly discuss the observed immobile peak in annealed profiles. An important observation is that the immobile peak in boron concentration appears to be above the solid solubility limit of boron in germanium as given by Sharma [129]. Bidwell [134] has studied boron-germanium system and has ruled out the possibility of precipitation or formation of intermetallic compounds such as GeB or GeB_2. It is possible however that boron atoms get associated with implantation induced defects. At a boron concentration above its solid solubility value in germanium, the defects may act as nuclei for boron clusters. A thermodynamic driving force can be speculated to be present which favours stable configurations of boron clusters which does not become mobile even at very high temperatures. A better understanding of this behaviour can be achieved using TEM analysis in the region of immobile peak.

6.3 Silicon diffusion in germanium

6.3.1 Results

Annealing of samples implanted with silicon was performed in much the same way as the boron implanted samples using evacuated ampoules. The details of the samples are listed in Table 4.3 of chapter 4. Diffusion was investigated in the temperature range 750–890 °C. Note that except sample S2 all other samples were annealed without any surface cap. For diffusion anneal carried out at 750 and 825 °C (samples S1 and S3) the annealed profiles are shown in Fig. 6.12 along with the as implanted profile. One distinct characteristic found in these diffused profiles is the distinguishable peak near the surface region. Except for the lowest temperature of study i.e. at 750 °C, this anomalous peak was found to be present in all annealed profiles. Similar surface peaks in the annealed profiles have been reported in the literature previously [78] although their origin is not fully understood. Since silicon and germanium are completely soluble in each other, we can rule out the possibility of silicon precipitation. Therefore the peak could have been caused by immobility due to the trapping of silicon at the implantation defects. On the other hand, damage recovery might have been achieved during the 750 °C annealing procedure in which the sample was inserted slowly compared to sudden exposure to high temperatures during annealing at higher temperatures as mentioned in Sec. 6.1. Further investigation using e.g. TEM can shed more light into this behaviour but could not have been carried out within time frame available for this study.

The annealed silicon concentration profiles can be divided in two regions: the anomalous surface peak (~100 nm in Fig. 6.12) region and the in-diffused region. To extract diffusivity values from the annealed profiles, a procedure similar to that described in Sec. 6.2.2 for the case of boron is used. No attempts were made to fit the surface peak region. Due to the complete solubility of silicon in germanium, the solid solubility model was considered inappropriate.

A high values for the segregation and transport coefficient was chosen to implement the experimental condition of dose loss at the surface since most of the samples were annealed without surface protection. The point defect concentrations were chosen to be at their thermal equilibrium value by invoking PD.FERMI model. The as-implanted profile worked as the input and the diffusion coefficient (implemented by varying DIX.0 and setting DIX.E=0) was the only variable parameter in the optimisation procedure of the program. Result of fitting using such procedure is shown in Fig. 6.12. Due to the presence of the anomalous surface peak, one should be careful in extracting conclusive information from the absolute values of the calculated diffusion coefficients.

The values of the diffusion coefficient obtained from fitting are shown in Fig. 6.13 along with results from previous measurements from the literature in the form of an Arrhenius curve. The calculated values of activation energy and pre-exponential factor calculated

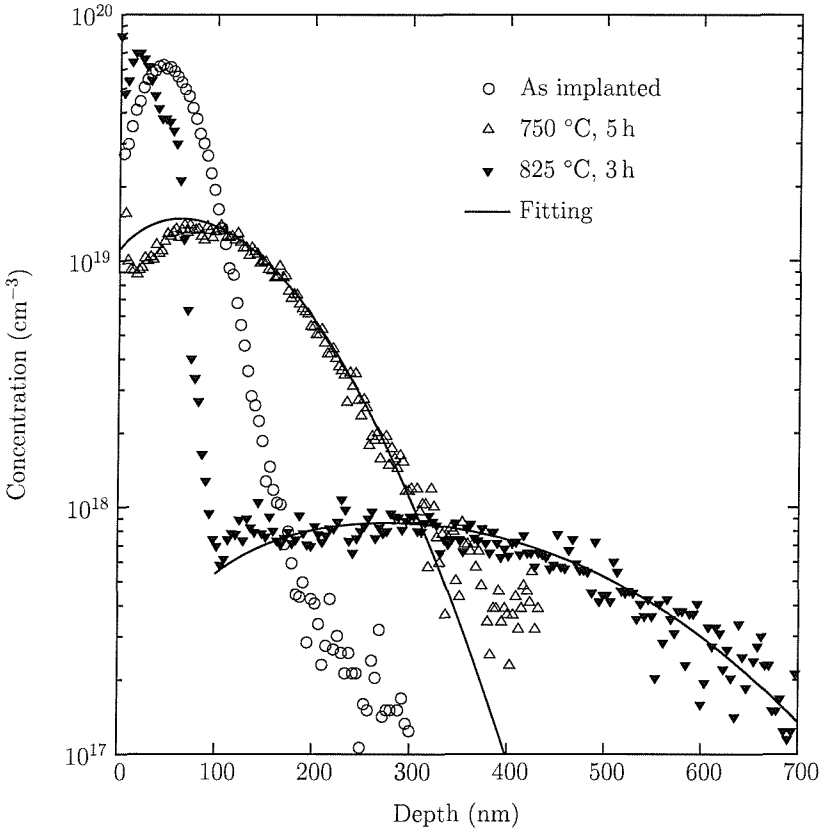

Figure 6.12: Silicon concentration profiles of as-implanted (sample S0) and diffused (samples S1 and S3) samples in germanium obtained using SIMS. Silicon was implanted in germanium with 50 keV *and* $5 \times 10^{14}\text{cm}^{-2}$ *fluence and annealed at temperatures and times mentioned in figure. No attempt was made to fit the anomalous peak in the diffused profile while fitting using TSUPREM.*

in this study are given in Table 6.3 along with literature values. Although the diffusion coefficients calculated in this study can be considered approximate due to the presence of an anomalous peak in these profile we find that the activation energy and pre-exponential factor assessed using these values are in remarkable agreement with values from literature.

6.3.2 Discussion

It must be emphasised that a comparison of diffusivity values and activation energy calculated in this work with literature values should be done with care. Nevertheless, one finds that the diffusion coefficient values from this work in agreement with literature values except that given by Strohm *et al.* [25]. Strohm *et al.* have presented silicon diffusivity values which are a factor 2–3 higher than those reported by others. We note that a short-lived-radiotracer of silicon with a half-life ~2.6 h, has been used in their study. The temperature range of the experiment is also limited to 843–904 °C with very short annealing times. These two factors may have caused an overestimation of silicon diffusivity in germanium in their experiment.

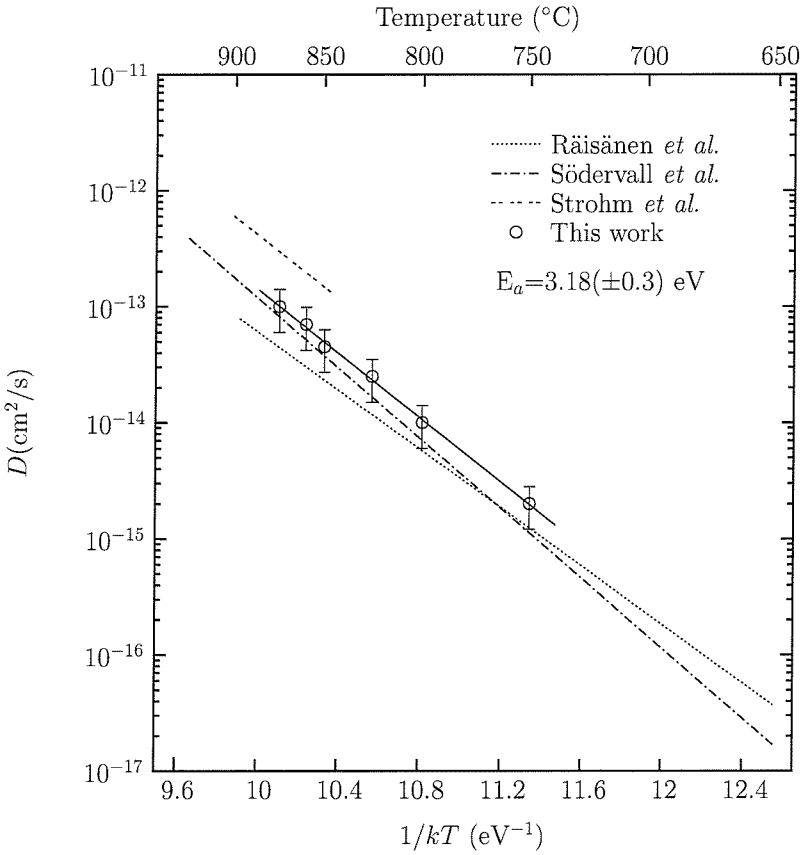

Figure 6.13: Diffusion coefficient of silicon in germanium plotted against inverse temperature. The measured values from this work though approximate match the values in literature within experimental errors.

Räisänen *et al.* [78] have also used the implantation technique to study silicon diffusion in germanium. The observation of a surface peak in their diffused profiles as shown in Fig. 6.14 is a peculiar similarity to this work. Such a surface peak was not observed when the diffusion is carried out using sputter deposited silicon on germanium surface [65]. Thus we can argue that the observed anomalous peaks in both studies be caused by implantation.

A comparison of activation energies of silicon diffusion in germanium with self-diffusion and other group IV elements can be made. In the literature [57], the values of activation energy for self-diffusion in germanium is found to vary between 2.95–3.14 eV. Recent measurements of Fuchs *et al.* [47] and Strohm *et al.* [25] are in complete agreement with these values. For another isovalent impurity Sn, one finds very similar activation energy values ranging between 2.68–3.26 eV [57, 58, 59, 60]. The values for silicon diffusion in germanium can be put in the range 2.9–3.47 eV and these values seem to be in agreement with the values for self- and Sn diffusion in germanium.

On the mechanism front, germanium self-diffusion is believed to be mediated by vacancies [8]. Considering the similarities (mainly the activation energy) among tin, silicon and self-diffusion in germanium, it has been concluded [8] that tin and silicon atoms diffuse using the same mechanism as that of self-diffusion. Our silicon diffusion results seem to agree

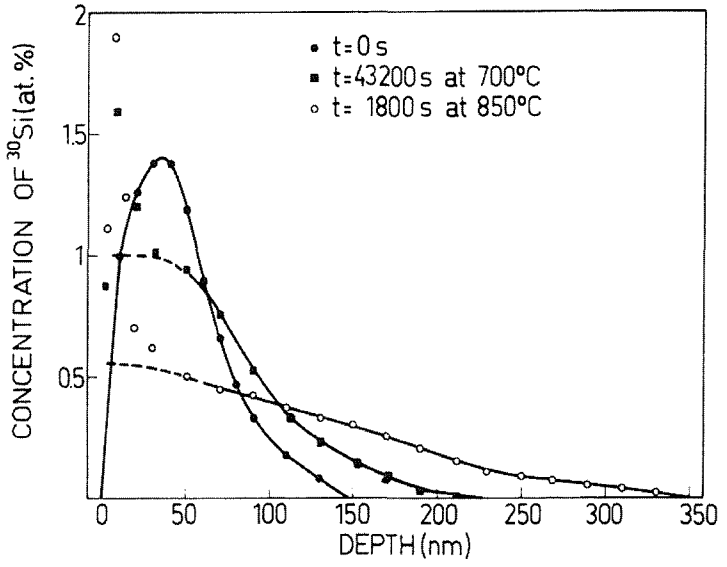

Figure 6.14: Experimental concentration profiles of ^{30}Si taken from Ref. [78]. The implantation dose and energy were $6 \times 10^{16}\,cm^{-3}$ and 50 keV, respectively. A clear surface peak of silicon in the annealed profile profile can be observed similar to results reported in this work.

with parameters from other studies and hence can be taken to argue that silicon diffuses in germanium mainly by vacancies.

However, it should be noted that absolute values of the diffusion coefficient of silicon in germanium from all studies are lower than those of the self-diffusion coefficient of germanium. Another recent measurement on silicon diffusion in $Si_{0.20}Ge_{0.80}$ [135] requires a mention here in which it was found that diffusion coefficient of silicon is lower than its counterpart germanium at the same alloy composition. The activation energy was calculated to be 3.57 eV for silicon diffusion which was higher than the germanium diffusion value of 3.48 eV in $Si_{0.20}Ge_{0.80}$ alloy. Thus we can safely conclude that like boron, silicon also diffuses slower in

D_o (cm^2/s)	E_a (eV)	Temperature range (°C)	Experimental technique	Reference
0.24	2.9	650–900	Implantation, (p-γ) resonance	[78]
140	3.47	650–930	Sputter deposition, SIMS	[65]
43	3.19	843–904	Radiotracer, sectioning by ion beam	[25]
9.7	3.18	750–890	Implantation, SIMS	This study

Table 6.3: Comparison of silicon diffusion parameters from literature with present work. Literature values are taken from individual studies. A close agreement of literature with present work can be noticed.

germanium than self-atoms. For the case of silicon atoms in germanium we do not expect any Coulombic interaction between vacancies and silicon atoms. Elastic interaction however may play a role. Thus a slightly larger activation energy for silicon diffusion in germanium than germanium self-diffusion can be brought into agreement to diffusion by vacancy mechanism by invoking Coulombic/elastic interaction of silicon atoms with vacancies. It should also be noted that doping dependence of silicon diffusion in germanium [78] is opposite to that shown by germanium self-diffusion. Thus contribution from a different charge state than responsible for self-diffusion in germanium or contribution from another defect can not be completely ruled out. Unfortunately, defect injection during diffusion anneals have not been characterised for germanium and hence independent confirmation on the dominating diffusion mechanism has not been feasible.

6.4 Implications for Si-Ge alloys

In Chap. 1, the importance of the study of boron diffusion in germanium as a tool to understand its diffusion behaviour in Si-Ge alloys as a function of germanium content has been highlighted. The current knowledge in self- and dopant diffusion in Si-Ge alloys was reviewed in Chap. 3. We refresh our knowledge with very recent developments and previous understanding.

For self-diffusion studies, germanium diffusivity in Si-Ge is found to increase with germanium content [25, 70, 76]. The activation energy reduces from germanium diffusion in silicon (~4.7 eV) to germanium diffusion in germanium (~3.1 eV). The reduction in activation energy and increase in diffusivity are correlated with the Arrhenius expression $D = D_0 \exp(E_a/kT)$. It should however be noted that there are two other important factors that may affect the diffusivity other than the activation energy: the temperature and pre-exponential factor. We must consider the effect of temperature. For an anneal carried out at say 900 °C (38 °C below melting point) in germanium, thermal activation is much pronounced than that in pure silicon as we are approx. 500 °C below the melting point. For Si-Ge alloy with say 20% germanium content, the melting point reduces to about 1260 °C causing more thermal activation than in silicon. Thus an increase in diffusivity is expected. It should be emphasised that the observed activation energy is assumed to be independent of temperature. Hence we can safely assume that a decrease in activation energy represents the reduction in the energy barrier to the flow of atoms through the lattice with the help of point defects.

For silicon self-diffusion and its diffusion in germanium differences in activation energy similar to germanium self-diffusion and its diffusion in silicon can be found. The same applies to dopant diffusion Si-Ge alloys. A representation of this fact is given in Table 6.4 where the values of activation energies for self- and dopant diffusion in silicon as well as in germanium are given. A pictorial representation of the Table 6.4 is given in Fig. 6.15.

	Activation energy eV	
Element	Si	Ge
Si	4.7	3.2
Ge	4.7	3.1
P	3.6	2.5
As	4.2	2.4
Sb	4.0	2.7
B	3.5	4.6
Al	3.98	3.45
Ga	3.34	3.31
In	3.77	3.63

Table 6.4: Trends of activation energy for self- and dopant diffusion in silicon and germanium. The mean values from literature [6, 57] have been tabled.

It was highlighted in Sec. 3.3 that except boron, self-and dopant diffusivity in relaxed Si-Ge alloys is higher than in silicon. We have noted from above the table that the activation energies for diffusion decrease from its value in pure silicon to germanium. The case of boron shows an exception where the activation energy in pure germanium is higher than in silicon. Also literature suggests a reduction in diffusion coefficient of boron with the addition of germanium at least up to 50% germanium. This reduction is against an expected increase in diffusivity due to the increase in thermal activation. Since the activation energy for dopant diffusion represents the formation and migration energy of the defect assisted diffusion (see Eq. 2.22), above mentioned facts imply that reduction in boron diffusion could be due to an increase in formation and/or migration energy of the defect responsible for diffusion.

In a recent measurement on boron diffusion in epitaxial Si-Ge alloys [136], the diffusion coefficient of boron was found to increase gradually for germanium content >50% to 86% at 900 °C to reach a value at pure germanium calculated in this study. This result is also an independent confirmation of our observation of slower boron diffusion in germanium as compared to self- and other group III and V dopants.

The explanation of the observed behaviour of self- and dopant diffusion has been discussed in Chap. 3. For the case of boron it has been argued by Kuo *et al.* [39] that a B-Ge pairing causes a slower diffusion in relaxed Si-Ge alloys compared to silicon. On the other hand, to explain almost no change in boron diffusivity from silicon to Si-Ge alloys with up to 24% germanium, Zangenberg [37] argued that the enhancement due to chemical effect counterbalances the retardation due to B-Ge pairing. The diffusivity values of Uppal *et al.* [136] measured on epitaxially grown Si-Ge using implantation sources match those of Kuo

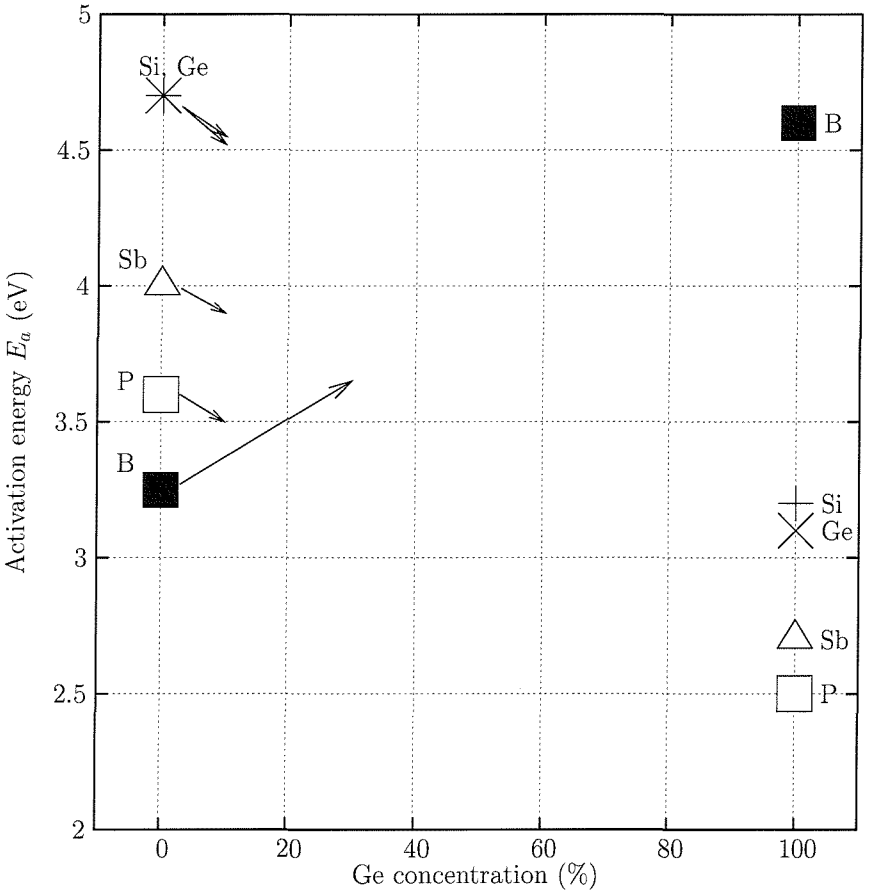

Figure 6.15: Activation energy of self- and dopant diffusion in silicon and germanium plotted against Ge content. The values are taken from Refs. [6] and [57]. We notice that activation energy for self- and dopant diffusion in germanium is lower than in silicon except boron. Accordingly the diffusion coefficient for self- and dopant diffusion increases as a function of germanium content except for boron.

et al. at 50% on epitaxially grown boron doped material and show a gradual increase towards 100% germanium. Pairing has been found insufficient to explain the observed behaviour of boron diffusion in Si-Ge alloys in the whole alloys spectrum.

The boron and phosphorus are believed to diffuse solely via the interstitialcy mechanism in silicon [6]. Antimony is known to diffuse primarily via the vacancy mechanism in both silicon and in germanium [137]. If boron was to diffuse via the vacancy mechanism in silicon as well as germanium, it would follow the trend of antimony. On the other hand if a changeover in mechanism from interstitial to vacancy has to occur as in the case of phosphorus, a behaviour similar to phosphorus in Si-Ge alloy spectrum can be expected. Thus a changeover in boron diffusion mechanism seems improbable. Theoretical calculations [81] have suggested a change in the formation energy of vacancies in Si-Ge alloys as compared to silicon as a function of the number of nearest neighbour atoms. The apparent increase in activation energy of boron diffusion in Si-Ge [37] is speculated to be caused by an increase in the self-

interstitial formation energy. We have also noted a higher value of activation energy for boron diffusion in germanium. Thus, it seems more likely that the reduction of boron diffusion in the silicon rich Si-Ge alloys is related to the increase in formation and/or migration energy of the defect(s) responsible for diffusion.

Following Zangenberg's [37] suggestion, it can be speculated that at low germanium content in Si-Ge alloys, boron diffusivity is dragged down by the increase in the self-interstitial formation energy. B-Ge pairing may also play a role. At germanium concentration above 50%, germanium interstitials start to control boron diffusion and the diffusivity recovers to its values at 100% germanium. From the arguments presented, it can be concluded that boron makes a special case in Si-Ge alloys. We speculate that boron diffuses via an interstitial-mediated i.e. interstitialcy mechanism in both silicon and germanium.

Chapter 7

Conclusions and future perspective

7.1 Conclusions

The main objective of this study was to calculate the diffusion coefficient of boron in germanium using the state of the art techniques. Earlier data on boron diffusion had been measured mainly by electrical methods 3–4 decades ago and disagreement over diffusivity value was large. Studying boron diffusion at the pure germanium end of Si-Ge alloys may help in further understanding the rather unique behaviour of boron in the silicon rich region. In addition to boron, silicon diffusion in germanium was also explored expecting that diffusion in this system would be similar to self-diffusion in germanium. The work carried out in this study constitutes the first measurement of boron and silicon diffusion in germanium using a combination of ion implantation and SIMS techniques.

It was soon realised that diffusion annealing of germanium requires special attention in view of the vulnerability of germanium surface to oxidation. Yet a limited study of diffusion as a function of temperature and implantation dose was successfully completed for boron diffusion in germanium. For silicon diffusion in germanium this study concentrated on the measuring diffusivity as a function of temperature.

Using a carefully designed set of experiments involving boron implantation in crystalline germanium wafers of different orientation and in pre-amorphised germanium it was confirmed that channelling phenomenon is present in the case of boron implantation in crystalline germanium and plays a dominant role in deciding the implantation profile. For diffusion studies, boron implantation in dose range 3×10^{13}–$6\times10^{14}\text{cm}^{-2}$ and energy range 5–20 keV has been utilised. Diffusivity values have been measured from the annealed profiles by subjecting samples to furnace annealing in the temperature range 800–900 °C in evacuated ampoules. A slower diffusion of boron in germanium compared to literature has been characterised by profiling elemental boron using SIMS. The measured diffusivity is found consistent with variation in implantation dose, annealing ambient and surface protective layer. Conducting diffusion experiments on epitaxial germanium layers doped with a boron delta layer grown

by MBE, it was established independently that boron diffusion is indeed slow and that implantation induced defects are not responsible for the observed slow diffusion. An activation energy of $4.6(\pm 0.3)$ eV and a pre-exponential factor of 1.2×10^5 cm^2/s can be assigned for boron diffusion in germanium in the temperature range studied. Based on the differences in boron diffusion in germanium and self-diffusion in germanium (activation energy as well as absolute diffusivity) it is suggested that the diffusion mechanism for boron in germanium should be reconsidered. In addition for the first time a direct estimation of solid solubility of boron in germanium has been made using diffused profiles and a value of $\sim2\times10^{18}$ atoms/cm^3 at 875 °C has been assigned.

Silicon diffusion in germanium has also been studied in the temperature range 750–875 °C using implantation doping and furnace annealing. Silicon diffusion in the temperature range studied can be described well by an Arrhenius curve corresponding to an activation energy of $3.2(\pm 0.3)$ eV and a pre-factor of 9.7 cm^2/s. The diffusion parameters are in close agreement with the values reported in literature. An anomalous peak in the diffused profiles has been observed and is attributed to implantation induced defects. The similarity of self- and silicon diffusion in germanium suggests that the two elements show diffuse via similar mechanism.

As an implication of the present study it is suggested that boron shows a unique diffusion behaviour in Si-Ge alloys where its diffusivity reduces, as compared to in Si, in the Si-rich end and finally recovers to its values in germanium. The boron diffusion behaviour in bulk germanium suggests that it is highly unlikely that a changeover of diffusion mechanism occurs as a function of germanium content in the whole alloys spectrum.

7.2 Further work

The experiments performed in this study leave opportunity to perform a more complete study in this area. In general, very little is known about dopant diffusion in germanium. Boron is an exception as only limited studies on boron diffusion have been performed. The present project can be extended to include the measurement of diffusivity of boron in germanium as function of time and temperature to improve our knowledge about its diffusion behaviour. The measurement of boron diffusivity as a function of implantation dose and energy is also important. Further characterisation of implantation induced defects in germanium using TEM and the effect of such defects on impurity diffusion is also required. The growth of epitaxial germanium with boron delta peak can be optimised and diffusion studies can be performed as a function of time and temperature which can be compared to studies involving implantation doping.

To understand the diffusion mechanism of boron in germanium more clearly one can utilise defect injection in germanium along similar lines to those performed in silicon. Rapid thermal annealing can be used as a technique under different ambient and/or with different protective layers which may provide direct indication of the underlying diffusion mechanism.

In addition, doping dependence using isoconcentration experiments similar to those used by Willoughby *et al.* [138] can be performed to study the Fermi level effect on diffusion. A combination of above mentioned experiments shall provide conclusive evidence on the dominant defect responsible for diffusion and its charge state.

An interesting extension to the present study would be to measure boron diffusivity as a function of temperature in Si-Ge at high germanium contents due to the importance of such material in p-MOSFET devices. Furthermore boron diffusivity as a function of germanium content needs to be established to understand the diffusion behaviour of boron in the whole Si-Ge alloys spectrum.

On silicon diffusion in germanium, characterisation of the implantation induced defects using TEM is a possible extension. Such studies may explain the anomalous surface peak observed in this study. Also the studies suggested for the case of boron can also be extended to silicon in order to establish defect and the charge state of dominating defect responsible for diffusion of silicon in germanium.

Appendix A

Simulation proceedure

Following is an example of the input file for the TSUPREM.

Define a new material with material properties of germanium. It is important to name the material as "silicon" to invoke the solid solubility model

```
MATERIAL SILICON DY.DEFAU=.1 +
 E.FIELD AT.NUM=32 AT.WT=72.61 +
 DENSITY=5.323 MOL.WT=72.61 SEMICOND NI.0=7.58e18 NI.E=0.335 NI.F=1.5 +
 N.CONDUC=1.02e19 N.VALENC=3.87e16 BANDGAP=0.67 AFFINITY=4.05 G.DONOR=2 +
 G.ACCEPT=4 EPSILON=16.3
```

Define the mesh

```
LINE      X LOCATION=0 SPACING=0.1
LINE X LOCATION=2 SPACING=0.1
LINE Y LOCATION=0 SPACING=0.1
LINE Y LOCATION=2 SPACING=.1
```

Initialise

```
INITIALIZE <111> ROT.SUB=0.0 RATIO=1.5 CONCENTR ANTIMONY=1e14
```

Deposit germanium

```
DEPOSITION SILICON THICKNES=99.65 SPACES=100 CONCENTR ANTIMONY=1e15
DEPOSITION SILICON THICKNES=0.35 SPACES=500 CONCENTR ANTIMONY=1e15
```

load and plot the as-implanted file

```
PROFILE boron +
 IN.FILE=../data/A1test.dat +
 OFFSET=-.00225
SELECT    Z=log10(boron)
PLOT.1D   X.VALUE=0.0 LINE.TYP=1 COLOR=1 LEFT=-100 RIGHT=-99.5 BOTTOM=16 +
 TOP=20 X.SIZE=0.25 Y.SIZE=0.25 X.OFFSET=2.0 Y.OFFSET=2.0 T.SIZE=0.4 ^CLEAR
```

Optimisation loop with diffusivity and solid solubility as variable parameters

```
LOOP OPTIMIZE PLOT
ASSIGN NAME=DCOEF N.EXPRESS=1E-16 LOWER=9E-17 UPPER=9E-16 LOG
ASSIGN    NAME=SSLIMIT N.EXPRES=5e18 LOWER=3e18 UPPER=8e18 LOG
BORON     SILICON DIX.0=0 DIX.E=0 DVX.0=@DCOEF DVX.E=0 DIP.0=0 DIP.E=0 DVP.0=0 +
 DVP.E=0 DIPAIR.0=0 DIPAIR.E=0 DVPAIR.0=0 DVPAIR.E=0 R.I.S=0 E.I.S=0 R.IP.V=0 +
 E.IP.V=0 R.V.S=0 E.V.S=0 R.VP.I=0 E.VP.I=0 SS.TEMP=850 SS.CONC=@SSLIMIT +
 SS.CLEAR CM.SEC
METHOD    PD.FERMI
DEPOSITION OXIDE THICKNES=.002 SPACES=10 CONCENTR
DIFFUSION TIME=1440 TEMPERAT=850
ETCH      OXIDE ALL
EXTRACT   X=0 SILICON DISTANCE=100 Y.EXTRAC NAME=YSURF
SELECT Z=LOG10(BORON)
EXTRACT   X=0 SILICON VAL.EXTR NAME=DIFT +
 T.FILE=../data/X1test.dat V.COLUMN=1 +
 V.LOWER=-100 V.UPPER=-99.7 V.TRANSF=V+@YSURF T.COLUMN=2 T.LOWER=1E17 +
 T.UPPER=1e20 T.TRANSF=LOG10(T) WEIGHT=1.0 TOLERANC=.1 MIN.ABS=1e-10 +
 MIN.REL=1e-10
L.END
```

Plot the diffusion boron concentration profile

```
SELECT    Z=log10(boron)
PLOT.1D   X.VALUE=0.0 LINE.TYP=1 COLOR=2 SYMBOL=4 LEFT=-100 RIGHT=-99.5 +
 BOTTOM=16 TOP=20 X.SIZE=0.25 Y.SIZE=0.25 X.OFFSET=2.0 Y.OFFSET=2.0 T.SIZE=0.4 +
 ^CLEAR
```

Appendix B

Observations

B.1 Scanning Electron Microscopy

In initial set of experiments annealing was carried out at relatively low temperature of 675–725 °C in argon and forming gas ambient during which surface degradation was observed. Higher damage was observed at higher temperature. Strangely enough, for annealing at 700 and 725 °C anneal for 60 and 30 min respectively, apart from a high etch pit density on surface, the sample periphery lost its mirror like finish. Nomarski image of such a damage on sample periphery is given in Fig. B.1. For the two anneals samples were protected by a silicon-dioxide layer. It is believed that this damage has been caused by oxidation of the samples which starts at the periphery of the sample surface causing more damage there than in the middle of the sample as indicated by Nomarski image (Fig. B.1). It was observed that amount of surface damage observed was lesser if the ambient was changed from argon to forming gas flowing at a rate of 1–2 l/min

Fig. B.2 shows the SEM image of damaged region of the same sample. Regions marked (b) and (c) are the same as those in Fig. B.1. Region (c) is highly damaged and comes from close to the edge of the sample whereas regions marked (b) is seen relatively undamaged. It should be noted that the presence of etch pits hinders quantitative SIMS.

B.2 Hot probe measurement

A limited set of hot probe measurements were also performed on the as implanted as well as annealed boron implanted samples to check the electrical activity. Hot probe measurement makes use of two probes one of which is at a relatively higher temperature than the other. An observation of opposite voltage on the two sides of the samples means the two sides are oppositely doped. Since the starting wafer were n-type, for the case of boron implanted germanium this would mean that a pn-junction exists in the samples which would indicate electrically active (substitutional) boron. From the measurements, it was found that the

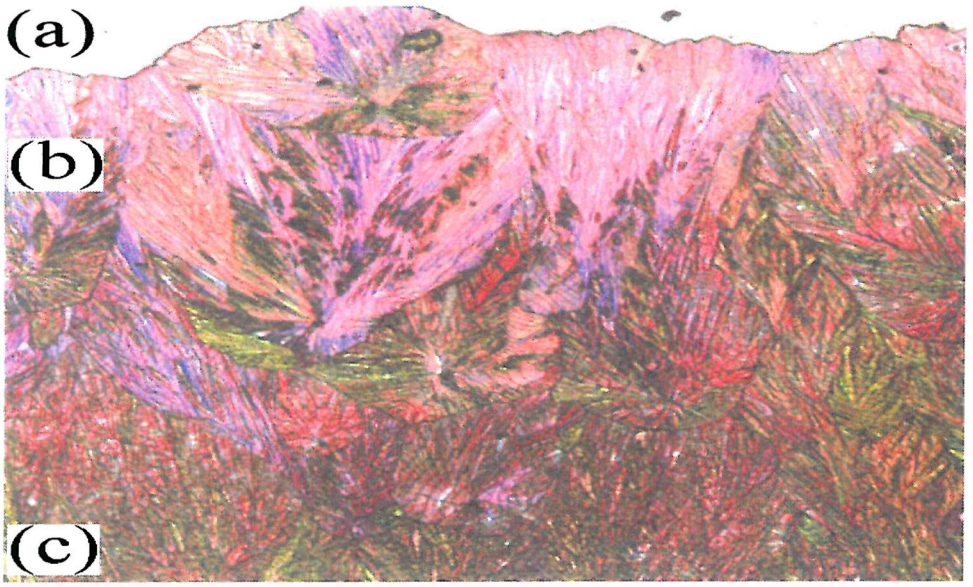

Figure B.1: Nomarski image of the damaged region of a sample after annealing. Region marked (a) *is polished surface. Region* (b) *and* c *are highly damaged as mirror like finish of the samples is lost during annealing.*

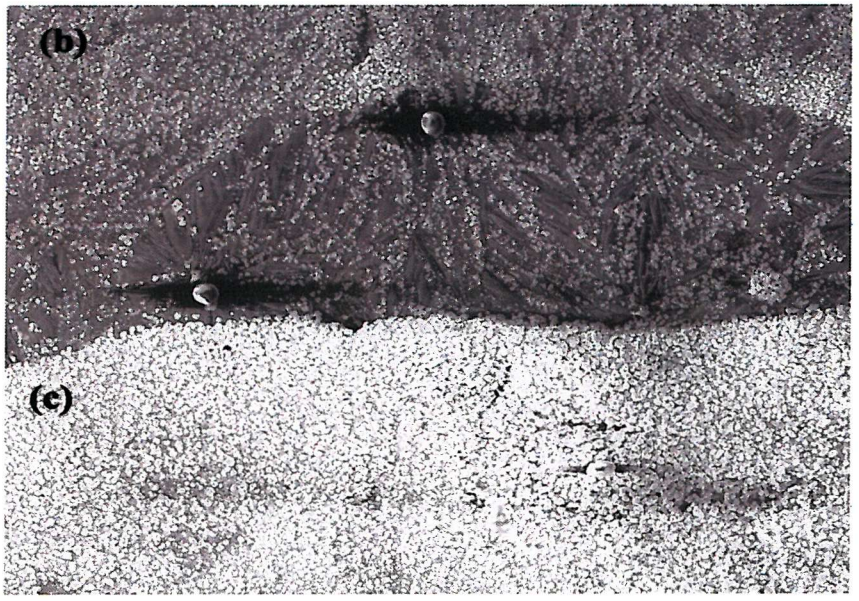

Figure B.2: SEM picture of the damage of a sample due to annealing. The picture is taken from the edge of the sample where maximum damage occurred. Region (c) *suffered more damage than region* (b) *as it is close to the edge.* (See also Fig. B.1)

samples implanted with dose $> 1\times10^{14}\text{cm}^{-2}$ did not show a p-type surface in as implanted state. However after heat treatment all the samples showed presence of a pn-junction. These measurements can be interpreted as that for dose $> 1\times10^{14}\text{cm}^{-2}$ boron is not electrically active in as implanted state but after annealing boron atoms occupy substitutional sites and become electrically active.

B.3 Atomic force microscopy

As discussed in Sec. 5.3 the implantation tails observed in boron concentration profiles could be caused by the non-uniform sputtering of germanium during SIMS analysis. In order to determine if roughening of the crater has occurred due to non-uniform sputtering, the crater bottom was profiled using atomic force microscopy. Image B.3 presents AFM image of a SIMS crater on Ge sample. Roughening of the order of 1–2 nm can be estimated suggesting that a largely uniform sputtering has taken place during SIMS analysis. This observation helped in concluding that implantation tails described in Chap. 5 were not artifact of SIMS.

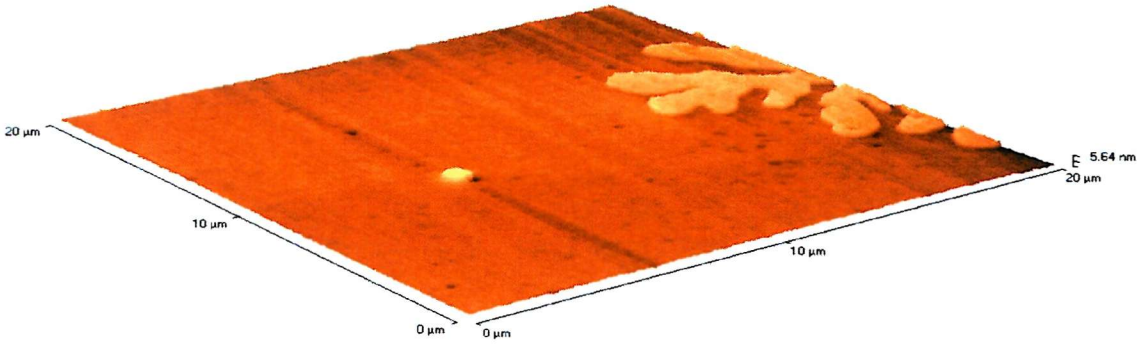

Figure B.3: Atomic force microscopy image of the crater bottom created during SIMS analysis. The measured roughness of the crater does not exceed 1–2 nm *which suggests that uniform erosion of germanium has been achieved during the SIMS.*

Appendix C

Characterisation of epitaxial germanium

To circumvent the effect of ion-implantation damage on boron diffusion, an epitaxial germanium layer with a boron delta layer was grown on <100> germanium substrate using MBE. The growth temperature was 275 °C. The growth quality of epitaxial germanium layer was checked using Nomarski imaging and transmission electron microscopy. The Nomarski image of the surface of epitaxial layer is shown in Fig. C.1. The defect density was estimated by

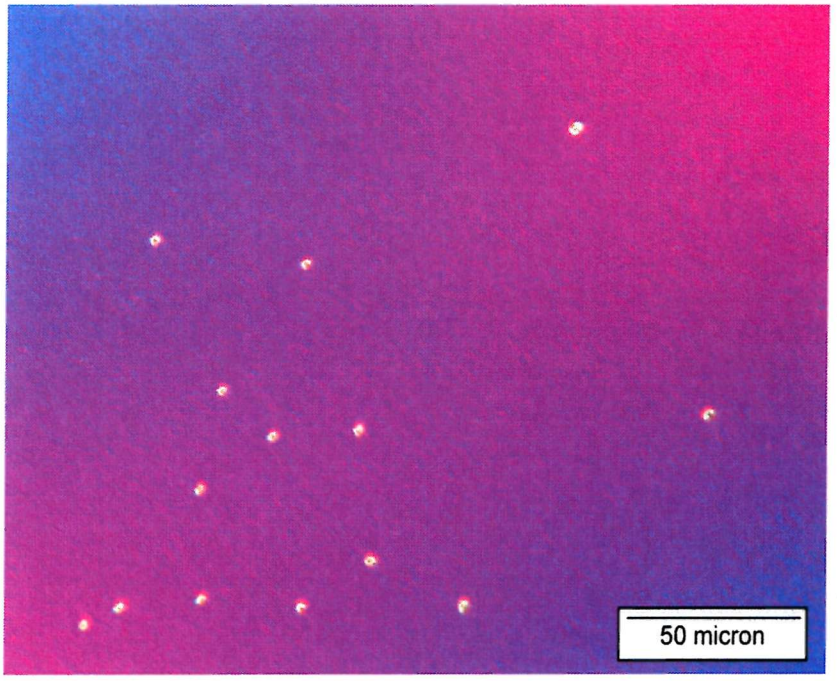

Figure C.1: Nomarski image of epitaxial germanium grown using Molecular Beam Epitaxy. Starting with germanium wafer as substrate a 375 nm *thick layer was grown at* 275 °C. *The epitaxial layer was crystalline but with some growth defects which can be seen in the figure as shining dots.*

measuring the pinholes on the surface, averaged over a large area and was found to be of the order of $10^7\,\mathrm{cm}^{-2}$. The epitaxial layer was crystalline but pinholes could be observed on the wafer surface.

A cross-sectional view of the epitaxial germanium layer is shown in Fig. C.2. The image shows the presence of defects which originate from the interface between the substrate and epitaxial layer and propagate up to the surface. The structure of the defects is typical of low temperature MBE growth.

Figure C.2: TEM image of epitaxial germanium grown using Molecular Beam Epitaxy. Starting with germanium wafer as substrate ~375 nm *thick layer was grown at* 275 °C. *The image shows cross-sectional view of the growth related defects.*

Bibliography

[1] A. S. Grove, *Physics and technology of semiconductor devices.* Wiely, 1967, ch. 2.

[2] M. L. Lee, C. W. Leitz, Z. Cheng, A. J. Pitera, T. Langdo, M. T. Curie, G. Taraschi, E. A. Fitzgerald, and D. A. Antoniadis, "Strained Ge channel p-type metal-oxide-semiconductor field-effect transistor grown on $Si_{1-x}Ge_x$/Si virtual substrates," *Applied Physics Letters*, vol. 79, pp. 3344–3346, 2001.

[3] A. F. W. Willoughby, "Diffusion mechanism in SiGe alloys," in *Semiconductor Silicon*, H. R. Huff, H. Tsuya, and U. Gösele, Eds., vol. 98-1. San Diago, California: Electrochemical Society, 1998, pp. 871–883.

[4] A. Seeger and K. P. Chik, "Diffusion mechanism and point defects in silicon and germanium," *Physica Status Solidi*, vol. 29, pp. 455–542, 1968.

[5] F. Seitz, "On the theory of diffusion in metals," *Acta Crystallographica*, vol. 3, pp. 346–360, 1950.

[6] P. Fahey, P. B. Griffin, and J. D. Plummer, "Point defects and dopant diffusion in silicon," *Reviews of Modern Physics*, vol. 61, pp. 289–384, 1989.

[7] S. M. Hu, "Nonequilibrium point defects and diffusion in silicon," *Materials Science and Engineering: R: Reports*, vol. 13, pp. 105–192, 1994.

[8] W. Frank, U. Gösele, H. Mehrer, and A. Seeger, "Diffusion in silicon and germanium," in *Diffusion in crystalline solids*, G. E. Murch and A. S. Nowick, Eds. New york: Academic, 1984, pp. 63–142.

[9] U. Gösele and F. Morehead, "Diffusion of zinc in gallium arsenide: A new model," *Journal of Applied Physics*, vol. 52, pp. 4617–4619, 1981.

[10] F. C. Frank and D. Turnbull, "Mechanism of diffusion of copper in germanium," *Physical Review*, vol. 104, pp. 617–618, 1956.

[11] B. Tuck, *Introduction to diffusion in semiconductors*, ser. IEE monograph series. Institute of Electrical Engineers, 1974.

[12] A. F. W. Willoughby, "Atomic diffusion in semiconducotrs," *Reports on Progress in Physics*, vol. 41, pp. 1665–1705, 1978.

[13] W. Meyer and H. Neldel, "Relation between the energy constant and the quantity constant in the conductivity-temperature formula of oxide semiconductors," *Zeitschrift für Technische Physik*, vol. 12, p. 588, 1937.

[14] S. M. Hu, "On interaction potential, correlation factor, vacancy mobility and activation energy of impurity diffusion in diamond lattice," *Physica Status Solidi (B)*, vol. 60, pp. 595–604, 1973.

[15] S. T. Dunham and C. D. Wu, "Atomistic modes for vacancy-mediated diffusion in silicon," *Journal of Applied Physics*, vol. 78, pp. 2362–2366, 1995.

[16] D. Shaw, "Self- and impurity diffusion in Ge and Si," *Physica Status Solidi (B)*, vol. 72, pp. 11–39, 1975.

[17] R. F. Peart, "Self-diffusion in intrinsic silicon," *Physica Status Solidi*, vol. 15, pp. K119–K122, 1966.

[18] B. J. Masters and J. M. Fairfield, "Silicon self-diffusion," *Applied Physics Letters*, vol. 8, pp. 280–281, 1966.

[19] J. M. Fairfield and B. J. Masters, "Self-diffusion in intrinsic and extrinsic silicon," *Journal of Applied Physics*, vol. 38, pp. 3148–3154, 1967.

[20] H. J. Mayer, H. Mehrer, and K. Maier, "Self-diffusion in silicon between 1320 K and 1660 K," in *Defects and radiation effects in semiconductors*, ser. Institute of Physics Conference Series, J. H. Albany, Ed., vol. 31. Institute of Physics, Bristol and London, 1978, pp. 186–193.

[21] R. N. Ghoshtagore, "Method for determining silicon diffusion coefficients in silicon and in some silicon compounds," *Physical Review Letters*, vol. 16, pp. 890–892, 1966.

[22] J. Hirvonen and A. Anttila, "Self-diffusion in silicon as probed by the (p,γ) rasonance boradening method," *Applied Physics Letters*, vol. 35, pp. 703–705, 1979.

[23] F. J. Demond, S. Kalbitzer, H. Mannsperger, and H. Damjantschitsch, "Study of Si self-diffusion by nuclear techniques," *Physics letters A*, vol. 93, pp. 503–506, 1983.

[24] T. Voss, A. Strohm, S. Matics, P. Scharwaechter, and W. Frank, "A novel technique for measuring diffusivities of short-lived radioisotoped in solids," *Zeitschrift für Metallkunde*, vol. 93, pp. 1077–1082, 2002.

[25] A. Strohm, T. Voss, W. Frank, P. Laitinen, and J. Räisänen, "Self-diffusion of Ge and Si in SiGe alloys," *Zeitschrift für Metallkunde*, vol. 93, pp. 737–744, 2002.

[26] L. Kalinowski and R. Seguin, "Self-diffusion in intrinsic silicon," *Applied Physics Letters*, vol. 35, pp. 211–212, 1979.

[27] H. Bracht, E. E. Haller, and R. Clark-Phelps, "Silicon self-diffusion in isotope heterostructures," *Physical Review Letters*, vol. 81, pp. 393–396, 1998.

[28] A. Ural, P. B. Griffin, and J. D. Plummer, "Fractional contributions of microscopic diffusion mechanisms for common dopants and self-diffusion in silicon," *Journal of Applied Physics*, vol. 85, pp. 6440–6446, 1999.

[29] A. Ural, P. B. Griffin, and J. D. Plummer, "Experimental evidence for a dual vacancy-interstitial mechanism of self-diffusion in silicon," *Applied Physics Letters*, vol. 73, pp. 1706–1708, 1998.

[30] A. Ural, P. B. Griffin, and J. D. Plummer, "Self-diffusion in silicon: similarity between the properties of native point defects," *Physical Review Letters*, vol. 83, pp. 3454–3457, 1999.

[31] A. Ural, P. B. Griffin, and J. D. Plummer, "Silicon self-diffusion under extrinsic conditions," *Applied Physics Letters*, vol. 79, pp. 4328–4330, 2001.

[32] Y. Nakabayashi, H. I. Osman, T. Segawa, K. Saito, S. Matsumoto, J. Murota, K. Wada, and T. Abe, "Self-diffusion in extrinsic silicon using isotopically enriched ^{31}Si layer," *Japanese Journal of Applied Physics*, vol. 40, pp. L181–L182, 2001.

[33] H. H. Silvestri, I. D. Sharp, H. Bracht, S. P. Nicols, J. W. Beeman, J. L. Hansen, A. N. Larsen, and E. E. Haller, "Dopant and self-diffusion in extrinsic n-type silicon isotopically controlled heterostructures," in *Defect- and impurity- engineered semiconductors and devices III*, S. Ashok, J. Chevallier, N. M. Johnson, B. L. Sopori, and H. Okushi, Eds., vol. 719, Materials Research Society Symposium Proceedings. Materials Research Society, San Fransisco, CA, 2002.

[34] I. D. Sharp, H. Bracht, H. H. Silvestri, S. P. Nicols, J. W. Beeman, J. L. Hansen, A. N. Larsen, and E. E. Haller, "Self- and dopant diffusion in extrinsic boron doped isotopically controlled silicon multilayer structure," in *Defect- and impurity- engineered semiconductors and devices III*, S. Ashok, J. Chevallier, N. M. Johnson, B. L. Sopori, and H. Okushi, Eds., Materials Research Society Symposium Proceedings. Materials Research Society, San Fransisco, CA, 2002.

[35] R. J. Needs, "First-principles calculations of self-interstitial defect structures and diffusion paths in silicon," *Journal of Physics: Condensed Matter*, vol. 11, pp. 10 437–10 450, 1999.

[36] R. J. Leung, W.-K. Needs, R. G., S. Itoh, and S. Ihara, "Calculations of silicon self-interstitial defects," *Physical Review Letters*, vol. 83, pp. 2351–2354, 1999.

[37] N. R. Zangenberg, "Defects and diffusion studies in Si and SiGe," Ph.D. dissertation, University of Aahrus, Denmark, 2003.

[38] R. B. Fair, "Concentration profiles of diffused dopants in silicon," in *Impurity doping processes in silicon*, F. F. Y. Wang, Ed. Amsterdam: North-Holland, 1981, vol. 1, pp. 314–442.

[39] P. Kuo, J. L. Hoyt, J. F. Gibbons, J. E. Turner, and D. Lefforge, "Boron diffusion in Si and $Si_{1-x}Ge_x$," in *Strained layer epitaxy-material, processing and device applications*, E. A. Fitzgerald, J. H. Hoyt, K.-Y. Cheng, and J. Bean, Eds., vol. 379, Materials Research Society Symposium Proceedings. Materials Research Society, San Fransisco, CA, 1995, pp. 373–378.

[40] R. N. Ghoshtagore, "Intrinsic diffusion of boron and phosphorus in silicon free from surface effects," *Physical Review B*, vol. 3, p. 389, 1971.

[41] T. T. Fang, W. T. C. Fang, P. B. Griffin, and J. D. Plummer, "Calculation of the fractional interstitial component of boron diffusion and segregation coefficient of boron in $Si_{0.8}Ge_{0.2}$," *Applied Physics Letters*, vol. 68, pp. 791–793, 1996.

[42] H.-J. Gossmann, T. E. Haynes, P. A. Stolk, D. C. Jacobson, G. H. Gilmer, J. M. Poate, H. S. Luftman, T. K. Mogi, and M. O. Thompson, "The interstitial fraction of diffusivity of common dopants in Si," *Applied Physics Letters*, vol. 71, pp. 3862–3864, 1997.

[43] H. Letaw Jr., W. M. Portnoy, and L. Slifkin, "Self-diffusion in germanium," *Physical Review*, vol. 102, pp. 636–639, 1956.

[44] M. W. Valenta and C. Ramasastry, "Effect of heavy doping on the self-diffusion of germanium," *Physical Review*, vol. 106, pp. 73–75, 1957.

[45] G. Vogel, G. Hettich, and H. Mehrer, "Self-diffusion in intrinsic germanium and effects of doping on self-diffusion in germanium," *Journal of Physics C: Solid State Physics*, vol. 16, pp. 6197–6204, 1983.

[46] M. Werner, H. Mehrer, and H. D. Hochheimer, "Effect of hydrostatic pressure, temperature, and doping on self-diffusion in germanium," *Physical Review B*, vol. 32, pp. 3930–3937, 1985.

[47] H. D. Fuchs, W. Walukiewicz, E. E. Haller, W. Dondl, R. Schorer, and G. Abstreiter, "Germanium $^{70}Ge/^{74}Ge$ isotope heterostructures: an approach to self-diffusion studies," *Physical Review B*, vol. 51, pp. 16 817–16 821, 1995.

[48] H. Widmer and G. R. Gunther-Mohr, *Helvetica Physica Acta*, vol. 34, p. 635, 1961.

[49] E. E. Haller and L. Wang, "Self-diffusion studies using semiconductor isotope heterostructures," *Defect and Diffusion Forum*, vol. 143-147, pp. 1067–1078, 1997.

[50] D. R. Campbell, "Isotope effect for self-diffusion in germanium," *Physical Review B*, vol. 12, pp. 2318–2324, 1975.

[51] N. A. Stolwijk, W. Frank, J. Holzl, S. J. Pearton, and E. E. Haller, "Diffusion and solubility of copper in germanium," *Journal of Applied Physics*, vol. 57, pp. 5211–5219, 1985.

[52] A. Giese, H. Bracht, N. A. Stolwijk, and H. Mehrer, "Diffusion of nickel and zinc in germanium," *Defect and Diffusion Forum*, vol. 143-147, pp. 1059–1064, 1997.

[53] A. Almazouzi, J. Bernardini, E. G. Moya, H. Bracht, N. A. Stolwijk, and H. Mehrer, "Diffusion, solubility, and thermodynamic properties of solid germanium studied by means of radiotracer and spreading-resistance analysis," *Journal of Applied Physics*, vol. 70, pp. 1345–1354, 1991.

[54] A. Strohm, T. Voss, W. Frank, J. Räisänen, and M. Dietrich, "Self diffusion of ^{71}Ge in SiGe alloys," *Physica B*, vol. 308-310, pp. 542–545, 2001.

[55] B. P. Uberuaga, G. Henkelman, H. Jónsson, S. T. Dunham, W. Windl, and R. Stumpf, "Theoretical studies of self-diffusion and dopant clustering in semiconductors," *Physica Status Solidi B*, vol. 233, pp. 24–30, 2002.

[56] B. P. Uberuaga, "First-principle study of self-diffusion in Ge using a cluster correction proceedure to improve supercell calculations," private communication.

[57] N. A. Stolwijk, in *Impurities and defects in group IV elements and III-V compounds*, ser. Landolt-Börnstein, New Series, M. Schulz, Ed. Springer, Berlin, 1989, vol. III/22b.

[58] P. Kringhøj and R. G. Elliman, "Diffusion of ion implanted Sn in Si, $Si_{1-x}Ge_x$, and Ge," *Applied Physics Letters*, vol. 65, pp. 324–326, 1994.

[59] M. Friesel, U. Södervall, and W. Gust, "Diffusion of tin in germanium studied by secondary ion mass spectroscopy," *Journal of Applied Physics*, vol. 78, pp. 5351–5355, 1995.

[60] A. Almazouzi, E. G. Moya, and J. Bernardini, "Bulk and grain boundary diffusion of Ge and Sn in intrinsic Germanium," *Defect and Diffusion Forum*, vol. 143-147, pp. 1047–1052, 1997.

[61] U. Södervall, H. Odelius, A. Lodding, U. Roll, B. Predel, W. Gust, and P. Dorner, "Gallium tracer diffusion and its isotope effect in germanium," *Philosophical Magazine A*, vol. 54, pp. 539–551, 1986.

[62] W. C. Dunlap, Jr., "Diffusion of impurities in germanium," *Physical Review*, vol. 94, pp. 1531–1540, 1954.

[63] W. Meer and D. Pommerring, "Diffusion von aluminium und bor in germanium," *Zeitschrift für Angewandte Physik*, vol. 23, pp. 369–372, 1967.

[64] S. Matsumoto and T. Niimi, "Concentration dependence of a diffusion coefficient of phosphorus diffusion in germanium," *Journal of the Electrochemical Society*, vol. 125, pp. 1307–1309, 1978.

[65] U. Södervall and M. Friesel, "Diffusion of silicon and phosphorus into germanium as studied by SIMS," *Defect and Diffusion Forum*, vol. 143-147, pp. 1053–1058, 1997.

[66] E. Vainonen-Ahlgren, T. Ahlgren, J. Likonen, S. Lehto, J. Keinonen, W. Li, and J. Haapamaa, "Identification of vacancy charge states in diffusion of arsenic in germanium," *Applied Physics Letters*, vol. 77, pp. 690–692, 2000.

[67] T. Ahlgren, J. Likonen, S. Lehto, E. Vainonen-Ahlgren, and J. Keinonen, "Fermi-level dependent diffusion of ion-implanted arsenic in germanium," in *AIP conference proceedings*, vol. 576, 2001, pp. 887–890.

[68] S. Mitha, S. D. Theiss, M. J. Aziz, D. Schiferl, and D. B. Poker, "Effect of pressure on As diffusion in Ge," in *Material Research Society Symposia Proceedings*, M. O. Manasreh, H. J. v. Bardeleben, G. S. Pomrenke, and M. Lannoo, Eds., vol. 325. USA: MRS, 1994, p. 189.

[69] M. Valenta, "Effect of heavy doping on the diffusion of impurities in germanium," Ph.D. dissertation, University of Illinois, United States of America, 1958.

[70] G. L. McVay and A. R. DuCharme, "The diffusion of germanium in silicon," *Journal of Applied Physics*, vol. 44, pp. 1409–1410, 1973.

[71] G. Hettich, H. Mehrer, and K. Maier, "Tracer diffusion of ^{71}Ge and ^{31}Si in intrinsic and doped silicon," in *International Conference on Defects and Radiation Effects in Semiconductors*, ser. Institute Physics Conferece Series, J. H. Albany, Ed., vol. 46. Nice, 1978: Institute of Physics, 1979, pp. 500–507.

[72] M. Ogino, Y. Oana, and M. Watanabe, "The diffusion coefficient of germanium in silicon," *Physica Status Solidi (A)*, vol. 72, pp. 535–541, 1982.

[73] A. L. Bouchetout, N. Tabet, and C. Monty, "Germanium impurity diffusion in boron doped silicon," *Material Science Forum*, vol. 10-12, pp. 127–132, 1986.

[74] P. Dorner, W. Gust, B. Predel, U. Roll, A. Lodding, and H. Odelius, "Investigation by SIMS of bulk impurity diffusion of Ge in Si," *Phil. Mag. A*, vol. 49, pp. 557–571, 1984.

[75] P. Fahey, S. S. Iyer, and G. J. Scilla, "Diffusion in silicon," in *Proceedings of the 14^{th} Nordic semiconductor meeting*, O. Hansen, Ed. Stockholm: Royal Swedish Academy of Sciences, 1990, pp. 55–59.

[76] N. R. Zangenberg, J. L. Hansen, J. Fage-Pedersen, and A. N. Larsen, "Ge self-diffusion in epitaxial $Si_{1-x}Ge_x$ layers," *Physical Review Letters*, vol. 87, pp. 125 901/1–125 901/4, 2001.

[77] P. Fahey, S. S. Iyer, and G. J. Scilla, "Experimental evidence of both interstitial-and vacancy-assisted diffusion of Ge in Si," *Applied Physics Letters*, vol. 54, pp. 843–845, 1989.

[78] J. Räisänen, J. Hirvonen, and A. Anttila, "The diffusion of silicon in germanium," *Solid-State Electronics*, vol. 24, pp. 333–336, 1981.

[79] H. Bracht, "Native point defects in silicon," in *Electrochemical society proceedings*, vol. 99-1, 1999, pp. 357–371.

[80] G. L. McVay and A. R. DuCharme, "Diffusion of Ge in SiGe alloys," *Physical Review B*, vol. 9, pp. 627–631, 1974.

[81] P. Venezulea, G. M. Dalpian, A. J. R. da Silva, and A. Fazzio, "Vacancy mediated diffusion in disordered alloys: Ge self-diffusion in $Si_{1-x}Ge_x$," *Physical Review B*, vol. 65, pp. 193 306/1– 193 306/4, 2002.

[82] K. Rajendran and W. Shoenmaker, "Studies of boron diffusivity in strained $Si_{1-x}Ge_x$ epitaxial layers," *Journal of Applied Physics*, vol. 89, pp. 980–987, 2001.

[83] P. Kuo, J. L. Hoyt, J. F. Gibbons, J. E. Turner, and D. Lefforge, "Effects of strain on boron-diffusion in Si and $Si_{1-x}Ge_x$," *Applied Physics Letters*, vol. 66, pp. 580–582, 1995.

[84] P. Kuo, J. L. Hoyt, J. F. Gibbons, J. E. Turner, and D. Lefforge, "Effects of Si thermal-oxidation on B diffusion in Si and strained $Si_{1-x}Ge_x$ layers," *Applied Physics Letters*, vol. 67, pp. 706–708, 1995.

[85] N. Moriya, L. C. Feldman, C. A. King, J. Bevk, and B. Freer, "Boron diffusion in strained $Si_{1-x}Ge_x$ epitaxial layers," *Physical Review Letters*, vol. 71, pp. 883–886, 1993.

[86] C. Chen, U. M. Gösele, and T. Y. Tan, "Dopant diffusion and segregation in semiconductor heterostructures: Part2. B in Ge_xSi_{1-x}/Si structures," *Applied Physics A: Material Science and processing*, vol. 68, pp. 19–24, 1999.

[87] P. Kuo, J. L. Hoyt, J. F. Gibbons, J. E. Turner, R. D. Jacowitz, and T. I. Kamins, "Comparison of boron diffusion in Si and strained $Si_{1-x}Ge_x$ epitaxial layers," *Applied Physics Letters*, vol. 62, pp. 612–614, 1993.

[88] N. E. B. Cowern, P. C. Zalm, P. v. Sluis, D. J. Gravesteijn, and W. B. de Boer, "Diffusion in strained Si(Ge)," *Physical Review Letters*, vol. 72, pp. 2585–2588, 1994.

[89] W. T. C. Fang, P. B. Griffin, and J. D. Plummer, "Implant enhanced diffusion of boron in silicon germanium," in *Strained layer epitaxy-material, processing and device applications*, E. A. Fitzgerald, J. H. Hoyt, K.-Y. Cheng, and J. Bean, Eds., vol. 379, Materials Research Society Symposium Proceedings. Materials Research Society, San Fransisco, CA, 1995, pp. 379–384.

[90] J. M. Bonar, B. M. McGregor, N. E. B. Cowern, A. H. Dan, G. A. Cooke, and A. F. W. Willoughby, "Furnace and RTA injection of points defects into cvd grown b doped Si and SiGe," in *Si front-end processing-physics and technology of dopant-defect interactions II*, A. Agarwal, L. Pelaz, H.-H. Vuong, P. Packan, and M. Kase, Eds., vol. 610, Materials Research Society Symposium Proceedings. Materials Research Society, San Fransisco, CA, 2000, pp. B4.9.1–B4.9.6.

[91] P. Kringhøj and A. N. Larsen, "Diffusion of Sb in $Si_{1-x}Ge_x$," *Defect and Diffusion Forum*, vol. 143-147, pp. 1125–1130, 1997.

[92] A. D. N. Paine, "Antimony diffusion in Silicon-Germanium alloys," Ph.D. dissertation, University of Southampton, 1998.

[93] A. Dan, A. F. W. Willoughby, J. M. Bonar, B. M. McGregor, M. G. Dowsett, and R. J. H. Morris, "Antimony diffusion in silicon germanium alloys under point defect injection," *International Journal of Modern Physics B*, vol. 16, pp. 4195–4198, 2002.

[94] A. Y. Kuznetsov, J. S. Christensen, M. K. Linnarsson, B. G. Svensson, H. H. Radamson, J. Grahn, and G. Landgren, "Diffusion of phosphorus in strained Si/SiGe/Si heterostructures," in *Si Front-end processing - physics and technology of dopant-defect interactions*, H.-J. L. Gossman, T. E. Haynes, M. E. Law, A. N. Larsen, and S. Odanaka, Eds., vol. 568, Materials Research Society Symposium Proceedings. Materials Research Society, San Fransisco, CA, 1999, pp. 271–276.

[95] J. Christensen, A. Y. Kuznetsov, H. H. Radamson, and B. G. Svensson, "Phosphorus and boron diffusion in silicon under equilibrium conditions," submitted to Journal of Applied Physics.

[96] A. N. Larsen and P. Kringhøj, "Diffusion in relaxed and strained SiGe layers," *Physica Scripta*, vol. T69, pp. 92–97, 1997.

[97] L. Zou, Z. G. Wang, D. Z. Sun, T. W. Fan, X. F. Liu, and J. W. Zhang, "Rapid thermal annealing of arsenic implanted $Si_{1-x}Ge_x$ epilayers," *Nuclear Instruments and Methods in Physics Research B*, vol. 122, pp. 639–642, 1997.

[98] S. Eguchi, J. L. Hoyt, C. W. Leitz, and E. A. Fitzgerald, "Comparison of arsenic and phosphorus diffusion behvior in silicon-germanium alloys," *Applied Physics Letters*, vol. 80, pp. 1743–1745, 2002.

[99] C. Cerrina, A. Nejim, Y. Wang, and P. L. F. Hemment, "Influence of Ge content on electrical properties: Sheet resistance and hall mobility in ion beam synthesized $Si_{1-x}Ge_x$ alloy," *Defect and Diffusion Data Part B -Solid State Phenomenon*, vol. 82-84, pp. 557–562, 2003.

[100] H. Bracht, "Diffusion mechanisms and intrinsic point-defect properties in silicon," *MRS Bulletin*, vol. 25, no. 6, pp. 22–27, 2000.

[101] H. Bracht, N. A. Stolwijk, and H. Mehrer, "Diffusion and solubility of copper, silver, and gold in germanium," *Physical Review B*, vol. 43, pp. 14 465–14 477, 1991.

[102] A. Giese, H. Bracht, N. A. Stolwijk, and D. Baither, "Microscopic defects in silicon induced by zinc out-diffusion," *Material Science and Engineering B*, vol. 71, pp. 160–165, 2000.

[103] R. Fisher, W. F. J. Frank, and K. Lyutovich, "Diffusion of gold in relaxed Si-Ge epi-layers," *Physica B*, vol. 273-274, pp. 598–602, 1999.

[104] H. Saito, N. Fukuoka, and H. Yoshida, "Interstitials in germanium," in *Institute Physics Conference Series*, vol. 59. Institute of Physics, 1981, pp. 45–55.

[105] A. Janotti, R. Baierle, A. J. R. Silva, R. Mota, and A. Fazzio, "Electronic and structural properties of vacancy and self-interstitial defects in germanium," *Physica B*, vol. 273-274, pp. 575–578, 1999.

[106] A. J. R. Silva, A. Janotti, A. Fazzio, R. Baierle, and R. Mota, "Self-interstitial defect in germanium," *Physical Review B*, vol. 62, pp. 9903–9906, 2000.

[107] R. Sielemann, H. Haesslein, L. Wende, and C. Zistl, "Frenkel pairs, vacancies, and self-interstitials in Ge: identification and properties from PAC- and Moessbauer spectrpscopy," *Physica B*, vol. 273-274, pp. 565–569, 1999.

[108] R. Sielemann, H. Haesslein, and C. Zistl, "Microscopic observation of interaction between self-interstitials ans In-acceptors in germanium," *Physica B*, vol. 302-303, pp. 101–105, 2001.

[109] H. Herzer and S. Kalbitzer, "Electrical properties of ion-implanted germanium," in *Proceedings of the 2nd international conference on ion implantation in semiconductors, physics and technology, fundamental and applied aspects*, I. Ruge and J. Graul, Eds. Springer Verlag, Berlin, West Germany, 1971, pp. 307–314.

[110] J. Lindhard, J. Scharff, and H. Schiøtt, "Range, concenpts and heavy ion ranges," *Mat. Fys. Medd. Dan. Vid. Selsk.*, vol. 33, pp. 1–42, 1963.

[111] J. P. Ponpon, J. J. Grob, R. Stuck, B. Burger, and P. Siffert, "Boron implanted contacts on high purity germanium," in *Second international conference on ion implantation in semiconductors*, I. Ruge and J. Graul, Eds. Springer-Verlag, 1972.

[112] J. P. Ponpon, R. Stuck, P. Siffert, H. Herzer, and S. Kalbitzer, "Further studies on implanted high purity germanium detectors," *IEEE transations on nuclear science*, vol. S-19, pp. 281–288, 1972.

[113] V. M. Gusev, M. I. Guseva, E. S. Ionova, A. N. Mansureva, and C. V. Starinin, "Electrical properties and structure of boron implanted germanium," *Physica Status Solidi (A)*, vol. 21, pp. 413–418, 1974.

[114] M. I. Guseva and A. N. Mansureva, "Radiation-enhanced diffusion of boron in germanium during ion implantation," *Radiation Effects*, vol. 20, pp. 207–210, 1973.

[115] P. J. Macdonald and D. W. Palmer, "Differences in defect production and annealing processes in boron- and carbon-irradiated germanium," in *Institute Physics Conference Series*, vol. 23. Institute of Physics, 1975, pp. 505–512.

[116] K. S. Jones and E. E. Haller, "Ion implantation of boron in germanium," *Journal of Applied Physics*, vol. 61, pp. 2469–2477, 1987.

[117] M. Metzger, Z. Zhang, B. Schmiedt, and H. Ryssel, "Implantation doping of germanium with Be, Mg, Zn, and B ions," in *Ion implantation: Equipment and Techniques*, H. Ryssel and H. Glawischnig, Eds. Berchtesgaden, West Germany: Springer-Verlag, Berlin, West Germany, 1983, pp. 458–464.

[118] A. Axmann, M. Schulz, and C. R. Fritzsche, "Implantation doping of germanium with Sb, As, and P," *Applied Physics*, vol. 12, pp. 173–178, 1977.

[119] G. Carter and W. A. Grant, *Ion implantation of semiconductors*, A. H. W. Beck and J. Lamb, Eds. Edward Arnold, 1967.

[120] S. K. Ghandhi, *VLSI fabrication principle: silicon and gallium arsenide*, 2nd ed. Canada: John Wiely and Sons, 1994, ch. 5, 7.

[121] R. G. Wilson, F. A. Stevie, and C. W. Magee, *Secondary Ion Mass Spectroscopy: A practical hand book for depth profiling and bulk impurity analysis.* John Wiley & Sons, 1989.

[122] E. L. Jordan, "A diffusion mask for germanium," *Journal of the Electrochemical Society*, vol. 108, pp. 478–481, 1961.

[123] R. Webb. (2001) Surrey University Sputter Profile Resolution from Energy deposition. Online. [Online]. Available: http://www.ee.surrey.ac.uk/SCRIBA/simulations

[124] J. F. Gibbons, W. S. Johnson, and S. W. Mylroie, *Projected range statistics: Semiconductors and related materials*, 2nd ed. Stroudsbury, PA, USA: Halsted Press, 1975.

[125] D. K. Brice, *Ion implantation range and energy deposition distribution.* New York: Plenum Press, 1975, vol. 1.

[126] J. F. Ziegler and J. P. Biersack. (2003) The Stopping Range of Ions in Matter. Online. [Online]. Available: http://www.srim.org

[127] H. Herzer, S. Kalbitzer, J. P. Ponpon, R. Stuck, and P. Siffert, "Ion implanted high-purity germanium detectors," *Nuclear instruments and methods*, vol. 101, pp. 31–37, 1972.

[128] S. S. Godakov, A. B. Klyukvin, and E. V. Mikhallutsa, "Interstitial diffusion of impurities from ion-implanted-doped layers in germanium," *Soviet Physics Semiconductors*, vol. 18, pp. 1372–1374, 1984.

[129] B. L. Sharma, "Diffusion in silicon and germanium," *Defect and Diffusion Forum*, vol. 70, pp. 1–102, 1990.

[130] *Two-dimensional process simulation program*, 7th ed., Avant! Corporation, July 2000.

[131] S. Uppal, A. F. Willoughby, J. M. Bonar, A. J. R. Evans, N. E. B. Cowern, R. Morris, and M. G. Dowsett, "Ion implantation and diffusion behaviour of boron in germanium," *Physica B*, vol. 308-10, pp. 525–528, 2001.

[132] A. Strohm, S. Matics, and W. Frank, "Diffusion of gold in germanium," *Defect and Diffusion Forum*, vol. 194-199, pp. 629–634, 2001.

[133] J. S. Nelson, P. A. Schultz, and P. A. Wright, "Valence and atomic size dependent exchange barriers in vacancy-mediated dopant diffusion," *Applied Physics Letters*, vol. 73, pp. 247–249, 1998.

[134] L. R. Bidwell, "The boron-germanium system," *Journal of less-common metals*, vol. 20, pp. 19–27, 1970.

[135] P. Laitinen, A. Strohm, J. Huikari, A. Nieminen, T. Voss, C. Grodon, I. Riihimäki, M. Kummer, J. Äystö, P. Dendooven, J. Räisänen, W. Frank, and the ISOLODE Collaboration, "Self diffusion of ^{31}Si and ^{71}Ge in relaxed $Si_{0.20}Ge_{0.80}$ layers," *Physical Review Letters*, vol. 89, pp. 085 902–085 904, 2002.

[136] S. Uppal, A. F. Willoughby, J. M. Bonar, N. E. B. Cowern, R. J. H. Morris, and M. Bollani, "Diffusion of boron in germanium and $Si_{1-x}Ge_x$ (x>50%) alloys," in *CMOS front end materials and process technology*, T. King, B. Yu, R. J. P. Lander, and S. Saito, Eds., vol. 765, Materials Research Society Symposium Proceedings. Materials Research Society, San Fransisco, CA, 2003.

[137] A. F. W. Willoughby, J. M. Bonar, and A. D. N. Paine, "Diffusion mechanism in SiGe alloys," in *Silicon front-end processingphysics and technology of dopant-defect interactions*, H.-J. L. Gossman, T. E. Haynes, M. E. Law, A. N. Larsen, and S. Odanaka, Eds., vol. 568, Materials Research Society Symposium Proceedings. Materials Research Society, San Fransisco, CA, 1999, pp. 253–263.

[138] A. F. W. Willoughby, A. G. R. Evans, P. Champ, K. J. Yallup, D. J. Godfrey, and M. G. Dowsett, "Diffusion of boron in heavily doped n- and p-type silicon," *Journal of Applied Physics*, vol. 59, pp. 2392–2397, 1986.